DOI: 10.31891/2079-1372

THE INTERNATIONAL SCIENTIFIC JOURNAL

PROBLEMS OF TRIBOLOGY

Volume 27 ***No 2/104-2022***

МІЖНАРОДНИЙ НАУКОВИЙ ЖУРНАЛ

ПРОБЛЕМИ ТРИБОЛОГІЇ

Присвячується 60-річчю Хмельницького національного університету

PROBLEMS OF TRIBOLOGY

INTERNATIONAL SCIENTIFIC JOURNAL

Published since 1996, four time a year

Volume 27 No 2/104-2022

Establishers:
Khmelnitskiy National University (Ukraine)
Lublin University of Technology (Poland)

Associated establisher:
Vytautas Magnus University (Lithuania)

Editorial board address:
International scientific journal "Problems of Tribology",
Khmelnitsky National University,
Institutskaia str. 11, Khmelnitsky, 29016, Ukraine
phone +380975546925

Indexed: CrossRef, DOAJ, Ulrichsweb, Google Scholar, Index Copernicus

E-mail: tribosenator@gmail.com

Internet: http://tribology.khnu.km.ua

ПРОБЛЕМИ ТРИБОЛОГІЇ

МІЖНАРОДНИЙ НАУКОВИЙ ЖУРНАЛ

Видається з 1996 р. ***Виходить 4 рази на рік***

Том 27 **№ 2/104-2022**

Співзасновники:
Хмельницький національний університет (Україна)
Університет Люблінська Політехніка (Польща)

Асоційований співзасновник:

Університет Вітовта Великого (Литва)

Адреса редакції:
Україна, 29016, м. Хмельницький, вул. Інститутська 11, к. 4-401
Хмельницький національний університет, редакція журналу "Проблеми трибології"
тел. +380975546925, **E-mail**: tribosenator@gmail.com

Internet: http://tribology.khnu.km.ua

Зареєстровано Міністерством юстиції України
Свідоцтво про держреєстрацію друкованого ЗМІ: Серія КВ № 1917 від 14.03. 1996 р.
(перереєстрація № 24271-14111ПР від 22.10.2019 року)

Входить до переліку наукових фахових видань України
(Наказ Міністерства освіти і науки України № 612/07.05.19. Категорія Б.)

Індексується в МНБ: CrossRef, DOAJ, Ulrichsweb, Google Scholar, Index Copernicus

Рекомендовано до друку рішенням вченої ради ХНУ, протокол № 18 від 30.06.2022 р.

Problems of Tribology, *V. 27, No 2/104-2022*

Problems of Tribology

Website: http://tribology.khnu.km.ua/index.php/ProbTrib
E-mail: tribosenator@gmail.com

CONTENTS

***Problems of Tribology**, V. 27, No 2/104-2022*

Problems of Tribology

Website: http://tribology.khnu.km.ua/index.php/ProbTrib

E-mail: tribosenator@gmail.com

ЗМІСТ

Problems of Tribology, V. 27, No 2/104-2022, 6-12

Problems of Tribology
Website: http://tribology.khnu.km.ua/index.php/ProbTrib
E-mail: tribosenator@gmail.com

DOI: https://doi.org/10.31891/2079-1372-2022-104-2-6-12

Creation of new technological methods for surface engineering based on broaching

I.V. Shepelenko*[1], E.K. Posviatenko[2], Ya.B. Nemyrovskyi[1], V.V. Cherkun[3], I.P. Rybak[2]

[1]Central Ukrainian National Technical University, Kropyvnytsky, Ukraine
[2]National Transport University, Kyiv, Ukraine
[3]Dmytro Motornyi Tavria State Agrotechnological University, Melitopol, Ukraine
**E-mail: kntucpfzk@gmail.com*

Received: 8 March 2022: Revised: 20 April 2022: Accept: 5 May 2022

Abstract

The article is devoted to the creation of new processing technologies through the use of drawing. It is determined that the most effective processes of surface engineering of machine parts are hybrid technologies. The advantages of such technologies due to obtaining a new effect from the impact on the part by two or more dissimilar processes belonging to one or different groups of surface engineering methods are noted. It is proved that the use of hybrid technologies on the basis of stretching allows to combine the advantages of different methods, first of all cold plastic deformation methods, in combination with others. The use of deforming drawing provides in the surface layer favorable for the part of the compressive residual stresses, increase the wear resistance of the surface, as well as the strength of the part. The results of the research allowed to classify the deforming drawing as a class of surface engineering methods. On the example of processing of cylinder liners of internal combustion engines the combined technology containing operations of deforming drawing and finishing antifrictional non-abrasive processing is developed. It is shown that the use of deforming drawing has significantly improved the quality of antifriction coating. The use of deforming drawing to the component of the hybrid method with the subsequent pulsed nitriding is considered.It is established that when nitriding cutting tool products, hybrid process modes should be set in order to create the most effective nitride zone. In the case of processing of road vehicle parts, special attention should be paid to obtaining a diffusion layer. The efficiency of the offered technologies on the basis of stretching is established. Determining the prospects for further use of deforming drawing as an integral part of hybrid technologies.

Key words: surface engineering, broaching, hybrid technologies, finishing antifriction non-abrasive treatment, nitriding

Introduction

Modern machines must have a set of operational, aesthetic, environmental, technological and other properties that are determined by the indicators system of the machine quality, which in turn are provided by the properties of the surface, surface layer or individual surface of the part. This means that when choosing structural materials for mechanical engineering should distinguish between the functions of the core and the surface layer. This design and technological concept of creating machines is not only strategic but also universal, as it dominates throughout the life cycle of the machine, in particular, in its manufacture, operation and repair, as well as in the restoration of individual components and parts. The general priority of modern mechanical engineering, which includes the development of known and creation of new technologies for influencing the surface layer of the part, the purpose of which is to control the composition, structure and properties of the latter, was defined as "surface engineering of machine parts" (SE).

Literature review

There are about two hundred methods of surface engineering, which should be classified as follows: coating, modification of the surface layer, technological and combined (hybrid) methods. Currently, researchers pay the most attention to coatings that can be obtained by gas-thermal and mechanothermic spraying, vacuum-condensation technologies, surfacing, galvanic and chemical deposition, enameling, plating, cladding, hot metal coating, solid lubricants application [1]. Having a number of advantages (thickness 0.005 ÷ 5 mm; high level of physical and mechanical properties; used equipment and technological equipment), coatings are still not securely held on the base, require finishing machining, create a large gradient of harmful residual stresses. Modification of the surface layer, including surface heat and chemical-thermal treatment and cold plastic deformation (CPD), is free from these disadvantages, as the means of influencing the properties of the metal are structural transformations, diffusion processes and changes in dislocation density in the base material. The disadvantage of the modification is the difficulty of managing the size of worn parts. Technological methods involve the impact on the surface layer of the part in order to change its properties by cutting or related processes. This group includes most methods of obtaining regular macro- and microreliefs. Hybrid methods involve obtaining a new effect from the impact on the part of two or more heterogeneous processes belonging to one or different groups of SE [2, 3].

Obviously, each of the methods affects the operational properties of machine parts through a set of geometric and physic-mechanical characteristics of the surface, primarily accuracy, roughness, support area, microrelief, macrorelief, porosity, hardness, microhardness, residual stresses, microstructure, texture, adhesion properties, adhesion strength to the base, the resource of plasticity used, etc. The obtained physic-mechanical and geometrical characteristics allow to increase wear resistance, corrosion resistance, fatigue strength, oxidation resistance, contact hardness, heat resistance, adhesion resistance, heat strength, antifriction or friction properties, tightness of joints, strength, lubricant retention efficiency, friction vapor compaction, heat and electrical insulating properties, fragmentation munitions efficiency, tool cutting properties.

In our opinion, hybrid technologies are the most effective processes of the surface engineering of machine parts, both in the main and in the secondary (repair and restoration) industries.

Special attention should be paid to the methods of parts finishing processing by CPD, among which should be noted deforming broaching (DB). The analysis of known sources showed that with all the variety of research in the field of DB application, despite its advantages, the use of this process requires more in-depth research, including the development of combined technologies. One of the examples of such a process is the technology of vehicle parts restoration, which includes volumetric CPD (shaping) followed by low-frequency finishing ionic pulsed nitriding [3, 4]. CPD by deposition, rolling, compressed liquid, drawing, hydroabrasive treatment, rolling, deforming broaching and stitching (mandrel) allows to obtain a number of useful from the standpoint of SE geometric and physic-mechanical characteristics of products surface layer. At the Institute of Superhard Materials named by V.M. Bakul of the NAS of Ukraine for the last few decades have been studying deforming broaching (DB) and related processes of CPD, which allowed to obtain important scientific results that formed the basis of many resource-saving technologies [5-9, etc.]. In this case, the DB was often considered as a finishing operation, the basis of which was the following [10, 11]. The accuracy of the holes in the circle, taking into account the shrinkage (+) and breakdown (-) after the DB was within ± 0.02 mm, and the curvature of the generator – 0.15-0.30 mm per 1000 mm of sleeve length. The roughness of the treated surface was guaranteed to be provided in the range of Ra = 0.05-0.15 μm, and the bearing surface – 90-95%. Studies have also shown that, depending on the modes of DB and the type of processed material, the thickness of the reinforced textured layer is 0.05-0.3 mm, and the degree of metal hardening in this layer is 50-300% (by microhardness index).

Thus, the analysis of literature sources showed the possibility and prospects of creating new technological methods of surface engineering on the basis of DB.

Purpose

The aim of the work is to expand the technological capabilities of DB by creating new technological methods of surface engineering to improve the quality of surface treatment.

Results

Studies [7-11] have shown that DB provides in the surface layer favorable for the part compressive residual stresses of the I kind, increase the wear resistance of the surface several times (except in the case of friction pair in abrasive wear), as well as the strength of the part. The last two effects are explained by the texturing of the surface layer, increasing the yield strength of the treated material, reducing the geometric parameters of stress concentrators and the favorable effect of compressive residual stresses.

This is confirmed by the distribution curves of some of the above characteristics of the DB surface layer, shown in Fig.1 and 2.

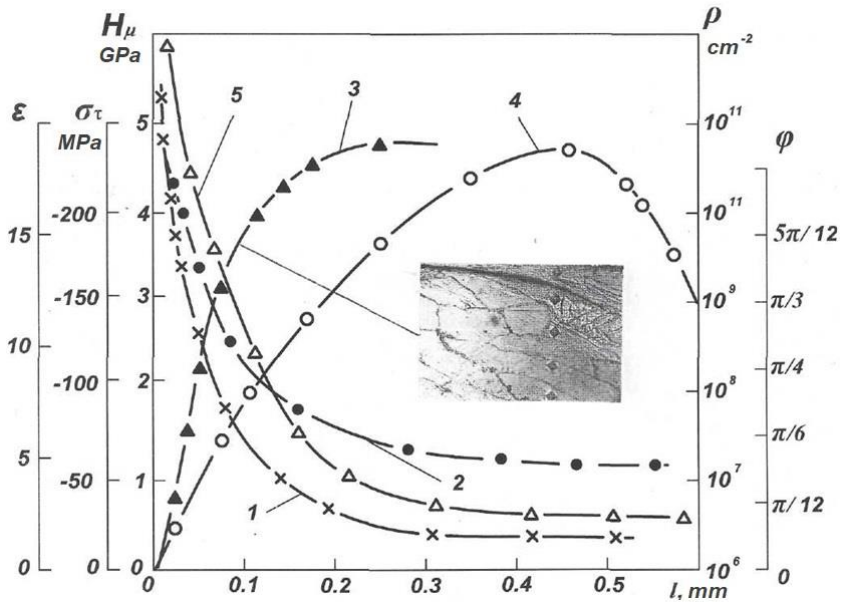

Fig. 1. Distribution of relative deformations of simple shear ε (1), microhardness $H\mu$ (2), tilt angle of texture grains large axes φ (3), compressive tangential residual stresses of the I kind σ_τ (4) and dislocation density ρ (5) by thickness of l liner surface layer from steel 10 processed by DB with 20 cycles. In the center – the microstructure of the sleeve surface layer, × 120

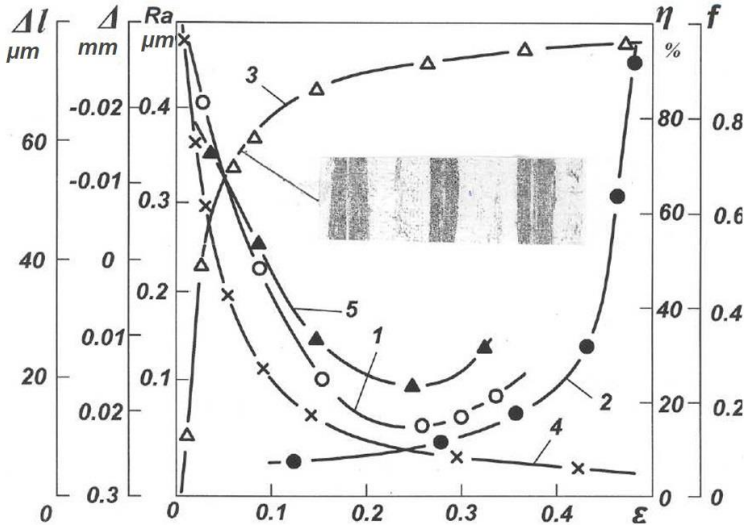

Fig. 2. Dependences of roughness Ra (1), accuracy Δ holes in a circle (2), bearing surface η (3), coefficient of friction f (4) and wear of a part Δl (5) on relative deformation ε at DB of a sleeve from steel 10. In the center – photomicrograph (× 80) of the hole area with regular annular microrelief: light stripes – support platforms, dark – grooves

The above research results allowed to classify CPD with the help of DB to the class of SE methods, combined with the concept of the surface layer modification during the manufacture and renovation of products [2].

At the same time, the results of careful analysis of some other surface layer properties after DB, which previously remained out of the researchers attention, led to the conclusion that this process can also be attributed to classes of technological and hybrid methods of SE. Thus, given the technological characteristics of the DB, in particular the magnitude and smallness of deformation, can be created on the treated surface of the part micro- and macroreliefs of the desired type, shape and height of each element, as well as control the number of elements per unit area, relative bearing surface and angles. Boring, cutting or other cutting processes should be used as the pre-DB treatment. As an example, Fig. 2 shows the curve of the support surface 3 and the area of the hole with a regular annular microrelief (η = 70%). The importance of technical solutions related to micro- and macro-reliefs is evidenced by the fact that they developed a state standard [12], defended several dissertations and published a number of monographs. We propose to use regular technological reliefs as micro-tanks for lubrication when working in sliding friction pairs of vehicles, such as power systems of hydraulic systems, shock absorbers, jacks, bearings. This protects the contacting parts from setting. For this purpose, it is advisable to use another property

of the surface layer after the DB – increasing the yield strength of the treated material by 40-70% and, as a consequence, – the allowable contact stresses by the criterion of setting bridges occurrence. This is confirmed by the curve of the friction coefficient on the level of deformation at DB (Fig. 2). This graph shows that even with small deformations, the reinforced by CPD surface receives reliable protection against adhesions (internal friction).

When using DB as part of one of the SE hybrid methods, including shape-forming CPD, followed by a finishing low-frequency ionic pulsed nitriding, the physical essence of the new joint effect on the product is as follows. When DB as a process that completes the formation of the part with the necessary increase (decrease) of its size, in the surface layer, along with obtaining the above useful geometric and physic-mechanical properties, a texture with variable tilt angle of a grain large axes relative to the movement direction of the tool (Fig. 1; curve 3; photomicrograph; $\varphi = 0 - \pi / 4$). Elongation of the microstructure grains is accompanied by their grinding and increasing the dislocations density by several orders of magnitude (ibid., curve 5). This preparation of the surface layer for further nitriding is extremely useful because it allows increasing several times the speed of this process, which is explained as follows.

The essence of low-frequency ionic nitriding in the pulsed mode, sometimes called nitriding in the glow discharge (NGD), is that in the rarefied gaseous environment between the cathode (part) and the anode (vacuum chamber wall) a glow discharge is excited. At the same time, positive ions with high energy, bombarding the surface of the part, heat it to saturation temperature and deepen into it, forming a solid solution of nitrogen in the metal, and when the solubility limit is reached – nitride phases. Pre-nitriding DB significantly accelerates the diffusion of nitrogen into the surface layers of the part, as it ensures the movement of atoms not only outside the grains of the base metal, but also mainly through the grains themselves behind dislocations. The structure of the nitrided layer consists of two zones: the outer nitride and the diffusion zone of the unsaturated solid solution with dispersed inclusions of intermediate phases [13]. The properties of the nitride zone, which has a thickness of several micrometers to several hundredths of a millimeter, are very different from the diffusion zone, the thickness of which can vary from several tenths of a millimeter to several millimeters. In the first case, the layer of material has a high hardness and fragility, and in the second – at lower hardness, the layer is stronger. Therefore, when NGD products such as cutting tools should be set modes of the hybrid process to create the most effective nitride zone. In the case of machining parts of road vehicles, a typical representative of which is the crankshaft, special attention should be paid to obtaining a diffusion layer. It should be borne in mind that the nitride zone can be a barrier to diffusion processes [14].

A promising area of further research of the described hybrid process is to obtain a duplex surface layer that would combine CPD, precision nitriding and coating application of TiN type with a thickness of $2 \div 5$ μm by the KIB method.

Another example of DB using as a component of a SE hybrid method is our technology of antifriction coatings, which includes mechanical surface preparation as a basis for creating regular microrelief, friction-mechanical coating and finishing processing – by deforming broaching [15]. The essence of the proposed and the participation of the DB are as follows. As noted in [16], the quality of the coating obtained by finishing antifriction non-abrasive treatment (FANT) mainly depends on the triggering of the following channels of contact surfaces activation: mechanical, chemical, thermal and vacancy-dislocation. At the same time, the authors of [17, 18] substantiated the feasibility of forming favorable shapes and sizes of microroughness in previous FANT operations, for example, creating a regular microrelief by turning as one of the conditions for obtaining a quality coating.

It is difficult to obtain a high-quality antifriction coating on a surface with a rough regular microrelief due to the peculiarities of filling the microroughness hollows with antifriction material. Thus, voids can occur between individual particles of antifriction material, which negatively affects the density and continuity of the coating.

The use of DB will significantly improve the quality of antifriction coating, namely:

- provide the individual elements packaging of the antifriction product in a solid mass and strengthening the coating material with the base by surface plastic deformation;
- increase the strength of antifriction material adhesion to the base;
- create a microrelief with a greater bearing capacity of the surface.

The proposed technological solution formed the basis of our developed technological process of processing the hole in the ICE sleeves using combined broaching and FANT [19, 20].

At the combined broaching there is a removal of an allowance by a cutting element and increase in the size of a hole by group of deforming elements. As a result of processing, the rough layer of the sleeve working surface has the necessary physic-mechanical and geometric properties. The change in the height parameter of the roughness *Ra* and the microrelief of the working surface during sleeves processing by FANT and DBR is shown in Fig.3.

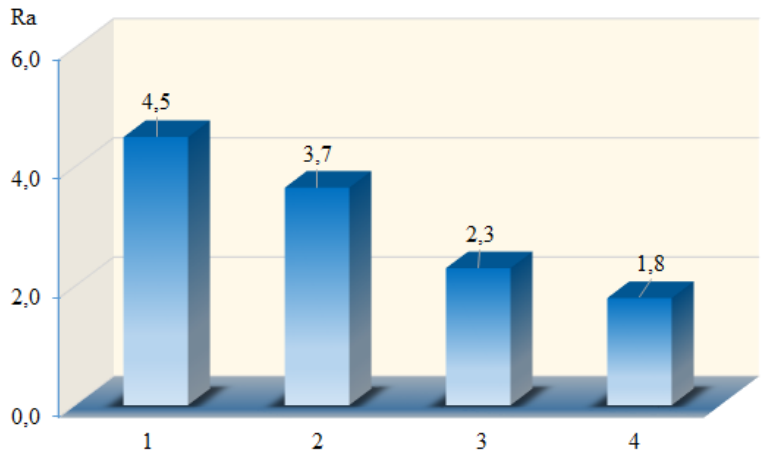

Fig. 3. Changing the parameter *Ra* when processing the sleeve: 1 – boring; 2 – FANT; 3 – DB with one deforming element; 4 – DB by two deforming elements

The use of DB allowed reducing the parameter Ra and creating a new technology for applying antifriction coatings using DB [21].

Conclusions

The application of the proposed hybrid technologies based on broaching allows to combine the advantages of different methods, including surface modification and coating application with the achievement of higher operational properties of parts that require further study.

The technological process of ICE sleeves processing has been developed, which includes operations of DB and FANT, which provides the obtaining of the sleeve working surface with improved physic-mechanical and tribological characteristics. The efficiency of the combination of DB and FANT operation has been established, which allows improving the quality of ICE sleeves processing.

The technology of details restoration containing DB with the subsequent finishing low-frequency ionic pulse nitriding is offered.

Determining the prospects for further research of DB as part of hybrid technologies.

References

1. Chernovol M.I., Shepelenko I.V. (2012) Sposoby formirovaniya antifrikcionnyh pokrytij na metallicheskie poverhnosti treniya [Zbirnyk naukovykh prats Kirovohradskoho natsionalnoho tekhnichnoho universytetu - Vyp. 25 (1)] – S.3-8.

2. Kanarchuk V.E., Posviatenko E.K., Lopata L.A. (2000) Inzheneriia poverkhni detalei transportnykh zasobiv: suchasnyi stan i perspektyvy [Visnyk Natsionalnoho transportnoho universytetu - Vyp. 4] – S.3-14.

3. Posviatenko E.K. (2008) Gibridnye processy inzhenerii poverhnostej detalej mashin [Inzheneriya poverhnosti i renovaciya izdelij] – S.195-198.

4. Posviatenko E.K., Alieksieiev V.V. (2007) Nyzkochastotne ionne impulsne azotuvannia yak metod inzhenerii poverkhni detalei DTZ [Visnyk Natsionalnoho transportnoho universytetu - Vyp. 15] – S.25-33.

5. Rosenberg A.M., Rosenberg O.A., Gricenko E.I., Posviatenko E.K. (1977) Kachestvo poverhnosti, obrabotannoj deformiruyushchim protyagivaniem. Kiev, Naukova dumka, 188 s.

6. Rosenberg A.M., Rosenberg O.A., Posviatenko E.K. (1978) Raschet i proektirovanie tverdosplavnyh deformiruyushchih protyazhek i processa protyagivaniya. Kiev, Naukova dumka, 256 s.

7. Rosenberg A.M., Rosenberg O.A. (1998) Mehanika plasticheskogo deformirovanija v processah rezanija i deformirujushhego protjagivanija. Kiev, Naukova dumka, 320 s.

8. Posviatenko E.K. (1993) Naukove obgruntuvannia efektyvnosti protsesu deformuiuche-rizhuchoho protiahuvannia [Avtoreferat dysertatsii doktora tekhnichnykh nauk] 35 s.

9. Posviatenko E.K., Nemyrovskyi Ya.B., Cherniavskyi O.V., Yeromin P.M. (2017) Mekhanika kombinovanoho protiahuvannia hrafitovmisnykh chavuniv. Kropyvnytskyi, Vydavets Lysenko V.F., 286 s.

10. Posviatenko E.K., Nemyrovskyi Ya.B., Shepelenko I.V. (2020) Protiahuvannia ta protiazhnyi instrument. Kropyvnytskyi, Vydavets Lysenko V.F., 298 s.

11. Posviatenko E.K., Nemyrovskyi Ya.B., Sheikin S.E., Shepelenko I.V., Cherniavskyi O.V. (2021) Inzheneriia detalei, obroblenykh protiahuvanniam. Kropyvnytskyi, Vydavets Lysenko V.F., 466 s.

12. Poverhnosti s regulyarnym mikrorel'efom: klassifikaciya, parametry i harakteristiki. GOST 24773-81 (1981) [Gosudarstvennyj komitet SSSR po standartam] 13 s.

13. Posvyatenko E.K., Alekseev V.V., Rutkovs'kij A.V. (2005) Vidnovlennia kolinchastykh valiv dvyhuniv vnutrishnoho zghoriannia ionno-impulsnym azotuvanniam [Visnyk Sumskoho derzhavnoho

universytetu: Tekhnichni nauky. Mashynobuduvannia - №11 – S.119-122.

14. Pastukh I.M. (2008) Fizyko-tekhnichna obrobka poverkhni metaliv bezvodnevym azotuvanniam v tliiuchomu rozriadi [Avtoreferat dysertatsii doktora tekhnichnykh nauk] 42 s.

15. Rasheed A Abdullah, Shepelenko I., Posviatyenko E. (2020) Experimental quality improvement of the application of antifriction coating [Journal of Physics: Conference Series, Volume 1706, First International Conference on Advances in Physical Sciences and Materials 13-14 August 2020, Coimbatore, India] – P. 1-11. https://doi:10.1088/1742-6596/1706/1/012187.

16. Shepelenko I.V., Posviatenko E.K., Cherkun V.V. (2109) The mechanism of formation of anti-friction coatings by employing friction-mechanical method [Problems of Tribology, №1] – S.35-39.

17. Shepelenko I., Ya. Nemyrovskyi, Y. Tsekhanov et al. (2020) Power Parameters of Micro-cutting During Finishing Anti-friction Non-abrasive Treatment [New Technologies, Development and Application III. NT 2020. Lecture Notes in Networks and Systems, vol 128. Springer, Cham] – P. 194-201. https://doi.org/10.1007/978-3-030-46817-0_22.

18. Shepelenko I., Tsekhanov Y., Nemyrovskyi Ya. et al. (2020) Improving the Efficiency of Antifriction Coatings by Means of Finishing the Antifriction Non-abrasive Treatment [Advanced Manufacturing Processes. InterPartner 2019. Lecture Notes in Mechanical Engineering. Springer, Cham] – P. 289-298. https://doi.org/10.1007/978-3-030-40724-7_30.

19. Chernovol M., Shepelenko I., Budar Mohamend R.F. (2015) Effectiveness increase in application of FANT of the components of mobile agricultural machines [Konstruiuvannia, vyrobnytstvo ta ekspluatatsiia silskohospodarskykh mashyn - Vyp. 45] – S.10-13.

20. Nemyrovskyi Ya., Shepelenko I., Osin R., Posviatenko E. (2022) Improving the processing quality of cylinder liners using combined technology [Cutting and Tools in Technological Systems, №96] – S.121-130. https://doi.org/10.20998/2078-7405.2022.96.13.

21. Shepelenko I.V. (2021) Naukovi osnovy tekhnolohii nanesennia antyfryktsiinykh pokryttiv z vykorystanniam plastychnoho deformuvannia [Avtoreferat dysertatsii doktora tekhnichnykh nauk] 43 s.

Шепеленко І.В., Посвятенко Е.К., Немировський Я.Б., Черкун В.В., Рибак І.П. Створення нових методів інженерії поверхні на основі протягування

Стаття присвячена створенню нових технологій обробки за рахунок застосування протягування. Визначено, що найбільш ефективними процесами інженерії поверхні деталей машин є гібридні технології. Зазначено переваги таких технологій за рахунок отримання нового ефекту від впливу на деталь двома або більше різнорідними процесами, що належать до однієї або різних груп методів інженерії поверхні. Доведено, що застосування гібридних технологій на основі протягування дозволяє поєднувати переваги різних методів, перш за все методів холодного пластичного деформування, у поєднанні з іншими. Розроблені комбіновані технології обробки, що вміщують деформуюче протягування і фінішну антифрикційну безабразивну обробку, також деформуюче протягування з наступним фінішним низькочастотним іонним імпульсним азотуванням. Встановлено ефективність запропонованих технологій на основі протягування.

Ключові слова: інженерія поверхні, протягування, гібридні технології, фінішна антифрикційна безабразивна обробка, азотування.

***Problems of Tribology**, V. 27, No 2/104-2022, 13--19*

Problems of Tribology
Website: http://tribology.khnu.km.ua/index.php/ProbTrib
E-mail: tribosenator@gmail.com

DOI: https://doi.org/10.31891/2079-1372-2022-104-2-13-19

Contact melting and structure formation in the system: α-iron-nanomaterials - common quality carbon steel

V.I. Savulyak*, A.A. Osadchuk

Vinnytsia National Technical University, Vinnytsia, Ukraine
**E-mail: korsav84@gmail.com*

Received: 10 March 2022: Revised: 5 April 2022: Accept: 15 May 2022

Abstract

In this paper, processes of contact melting between steel plates, which arises after feeding the contact pulse of a contact welding machine, are studied, for cases when nanomaterials in the form of carbon nanofibers and powders of refractory metals are being located between the plates. It was established that the addition of carbon nanotubes allows to ensure the passage of contact melting with lower energy costs and to obtain high carbonaceous layers of considerable hardness, and the addition of doping elements makes it possible to control the structure, grainy and physical and mechanical properties of the formed material.

Key words: contact melting, carbon nanofibers, nanopowders, scrap metal, high carbon structures, microhardness.

Introduction

Contact melting for a long time attracts the attention of researchers and engineers. Welding, obtaining fusible materials, consolidation of powder materials, coating - here is an incomplete list of applications of this process. The research and development of the theory of contact melting are devoted to a number of modern and earlier works, which have not lost their relevance yet. [1].

Analysis of the problem and the study of information sources revealed the existence of different concepts of the essence of contact melting and various hypotheses of the essence of the process. In the work, the definition of contact melting was adopted as the process of transition to a liquid state of solids that make eutectic pairs at a temperature lower than the melting points of each of the substances of the system [2]. During the contact of crystals of heterogeneous components, liquid eutectics are formed in the surface layers.

At contact melting, the aggregate state of substances varies (from solid to liquid), so it will be fair to use the Arrhenius formula to describe the process. By means of approximation using the package of mathematical programs, the value of the activation energy of the process of contact melting of *the iron – carbon* system is obtained.

It was investigated that in the Fe - X - C system there are exothermic effects [1], as follows:

- mixtures based on refractory metals (Cr, W, Mo, V) are characterized by exothermicity, insufficient for carrying out in them processes of synthesis of metal-carbide materials due to their own energy resources and need external heating;
- in closed systems on the basis of chromium and vanadium, eutectic melting is possible under heating to 1040 -1230°C;
- the use of high-dispersion powders (less than 10 microns) increases the thermality of mixtures by 10% or more;
- in the system "(*metal powders + carbon material*), metal substrates and gas phase" metal and carbon oxidation, the formation of a gas phase with a certain carbon potential, metal carbidization and carbon coagulation of the metal substrate may occur. Probability and mass flows of processes depend on thermodynamic and kinetic factors, in particular on the specific area of powders, heating temperature, density of the mixture.

An additional source of energy required to initiate contact melting may be nanomaterials in the form of metal powders, carbon nanofibers, fullerenes, graphene, and the like.

Methods of experiments

Initial samples from Armco iron plates (technically pure iron with a total content of impurities of about 0.16%, in particular not more than 0.025% C, 0.035% Mn, 0.05% Si, 0.015% P, 0.025% S, 0.05% Cu) 0.2 mm thick and standard quality steel of DSTU 2651: 2005 with a thickness of 2 mm was subjected to point welding with a compression force of 2400 N at a current of 3500 A, a pulse duration of ≈ 2 seconds. Between the plates at the welding site were installed carbon fiber nanofibers with a surface density of about 15 mg / mm2, as well as compositions in the form of carbon nanofibers with the addition of molybdenum nanopowders; Carbon nanofibers with the addition of vanadium nanopowders. The action with such parameters led to the formation of point connections, but the melting of the surface of the samples under the electrodes did not occur. This testifies that welding was carried out with minimal energy input. Microstructural studies of the surface layers of the samples were carried out using optical microscopes MBBS-6 and MIM-8. For the performance of microstructural studies, the welded plates were cut in the center of the weld joint and polished according to standard technology. Chemical etching of the surface of the samples was carried out in a 4% solution of HNO3 in alcohol. Microhardness was measured by a microhardness tester PMT-3M.

Characteristics of prototypes

The conducted studies of the source plates at point welding without additional gaskets showed the preservation of a clear boundary between the welded materials, the zone of thermal impact on steel common quality carbon steel length ≈ 1400 microns, while the signs of diffusion processes were not detected (Fig. 1) [3]. Fig. 2 shows the microhardness of welded joints of plates on the thickness of the cross-section.

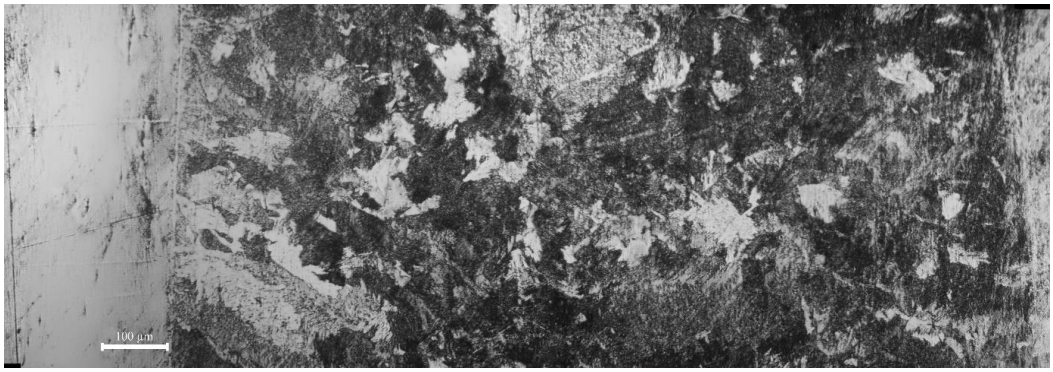

Fig. 1. Panorama of the point welded connection of the source materials (Armco iron and steel of common quality carbon steel)

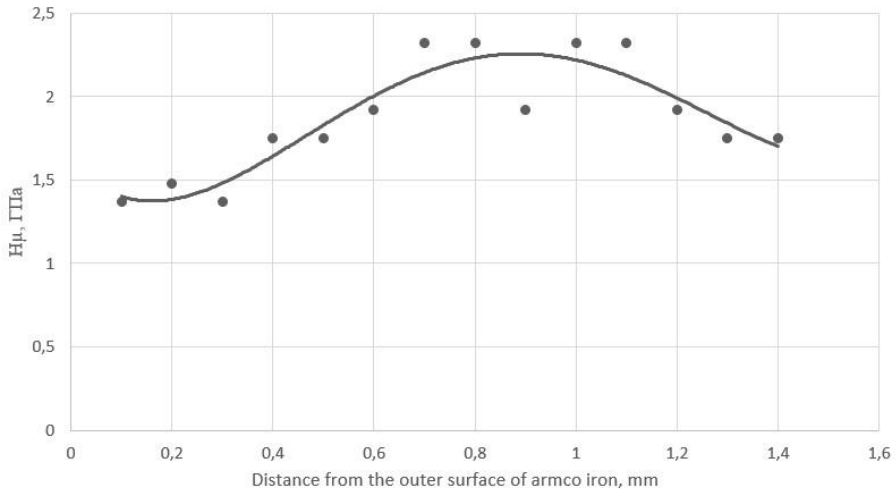

Fig.2. Distribution of microhardness in the sample of a point welded connection of raw materials

The following experiments with point welding of plates of Armco iron and common quality carbon steel and gaskets were conducted:

1 - carbon nanofibers;

2 - molybdenum powder Mo brand of PMC;

3 - vanadium powder V - VEL-1 (99.99% purity);
4 - carbon nanofibers and a layer of molybdenum powder in thickness up to 0,1 mm;
5 - carbon nanofibers and a layer of vanadium powder in the thickness of 0.1 mm.

From the above data on the chemical composition of the components, it can be seen that the main doping elements are vanadium or molybdenum in the presence of carbon. That is, systems of the type Fe-C-X were created, where X is molybdenum Mo or vanadium V. In stationary systems, the alloying element X forms, in the absence of carbon, solid substitution solutions in austenite or ferrite. In each of the experiments, we have two elements (Fe and X) which have comparatively small diffusion mobility and one element (C), which has 4-5 orders of magnitude a larger diffusion coefficient (carbon forms solid solutions and diffuses between the nodes of the iron lattice) [4].

Results of research and discussion

Microstructural studies have revealed some features of the microstructure, which were observed during spot welding without the use of gaskets made of carbon nanofibers or powders. Fig. 3 shows a series of panoramic microphotographs of the structure inward from left to right from the surface of Armco iron, to the main steel of common quality carbon steel

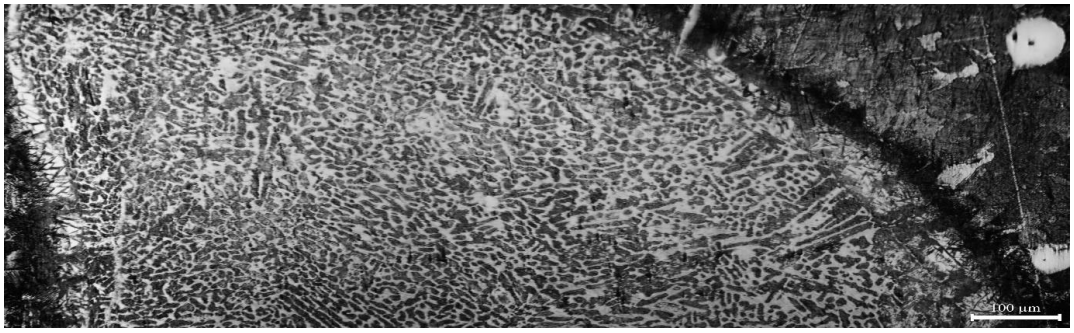

a) carbon fiber nanofibers

b) carbon fiber nanofibers with vanadium powder

c) vanadium powder

d) molybdenum powder

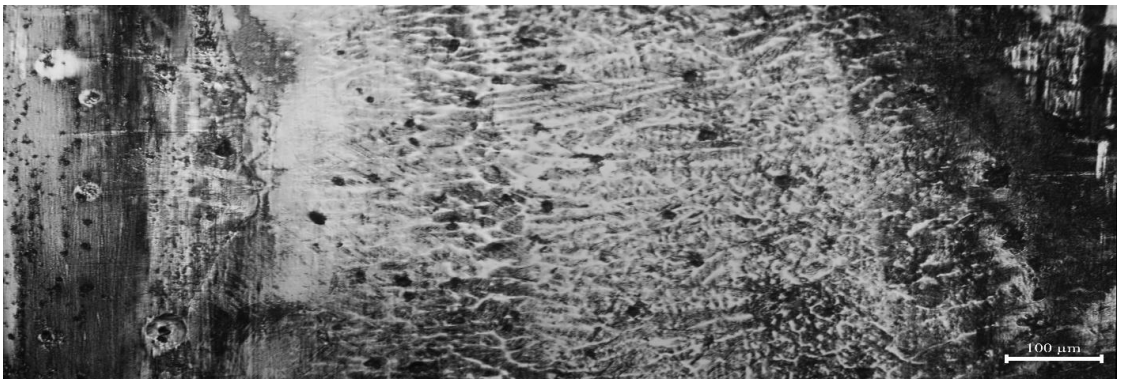

e) carbon fiber nanofibers with a molybdenum powder

Fig. 3. Panoramic photographs of microstructures of the nucleus of contact melting between Armco iron and common quality carbon steel in the presence of a gasket with doping components (on the left - Armco iron)

Study of the nucleus of contact melting between Armco iron and common quality carbon steel in the presence of carbon nanofibers between them (Fig. 3a) showed that a microstructure that corresponds to a high-carbon alloy with a structure of ledeburite was formed. Welding at the same time happened with a lower level of energy attachment, indicating the occurrence of contact melting processes [5, 6].

Fig. 3b shows a panoramic photo of a section of the nucleus of fusion of two steel plates, among which is a gasket of carbon nanofibers and vanadium powder. In the photograph on the left you can see the steel plaster of Armco iron, which practically did not melt and did not change its chemical composition. This is due to the fact that diffusion in α-iron does not occur[7, 8]. Almost all processes of melting and contact melting with diffusion processes are limited by the volume of common quality carbon steel. During the study of fig. 3b, the main three zones are observed: the first adjacent to α-iron, formed as a result of the carbide formation of vanadium carbonate from nano fabric that dissolved. This process is promoted by the high surface energy that this tissue has. The first zone is characterized by an increase in microhardness from Armco iron to the second zone (Fig. 4), which lies deeper. In the second zone, there was a process of intensive mixing of iron from common quality carbon steel, vanadium and carbon nano tissue. This led to the formation of a fine-grained composite structure with high hardness. The length of this zone is approximately 0.6 mm. The third zone directly touches the base metal [9, 10]. Structure formation in this zone takes place under conditions of higher heat transfer rate to common quality carbon steel. The result is a coarse-grained structure and less hardness.

Fig. 3c shows a panoramic photo of a section of a core of fusion of two steel plates between which is a gasket of vanadium powder. Study of microstructure and microhardness of structural components allows us to draw conclusions about the formation of vanadium-doped steel. On the left, we see a clear line of separation between Armco iron and crystallized melting zone. The microhardness of the melting core is much lower than for doping carbon nanotubes.

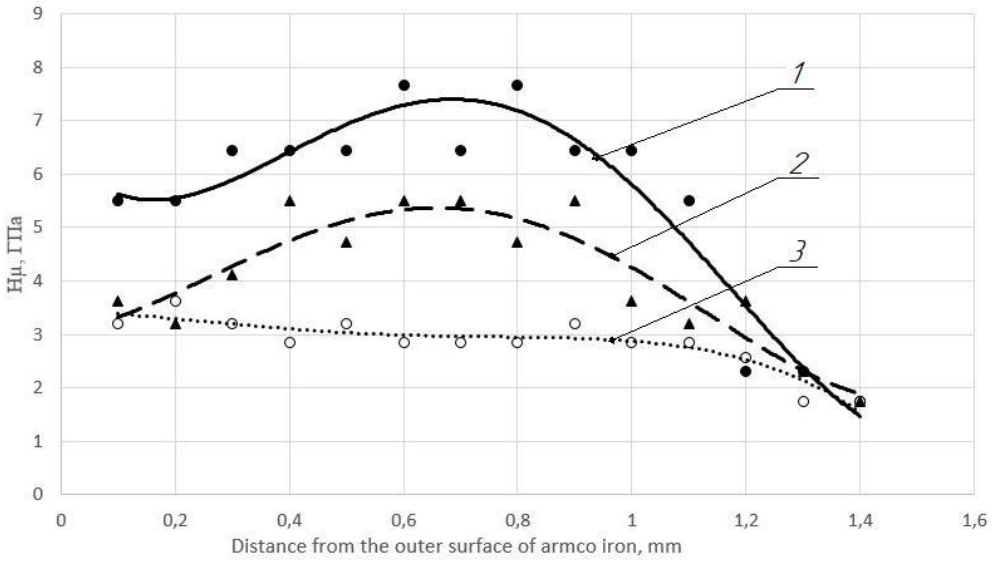

Fig. 4. Distribution of the microhardness of the cross-section of the fusion nucleus of two steel plates:
1) in the presence of carbon nanofibers between them;
2) in the presence of carbon nanotubes and powder vanadium between them
3) in the presence of vanadium powder

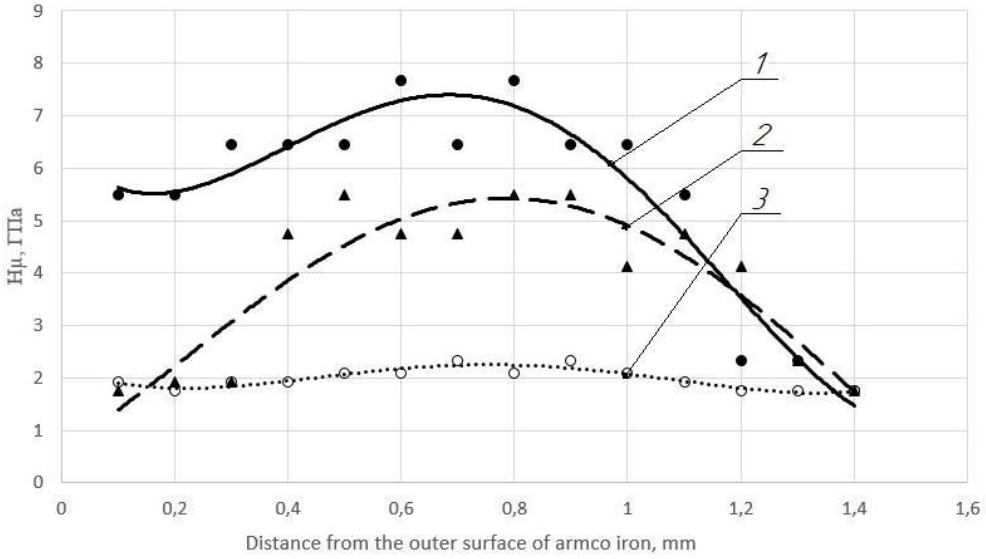

Fig. 5. Distribution of microhardness of the cross-section of the fusion nucleus of two steel plates:
1) in the presence of carbon nanofibers between them;
2) in the presence of carbon nanotubes and molybdenum powder between them
3) in the presence of molybdenum powder between them

In the case of doping with the addition of molybdenum (Fig. 3d) in the gap between the welded plates, the presence of a structure characterized by high uniformity and fine grains and uniform microhardness throughout the cross section was revealed. At the same time, the layer of Armco iron (α-Fe) disappeared due to doping with molybdenum.

When doped with the addition of a double layer of carbon nanofibers and molybdenum powder (Fig. 3e), the processes of structure formation proceed with much more complex kinetics. On microstructure photographs, appeared defects in the form of gas vapors. This is a consequence of the large sorption capacity of carbon nanofibers. As the process takes place in the air, a sufficient amount of gases is released into the fiber, which is released when the composition is heated. The process of melting and crystallization occurs within a fraction of a second and is not sufficient to isolate the gas bubbles from the melting zone. It should also be noted that Armco iron did not take part in the process of formation of the structure. In addition, the process of stratification into separate zones is viewed. Under the plate with Armco iron formed the structure of doped with molybdenum white cast iron, which continues onto the high-carbon zone with columnar crystals and high hardness.

Conclusions

1. For the first time contact melting between sheet metal reinforcement (0.2 mm) and a common quality carbon steel plate with the addition of layers of molybdenum and vanadium nanopowders and carbon nanotubes between them was studied.

2. It was established that the addition of carbon nanotubes allows ensuring contact melting with fewer energy costs.

3. Adding carbon nanotubes allows you to obtain high-carbon layers of high hardness, and adding doping elements allows you to control the structure, grainy and physicomechanical properties of the material.

4. It was established that Armco iron does not participate in super-rapid processes of carbonization, leaving its structure and properties. This allows using such contact welding technology to form wear-resistant surface layers that correspond to Sharp's principle, after mechanical removal of a soft layer of iron armor.

References

1. Savulyak V. I. Contact melting of unalloed steel with graphite in diffusive unstazinary mode./ V. I. Savulyak A.Yu. Osadchuk V. V. Savulyak / Bulletin of the Polytechnic Institute. Iasi, Romania . – №LIV (LVIII). 2008. P. 85-90.

2. Zalkin V.M The nature of eutectic alloys and the effect of contact melting “Metallurgy” / V.M Zalkin/ “Metallurgy”, 1987, 152 p.

3. Ahtubekov A. A. Diffusion kinetics of growth of the liquid phase upon contact of heterogeneous crystals / A. A Ahtubekov B. S Karamuzov Electronic journal "Research in Russia", 34, 465 - 474, 2000. http: // zhurnal.ape.relarn.ru / articles / 2000 / 034.

4. Savulyak V. I. On the influence of elements on the equilibrium temperature of eutectic transformations . / V. I. Savulyak, A.A. Zhukov, T.F. Arhipova //Metal science and heat treatment of metals. – 2000. - №2. – P. 3 – 8.

5. Ahkubekov A.A. Contact melting of metals and nanostructures based on them / A.A. Ahkubekov, T.A. Orkvasov, V.A. Sozaev. M.: Fizmatlit, 2008. – 152 p.

6. Korotkov P.K. The microstructure of the contact layers formed during the contact melting of copper with aluminum Surface / P.K. Korotkov, M.Z. Laypanov, A.R. Manukyants, M.H. Ponezhev, V.A. Sozaev / X-ray, synchrotron and neutron studies. – 2014. – № 7. – P. 109-112.

7. Hayrulaev M.R. Thermal effect during contact melting in the Pb-Te system. / M.R. Hayrulaev, D.H. Dadaev // Fizika, Baki: Elm, 2007. C. XIII, No 12, P. 7173.

8. Dadaev D.H. Contact melting in simple systems // Universum: Technical sciences: electronic scientific journal 2013. № 1(1). URL: http://7universum.com/ru/tech/archive/item/789

9. Savvin B.C. Contact melting kinetics in the nonstationary-diffusion mode. / B.C. Savvin, O.V.Mihalyova, A.A. Povzner /URasplavy-2001 -№2.-C.43-50

10. Thermokinetics of the initial stage of contact melting in peritectic systems with a chemical compound / V.P. Solntsev, V.V. Skorohod, K.N. Petrash, A.M. Shahnovskiy // Modern problems of physical materials science. Collection of scientific papers -- IPM NAS of Ukraine, 2013. — release. 22. — C. 181-185. — bibliography. 4 name. — poc.

Савуляк В.І., Осадчук А.А. Контактне плавлення та структуроутворення в системі: α-залізо – наноматеріали – сталь звичайної якості.

В роботі вивчені процеси контактного плавлення між сталевими пластинами, яке виникає після подачі на контакт імпульсу струму від машини контактного зварювання для випадків, коли між пластинами розміщені наноматеріали у вигляді вуглецевих нановолокон та порошків тугоплавких металів. Встановлено, що додавання вуглецевої нанотканини дозволяє забезпечити проходження контактного плавлення з меншими енергетичними витратами та отримати високовуглецеві шари значної твердості, а додавання легувальних елементів створює можливість керувати структурою, зернистістю та фізико-механічними властивостями утвореного матеріалу.

Ключові слова: контактне плавлення, вуглецеві нановолокна, нанопорошки, тугоплавкі метали, високовуглецеві структури, мікротвердість.

***Problems of Tribology**, V. 27, No 2/104-2022, 20--27*

Problems of Tribology
Website: http://tribology.khnu.km.ua/index.php/ProbTrib
E-mail: tribosenator@gmail.com

DOI: https://doi.org/10.31891/2079-1372-2022-104-2-20-27

Increasing warning resistance of engine valves by gas nitrogenization method

D.D. Marchenko*, K.S. Matvyeyeva

Mykolayiv National Agrarian University, Mykolayiv, Ukraine
**E-mail: marchenkodd@mnau.edu.ua*

Received: 20 March 2022: Revised:15 April 2022: Accept: 25 May 2022

Abstract

The article presents the results of tribological research on the most promising way to restore and increase the wear resistance of engine valves by developing a method of gas nitriding. It is established that with increasing operating time the guide bushings of the outlet connections wear out with the displacement of the axis of the forming surfaces of the hole. Characteristic significant displacement of the axes of the inlet connections is not detected, ie. their wear on the diameter of the hole is 1.5 ... 3 times less than the wear of the exhaust bushings, the values of the displacement of the axes are within the error of the measuring instrument. The average value of ovality is greater in the exhaust seats - the maximum beating values of the intake seats are 0.34 mm, exhaust - 0.22 mm. It is proved that the non-uniformity of the wear of the sleeve hole is determined by the balance of acting forces, which, in turn, are determined by deviations from the optimal ratios μ and e. the side of the rocker arm axis. Distortions of the valve in the longitudinal axis of the engine contribute to an earlier reduction in the tightness of the valve pairs. Redistribution of the valve end material with the formation of a wavy concentric surface, the shape of the contact spot on the rocker arm and the corresponding direction of wear of the saddle chamfer was observed in 43% of the studied connections. Technological means and methods for improving the quality of repair, measuring instruments for accurate study of the parameters of parts and connections of the valve group are given. The results of laboratory and operational tests are presented. A method of gas nitriding with an installation for its implementation has been developed, which provides an environmentally friendly method of low-temperature and high-temperature hardening, obtaining deeper and well-developed layers of the diffusion near-surface zone and reduces training, technological time in the process of strengthening and reducing energy consumption.

Key words: gas nitriding, wear resistance, friction steam, engine valves, recovery technology, wear intensity.

Introduction

The urgent need to reduce engine oil consumption during engine operation has led to many changes in the design of engine parts, including the design and choice of valve stem material. Which is once again confirmed by the expression: "For every action there is opposition."

As the amount of oil entering the orifice of the valve guide sleeve has decreased, there is an urgent need for such treatment of the valve stem, which will withstand abrasion resistance or other types of wear at high temperature fluctuations and loads.

Nitriding is widely used to strengthen a variety of steels and alloys, machine parts, tools operating in different conditions and environments, as well as to increase hardness, wear resistance, abrasion resistance, fatigue and corrosion resistance. Deformation of products during nitriding is minimal, nitrided layer is well polished and polished [1].

This process is the most modern metal nitriding technology in the world. This method is based on the strengthening treatment of heavily loaded parts of machines, tools, stamping equipment by diffusion saturation of the surface layer with nitrogen nitrogen-hydrogen plasma pulsating current. In this process, the phenomenon

of ionic deposition in a dilute gaseous medium is used to saturate the surface layer of metals with nitrogen. Pulsed ion-plasma nitriding is a modern type of gas nitriding, in which ammonia is replaced by nitrogen and hydrogen, which do not pose a threat to the environment.

The process is carried out at low temperatures (starting from 400 °C, which is also one of the many advantages of ion-plasma nitriding) and under reduced pressure. The main result of this process is to obtain nitrided layers of high hardness. Control of process temperature in the working range from 400 °C to 600 °C allows to receive various indicators of hardness of a surface layer. The highest hardness of the nitrided surface is formed when using operating temperatures in the range of 400 °C - 500 °C. The nitriding process itself takes place in a chamber with a vacuum of 1-10 hPa. The workpiece is the negative electrode (cathode) and the chamber walls are the positive electrode (anode). When a constant voltage (400-700 V) is applied between the cathode (negative potential) and the anode (positive potential), a heterogeneous electric field arises and a glow discharge is excited. Due to the collision of electrons and gas atoms, the latter accelerate and bombard the cathode surface, knocking out atoms of iron, its compounds, carbon, nitrogen and electrons required for ion deposition. Iron atoms combine with active nitrogen atoms and are deposited on the surface of the part as nitrides and saturate the surface layers with nitrogen during diffusion. As a result of pulsed ion-plasma nitriding, a diffusion layer with a developed nitride zone is obtained, which provides high corrosion resistance and workability of friction surfaces. Optimization of the properties of the reinforced surface is ensured by the necessary combination of nitride and diffusion layers, ensuring a significant increase in wear resistance, burr resistance and fatigue [2].

The range of steel grades is constantly expanding, which develops individual technological parameters of the process of pulsed ion-plasma nitriding.

As a result of surface hardening by the above method we obtain a diffusion layer, which provides a 5-fold increase in service life, wear resistance and increase the anti-emergency properties of parts. The use of this technology can significantly improve the performance of the pair "valve rod - guide", reduce the adhesion of soot in the area of the valve plate and increase the corrosion resistance of the valve and its overall service life. The results of tests of valve steels before and after nitriding by the method of linear wear measurement show more than 5-fold reduction in wear of nitrided steel.

Literature review

Nitriding as a method of strengthening machine parts and tools has come a long way of development and improvement. Currently, in terms of ensuring the functional properties of numerous parts and tools, it is one of the most effective and common methods of strengthening in various fields of mechanical engineering (automotive, aerospace, engine, machine tool, chemical industry, etc.).

Among the advantages of the nitriding process should be noted:

1. High hardness (up to HV 1300), which is achieved without hardening;
2. Insignificant in comparison with other methods of strengthening deformation of details;
3. Heat resistance of the surface saturated layer up to 500… 600 °C;
4. High wear resistance;
5. Corrosion resistance (especially in the air);
6. High fatigue resistance;
7. High resistance to alternating loads.

The disadvantages of this method of strengthening are as follows:

1. Long duration of the saturation process (up to 100 hours);
2. Low in comparison with cement details contact strength;
3. High fragility of the surface layer;
4. Reduced viscosity of nitrided parts;
5. Instability of nitriding results in its implementation in industry [3].

Although many varieties and methods have been developed and implemented since the industrial development of the nitriding process (laser and plasma nitriding, vibration in the vibrating fluidized bed, in salt melts, etc.), however, practical experience shows that the most common process in industrial conditions is the vast majority. machine-building industries are gas nitriding using as saturating the atmosphere products of partial dissociation of ammonia NH_3.

In particular, the so-called classical process of gas nitriding, which was developed by Lakhtin Y.M., Kosolapov G.F., Minkevich A.N., Beloruchev A.V., Jurgenson A.A., Arzamasi B.N., Kogan I.D., is actively used to strengthen parts of machines and tools in the current production. This is due to the relative simplicity of the technological implementation of the gas nitriding process using ammonia as a saturated medium, the relatively low cost of equipment and equipment required for this process (compared, for example, with equipment for ionic nitriding), as well as fairly well-established chemical regimes - heat treatment of various steels and alloys using this type of saturation. However, based on empirical observations and practical experience of gas nitriding of some of the above companies, it was observed that this type of nitriding leads to significant embrittlement of products, some time after their saturation in ammonia.

In high-speed engines, the end working surfaces of the pushers are also welded with high-strength alloys. Phosphating of pusher working surfaces and molybdenum dioxide treatment (to prevent burrs during operation) are also used. Improving the wear resistance of pushers is achieved by using the most advantageous forms of their working surfaces. The surface of the collision of the pusher with the cam is made, for example, spherical, which significantly reduces the compression stress due to the inability to maintain parallelism in the plane of the cam of the cam of the camshaft. For the same purpose, the barrel-shaped shape of the pusher guide surface is used in combination with a flat end surface. To increase the wear resistance of the valves and use a device that ensures their rotation during engine operation. At the same time the term between grinding of valves doubles.

Serviceable valves must quickly and reliably seal the combustion chamber, withstand large temperature fluctuations and have good wear resistance to ensure the longevity of the engine. Failure of the valves (or even one valve) disables the engine. And in the most severe case - to the destruction of the piston, cylinder or cylinder head. Therefore, thorough defecting of valves and bushings is very important when repairing the motor [4].

At pushers surfaces of a core and a plate wear out. Pusher rods are restored by vibro-arc surfacing, using high-carbon steel wire, or baking metal powders. After surfacing or baking, the pusher rod is ground on a grinder. It is not recommended to restore the push rods by chrome plating, as this leads to rapid wear of the guides in the unit. The pusher plates of modern engines are welded with a thin layer of bleached cast iron, so when grinding they remove a very thin layer (up to 0.3 mm), necessary only to remove traces of wear.

The valve in the sleeve makes not only reciprocating movements, but also rotational-angular. If you take into account the speed of such movements, you can understand what the load will be on the sleeve. Naturally, wear occurs over time. Due to the radial beating the load increases, the rotational movement of the valve becomes more difficult and production increases.

This leads to one-sided wear not only of the bushing, but also the valve with the seat. Increased clearance in the pair of "valve-sleeve rod" leads to increased oil consumption, as the oil cap is not able to hold oil, which again is caused by increased side beats of the valve. With the untimely intervention of the master, this can lead to irreversible consequences - the replacement of seats, valves, bushings, and sometimes the replacement of the entire head of the unit.

The shape and material of the guide sleeve of the valve are selected taking into account the high speed of movement of the valve in the sleeve, the high temperature load and the limitation of the lubrication of the friction pair "sleeve-valve". If the head of the cylinder block is made of cast iron, then often the seats and guide bushings of the valves are integral with the head of the block. This design ensures alignment and, consequently, a more accurate fit of the valve on the seat, which reduces the temperature of the inlet and outlet valves. Cast iron cylinder heads were used on some engines from Opel, Ford and other manufacturers. But the technology of production of cast iron heads is complex and requires expensive equipment, so most of the heads of modern car units are made of aluminum alloys. In their production, the guide bushings and valve seats are made separately, and then pressed into their seats in the cylinder head [5].

Guide bushings are made of wear-resistant materials with good thermal conductivity. These are special cast iron, cermets, bronze and brass. Higher thermal conductivity in bronze and brass, so they are used on most boosted engines, such as BMW, Audi, Volvo. To fix the sleeve in height in the cylinder head on its outer surface there is usually a support flange. Sometimes a split support ring is used instead. If the sleeve is smooth on the outside, you will need a special border or a remote sleeve to install it in the head.

The intake manifold guide bushings should not protrude too much into the intake manifold so as not to increase its aerodynamic drag. But the exhaust valve bushes, on the other hand, should close the valve stem to the maximum length for protection against hot exhaust gases and for better heat dissipation from the exhaust valve rod. If the guide bushings are made of bronze or brass, they usually have the same length, as these alloys have high thermal conductivity.

To ensure the alignment of the seat and the plate of the valve requires high precision manufacturing of the sleeve. In addition, the outer surface of the sleeve, pressed into the head of the unit, should be treated with a high degree of surface cleanliness and should not have scratches and scratches. This is done to improve heat dissipation from the bushing to the cylinder head.

The main defect of the guide bushings is the increased wear of the inner surface caused by prolonged (at least 60-100 thousand km for domestic and 150 - 200 thousand km for foreign cars) operation of the engine. However, the use of poor quality oils dramatically reduces the life of the bushings, not to mention the engine as a whole. Prolonged operation of the engine with incorrectly set thermal gaps of the valves is also the cause of uneven wear of the guide sleeve. This is due to the increase in lateral loads on the rod and the deterioration of the rotation of the valve.

In the presence of repair valves, the sleeve is first deployed under the repair diameter of the valve stem, and then under the required clearance between the sleeve and the valve. The clearance is the same as for standard valves. When deploying the sleeve to obtain the correct geometry, the deployment holes must start from the oil cap side, as this part of the sleeve is subject to less wear.

The method of knurling the inner surface of the sleeve with subsequent scanning to the desired inner diameter. This method requires a special tool. When using it, the seat under the guide in the head of the unit is

not damaged. However, its inner surface, erased by the valve stem, will have a greater hardness than the body of the sleeve, which occurs due to plastic deformation.

This method is especially suitable for engines that have a cast iron block head, and the valve guides are made directly in the block head. At wear to 0.3 mm it is easier and cheaper to restore them by unrolling, than by boring and pressing of new directing plugs.

In addition, before pressing the sleeve, be sure to check the diameter of the seat under the oil cap. If this diameter is smaller than on the old bushings, the caps may simply fly off while the engine is running. Many companies, such as Volvo, BMW, Volkswagen, produce repair guide bushings with increased outer diameter for pressing. The seat under such a sleeve in the head of the unit must be expanded to a size that provides a landing with a tension of 0.02 to 0.1 mm [6].

Before pressing the new bushings, the block head is heated again to 90 °C - 100 °C, and the bushings are cooled, which is most desirable to do in liquid nitrogen.

To increase the wear resistance of the valves and bushings crystallize on nickel-phosphorus-copper coatings. Immediately after precipitation, all coatings containing more than 4% P were amorphous. The only composition that was obtained with a crystalline structure was a coating containing 4% R. Its structure consisted of supersaturated phosphorus - Ni from a strongly distorted crystal lattice.

Ni-P-Cu coatings are also used. The processes of joint chemical reduction of metals, as well as the processes of their electrochemical reduction, are subject to the same thermodynamic laws. Therefore, the equilibrium potentials of metals and their change as a result of complexation in solution and formation of alloys play a special role in these processes. Assuming that the chemical reduction of metals proceeds by electrochemical mechanism, we can assume that the processes of chemical and electrochemical deposition of metals are similar. However, it should be borne in mind that the rate of entry into the metal of active agents of the reduction reaction - electrons, is determined by the rate of anodic oxidation of the reducing agent, sensitive to nature and the state of the reaction surface. This leads to the lack of a complete analogy between chemical and electrochemical deposition of alloys, which is primarily expressed in the effect on the rate of chemical deposition of alloy components of the catalytic properties of metals.

The composition of solutions is empirically substantiated in most works on chemical deposition of alloys and the simplest regularities of deposition processes are revealed, and only in some the structure of sludge, influence of deposition conditions on its composition, kinetics and process mechanism are considered [7].

Purpose

The purpose of scientific research is to increase the wear resistance of engine valves by developing a method of gas nitriding and a technology for its implementation.

Research methodology

The main characteristic of wear of a detail is linear wear which is measured in the direction perpendicular to a friction surface. Due to a number of reasons, wear can be uneven. Therefore, to fully characterize the amount of wear of the part, it is necessary to know the distribution on the friction surface the shape of the worn surface [8].

To obtain the dependences of the size of the contact site *a* on the friction path *S*, wear tests of two friction pairs were performed. The tests were performed on a lathe equipped with a special device. The scheme of the device is shown in Fig. 1.

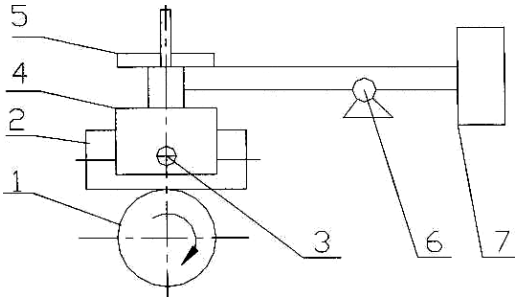

Fig. 1. Scheme of the device for tests on wear according to the scheme of cross cylinders: 1 - shaft; 2 - sample; 3 - screw; 4 - mandrel; 5 - cargo; 6 - support; 7 - counterweight

A shaft 1 made of steel 45 (HRC 48 ... 55, counter body) is mounted in the machine spindle, on which a cylindrical specimen 2 is mounted and pressed by a force *Q* (load 5 with known mass). The sample is fixed to the mandrel 4 with screw 3. To compensate for the mass of the device at the other end of the holder is screwed counterweight 7.

A lubricating cup is installed on the machine for lubrication testing, then both cylinders are immersed in the oil [9, 10].

The tests are performed in the following sequence:
- install the sample in the clamp 4;
- press the sample 2 with screw 3;
- counterweight 7 compensate for the mass of the sample and other elements of the device;
- on the axis of the clamp set the load with a known mass;
- turn on the machine and record the time;
- after a certain period of time we take out the sample in the reverse sequence and measure the size of the contact area;
- install the sample in the clamp so that the contact spot rises to its previous place.

Research results

Friction pair 1: 40X hardened steel - cast iron SC 20.

The test results of the samples are entered in the table (Table 1), having previously determined the equivalent radius of the circle by the formula:

$$a = (a^* b^*)^{1/2}.$$

According to these results, we construct a graph of the dependence of the contact spot on the friction path ($S = \pi d\, n\, T$) - Fig. 2.

S_1 = 3.14 x 20 x 100 x 1 = 6280 mm = 6,280 10^3 mm

S_5 = 3.14 x 20 x 100 x 5 = 31.4 10^3 mm

S_{10} = 3.14 x 20 x 100 x 10 = 62.80 10^3 mm

S_{15} = 3.14 x 20 x 100 x 15 = 94.2 10^3 mm

Table 1

The results of the test of cast iron midrange 20 (Friction pair 1: Cast iron SC 20 - steel 40X hardened)

T, min	*S* 10^3, mm	2*a**, mm	2*b**, mm	*a*, mm
1	6,280	0,554	1,167	0,211
5	31,40	0,634	1,428	0,234
10	62,80	0,75	1,598	0,267
15	94,2	0,943	1,761	0,315

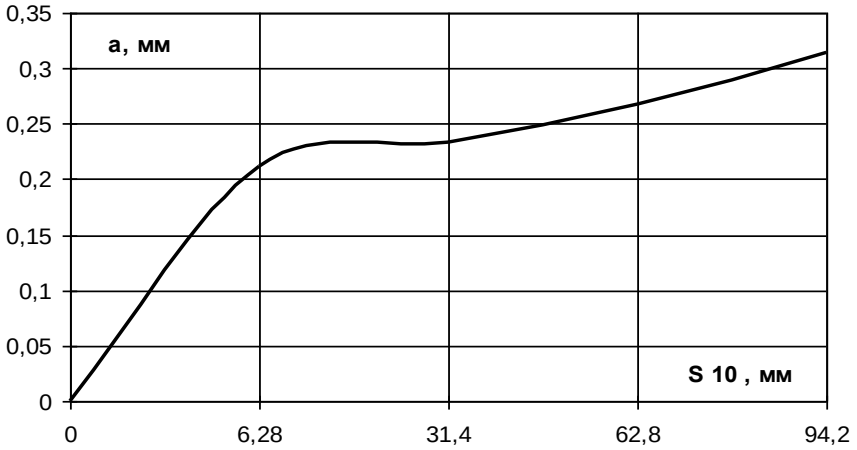

Fig. 2. The plot of the equivalent radius is spotted cast iron SC 20 from the friction path

Friction pair 2: Cast iron SC 20 - steel 40X nitrided.

Table 2

The results of the test of cast iron midrange 20 (Friction pair 1: Cast iron SC 20 - steel 40X nitrided)

T, min	*S* 10^3, mm	2*a**, mm	2*b**, mm	*a*, mm
1	6,280	0,554	1,167	0,203
5	31,40	0,634	1,428	0,227
10	62,80	0,75	1,598	0,243
15	94,2	0,943	1,761	0,277

According to these results, we plot the dependence of the contact spot on the friction path (Fig. 3.)

It is established that with increasing operating time the guide bushings of the outlet connections wear out with the displacement of the axis of the forming surfaces of the hole. Characteristic significant displacement

of the axes of the inlet connections is not detected, their wear on the diameter of the holes is 1.5 ... 3 times less than the wear of the exhaust bushings, the values of the displacement of the axes are within the error of the measuring instrument [11, 12].

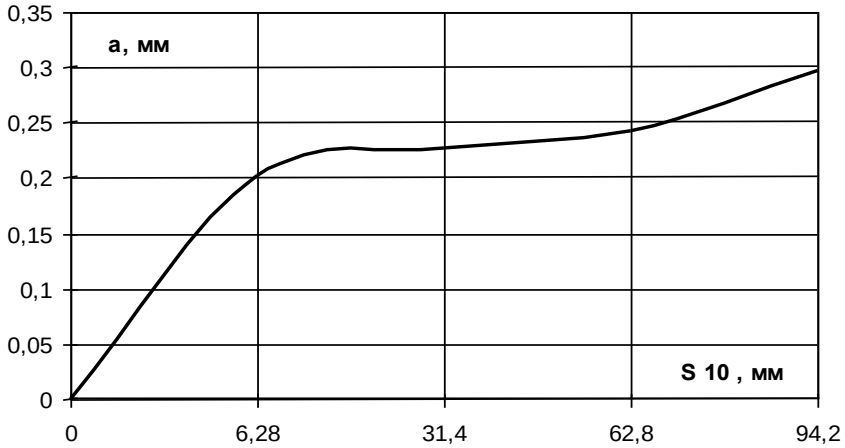

Fig. 3. Graph of the dependence of the sizes of the equivalent radius the spot of contact of cast iron SC 20 from the friction path

In Fig. 4 combined Fig. 2 and 3.

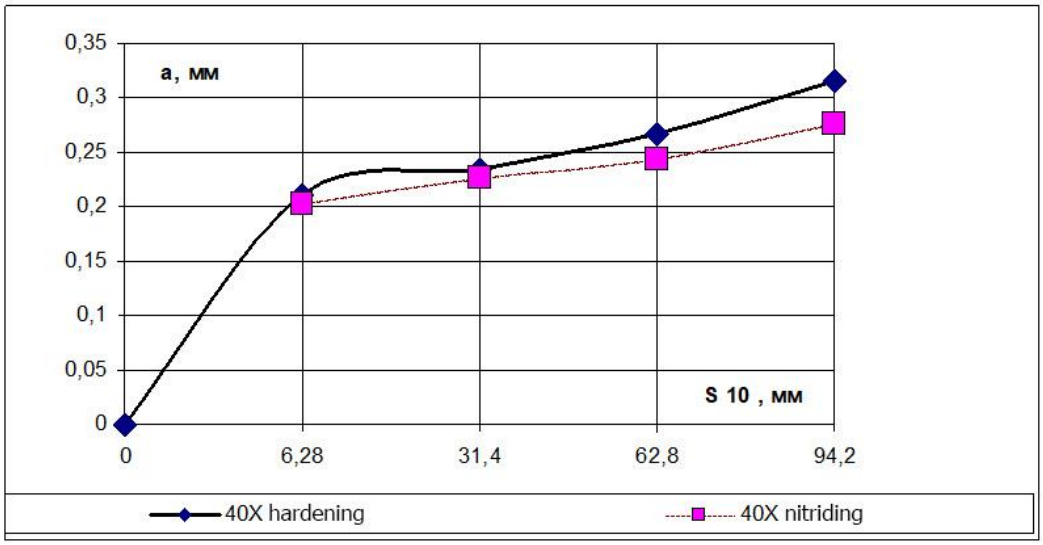

Fig. 4. Graphs of the dependence of the dimensions of the equivalent radius of the contact spot on the friction path of cast iron SC 20 (counterbody - nitrided and hardened steel 40X)

The nature of the distortion of the shape of the saddle chamfer inherits the main direction of displacement of the axis and the shape of the distortion of the guide sleeve during wear. The most frequent deviations of relative displacement occur not in the plane of rocking of the rocker arm, but at an angle to it and directed to the center of the combustion chamber. In contrast to the bushings, the relative displacement of the axes of the inlet seats is the same pattern [13]. Moreover, the average value of the ovality is greater than that of the exhaust seats - the maximum beating values of the intake seats are 0.34 mm, exhaust - 0.22 mm.

Conclusions

The analysis of materials to increase the wear resistance of the friction pair "valve - bushing" and identified the main faults, causes of wear and existing repair technologies. It was found that severe wear of the guide bushings leads to a violation of the geometry of the seats and even to their destruction. The surface of the collision of the pusher with the cam is made, for example, spherical, which significantly reduces the compression stress, which occurs due to the inability to maintain parallelism in the plane of the cam of the cam of the camshaft. The purpose of repair of valve seats - to provide the correct geometry of connections "valve-seat" and their tightness which are defined in turn mainly by vacuum pressure and "beating" of a facet of the valve and a seat. Existing technologies for repairing valves and bushings are determined by the high cost of processing equipment and consumables. Therefore, we have proposed a method of gas nitriding, which has significant advantages over existing methods. Researches of technology of repair of conjugation of valve group of engines

are carried out. It is established that the non-uniformity of wear of the sleeve hole is determined by the balance of acting forces, which, in turn, are determined by deviations from the optimal ratios μ and e. the side of the rocker arm axis.

References

1. Archard J.F. Contact and rubbing of flat surfaces. *J Appl Phys* 1953; 24: 981–988.

2. Lai F.Q., Qu S.G., Yin L.M., et al. Design and operation of a new multifunctional wear apparatus for engine valve train components. Proc IMechE, Part J: *J Engineering Tribology* 2018; 232: 259–276.

3. Lewis R., Dwyer-Joyce R.S. Wear of diesel engine inlet valves and seat inserts. Proc IMechE, Part D: *J Automobile Engineering* 2002; 216: 205–216.

4. Worthen R.P., Rauen D.G. Measurement of valve temperatures and strain in a firing engine. SAE paper 860356, 1986.

5. Forsberg P., Debord D., Jacobson S. Quantification of combustion valve sealing interface sliding – a novel experimental technique and simulations. Tri Int 2014; 69: 150–155.

6. Mascarenhas L.B., Gomes J.D., Beal V.E., et al. Design and operation of a high temperature wear test apparatus for automotive valve materials. *Wear* 2015; 342–343: 129–137.

7. Marchenko D.D., Matvyeyeva K.S. Improving the contact strength of V-belt pulleys using plastic deformation. *Problems of Tribology*. Khmelnitsky, 2019. Vol 24. No 4/94 (2019). S. 49–53. DOI: https://doi.org/10.31891/2079-1372-2019-94-4-49-53.

8. Chun K.J., Kim J.H., Hong J.S. A study of exhaust valve and seat insert wear depending on cycle numbers. *Wear* 2007; 263: 1147–1157.

9. Marchenko D.D., Matvyeyeva K.S. Investigation of tool wear resistance when smoothing parts. *Problems of Tribology*. Khmelnitsky, 2020. Vol 25. No 4/98 (2020). S. 40–44. DOI: https://doi.org/10.31891/2079-1372-2020-98-4-40-44

10. Dykha A.V. Marchenko D.D., Artyukh V.A., Zubiekhina–Khaiiat O.V., Kurepin V.N. Study and development of the technology for hardening rope blocks by reeling. Eastern–European Journal of Enterprise Technologies. Ukraine: PC «TECHNOLOGY CENTER». 2018. №2/1 (92) 2018. pp. 22–32. DOI: https://doi.org/10.15587/1729-4061.2018.126196.

11. Blum M., Jarczyk G., Scholz H., et al. Prototype plant for the economical mass production of TiAl-valves. Mat Sci Eng A-Struct 2002; 329–331: 616–620.

12. Dykha A.V., Marchenko D.D. Prediction the wear of sliding bearings. International Journal of Engineering and Technology (UAE). India: “Sciencepubco–logo” Science Publishing Corporation. Publisher of International Academic Journals. 2018. Vol. 7, No 2.23 (2018). pp. 4–8. DOI: https://doi.org/10.14419/ijet.v7i2.23.11872.

13. Marchenko D.D., Artyukh V.A., Matvyeyeva K.S. Analysis of the influence of surface plastic deformation on increasing the wear resistance of machine parts. Problems of Tribology. Khmelnitsky, 2020. Vol 25. No 2/96 (2020). S. 6–11. DOI: https://doi.org/10.31891/2079-1372-2020-96-2-6-11.

Марченко Д.Д., Матвєєва К.С. Підвищення зносостійкості клапанів двигунів методом газового азотування

В статті приведено результати трибологічних досліджень з найбільш перспективного способу відновлення і підвищення зносостійкості клапанів двигунів шляхом розробки методу газового азотування. Встановлено, що із збільшенням напрацювання напрямні втулки випускних сполучень зношуються зі зміщенням осі утворюючих поверхонь отвору. Характерного значного зміщення осей втулок впускних сполучень не виявлено, т. я. їх знос по діаметру отвору в 1,5 ... 3 рази менше зносу випускних втулок, значення зміщення осей знаходяться в межах похибки засобу вимірювання. Середня величина овальності більше у випускних сідел - максимальні значення биття впускних сідел складають 0,34 мм, випускних - 0,22 мм. Доведено, що нерівномірність зношування отвору втулки визначається балансом діючих сил, які, в свою чергу, задаються відхиленнями від оптимальних співвідношень μ і e. З урахуванням сил тертя, що виникають на поверхні втулки, зношування отвору втулки відбуватиметься з поворотом її осі в нижній частині в сторону осі коромисла. Перекоси клапана в поздовжній осі двигуна сприяють більш раннього зниження герметичності клапанних пар. Перерозподіл матеріалу торця клапана з утворенням хвилястої концентричної поверхні, форма плями контакту на бойку коромисла і відповідний напрям зносу фаски сідла спостерігалося у 43% досліджуваних сполучень. Приведені технологічні засоби і методи, що забезпечують підвищення якості ремонту, засобів вимірювань для точного дослідження параметрів деталей і сполучень клапанної групи. Представлені результати лабораторних та експлуатаційних випробувань. Розроблено метод газового азотування з установкою для його здійснення, який забезпечує екологічно чистий спосіб низькотемпературного і високотемпературного зміцнення, отримання глибших і добре розвиненіших шарів дифузійної приповерхневої зони і дозволяє скоротити підготовку, технологічний час при проведенні процесу зміцнення та скорочення витрати енергоносіїв.

Ключові слова: газове азотування, зносостійкість, пара тертя, клапани двигуна, технологія відновлення, інтенсивність зношування.

***Problems of Tribology**, V. 27, No 2/104-2022, 28-34*

Problems of Tribology
Website: http://tribology.khnu.km.ua/index.php/ProbTrib
E-mail: tribosenator@gmail.com

DOI: https://doi.org/10.31891/2079-1372-2022-104-2-28-34

Tribological properties of anode-spark coatings on aluminum alloys

O. Dykha*, O. Babak, O. Makovkin, S. Posonskiy

Khmelnitskyi National University, Ukraine
**E-mail: tribosenator@gmail.com*

Received: 18 March 2022: Revised: 25 April 2022: Accept: 20 May 2022

Abstract

It is established that at present the technology of anode-spark coatings in general is well studied. However, the lack of recommendations for the choice of modes of technological processes and tribological characteristics in different operating conditions limit the widespread introduction of this technology. The task of this work was to analyze the processes of anode-spark coatings, improve technology and study the wear resistance of samples processed by this and traditional anode technology. The development of technology for the application of protective coatings on valve metals in the conditions of spark discharge included the choice of electrolyte and mode of operation of the bath: voltage, current density, hydrodynamic conditions and other parameters. Wear resistance tests were performed on a special installation. Structurally, the installation is made in two positions, which allows you to test two samples with different load conditions at a constant sliding speed. The design of the installation implements the friction scheme of the liner shaft. The study of anode-spark coatings in the mode of limiting lubrication was studied in the environment of industrial oil. The wear criterion was the weight wear of the samples according to the results of weight measurements before and after wear. It is established that prolonged electrolysis in the conditions of sparking leads to the formation of anode coatings that exceed in their properties the films obtained by non-sparking oxidation. Comparative studies of the wear resistance of anode-spark coatings and galvanic anode coatings under the same test conditions showed that the wear of anode-spark coatings is almost twice lower for the entire load range. The considered technology is recommended for increase of wear resistance of elements of devices from the aluminum alloys working in the conditions of corrosion and mechanical wear.

Keywords: anode-spark coatings, aluminum alloys, tribological tests, wear, friction coefficient.

Introduction

For a long time, it was believed that the coating formed in the spark mode has lower protective properties than the traditional anode coating. Because of this, the anodizing was usually stopped at a voltage lower than the breakdown voltage. More recently, it has been established that prolonged electrolysis under sparking conditions leads to the formation of fairly thick anode coatings that exceed in their properties the films obtained by sparkless oxidation. Analysis of anode-spark coatings shows that in them, along with the metal oxides of the substrate in large quantities are atoms and groups of atoms that are part of the electrolyte. In the thickness of the amorphous oxide there are areas of the solidified melt. The latter indicates a strong thermal effect of electrical breakdown on the material of the formed oxide. There is every reason to believe that effective anode-spark molding occurs only if the breakdown is thermal.

Analysis of research and publications

As a result of many studies, at present, it is established that the anode-oxide films consist of two layers: a barrier layer, which has a dense structure and is directly adjacent to the oxidized metal, and a porous layer.

The use of electron microscopy has made the most significant contribution to the studied structures of anode-oxide coatings. The results of these tests performed by Keller, Kanter, Robinson and other researchers allowed us to propose a so-called model of a porous anode oxide film based on physical and geometric images.

According to this model, in the first seconds of anodizing on aluminum, a non-porous barrier layer is formed, the beginning of the formation of which is associated with the corresponding active oxidation centers on the metal surface. Hemispherical lenticular microelements grow from these embryos. First isolated, then grow and fill the metal surface with the formation of a solid barrier layer. Under the action of local influence of electrolyte ions in the barrier layer, pores begin to emerge, the number of which is associated with the magnitude of the stress of the forming oxide. As a result, an oxidizing element is formed, similar in shape to a spherical segment, the center of which lies in the area of the porous layer. The growth of the anode-spark coating occurs in two ways that run in parallel. The first of them is the formation of the anode coating by the mechanism of growth of oxide films in the metal-oxide-electrolyte (MOE) system, and the second is the formation of chemical compounds on the electrode surface with the participation of electrolyte components. In the process of forming anode-spark coatings. Along with the formation of the film may occur side chemical and electrochemical reactions that lead to unproductive energy consumption and accumulation of substances in the bath, affecting the quality of sludge. The main side processes are the formation of oxygen and hydrogen due to electrolysis in the area of spark discharges. which lead to unproductive energy costs and the accumulation of substances in the bath, affecting the quality of sludge. The main side processes are the formation of oxygen and hydrogen due to electrolysis in the area of spark discharges. which lead to unproductive energy costs and the accumulation of substances in the bath, affecting the quality of sludge. The main side processes are the formation of oxygen and hydrogen due to electrolysis in the area of spark discharges.

Let us pay attention to the most urgent problems in the field of anodic oxidation that are currently being considered.

In work [1], it was noted that tlectrochemical oxidation is an effective wastewater treatment method. Metal oxide-coated substrates are commonly used as anodes in this process. This article compiles the developments in the fabrication, application, and performance of metal oxide anodes in wastewater treatment. It summarizes the preparative methods and mechanism of oxidation of organics on the metal oxide anodes. The discussion is focused on the application of SnO_2, PbO_2, IrO_2, and RuO_2 metal oxide anodes and their effectiveness in wastewater treatment process.

In work [2] it is said that during plasma electrolytic oxidation (PEO) processes, the factors, such as the shape of the specimen, the location of the cathode electrode, and others have a critical influence on the anode (specimen to be treated) current. This may lead to different oxidation dynamics at different locations on the samples resulting in the non-uniform coating thickness and surface properties. In this work, the current through samples made of 2024 aluminum alloy was monitored in a sodium silicate solution during plasma electrolytic oxidation. The experimental results demonstrate that the distance between the cathode and anode affects the anode current and the oxidation efficiency. The current flowing through the front surface of the specimen is larger than that flowing through the back surface of the same specimen. The measured tribological properties and corrosion-resistance agree well with the effects of the current. The front surface exhibits more superior wear and corrosion resistance than the back surface.

In aqueous zinc-ion batteries, metallic zinc is widely used as an anode because of its non-toxicity, environmental benignity, low cost, high abundance and theoretical capacity. However, growth of zinc dendrites, corrosion of zinc anode, passivation, and occurrence of side reactions during continuous charge-discharge cycling hinder development of zinc-ion batteries. In study [3], a simple strategy involving application of a HfO_2 coating was used to guide uniform deposition of Zn^{2+} to suppress formation of zinc dendrites. The HfO_2-coated zinc anode improves electrochemical performance compared with bare Zn anode.

In [4] the deactivation of an IrO_2–Ta_2O_5 coated titanium anode was studied during an accelerated life test at 2 A cm^{-2} in 1 mol dm^{-3} H_2SO_4 solution using CV, EIS, SEM and EDX. The changes of voltammetric charge, double layer capacitance, oxide film resistance and charge transfer resistance of oxygen evolution with time during the electrolysis were monitored. The morphology and surface composition of the oxide anode before and after electrolysis test were analysed. A comprehensive process of deactivation of the oxide anode was proposed based on the test results and analysis.

The wettability of coatings, including ceramic ones, which show considerable promise for the use on bioengineering products, with physical solution (0.9% NaCl) have been studied in [5]. It has been found that the use of coatings of all types under study increases the wetting angles on the surface as compared with the initial metal materials (stainless steel of the 12X18H10T grade, titanium alloy of the BT6-grade, Co-Cr-Mo alloy), which serves as a prerequisite for an improvement in the biocompatibility of implants.

Protective α-Al_2O_3 coatings on the surface of a graphite article have been obtained in [6] by method of electric-arc metallization with aluminum and microarc oxidation (anodic spark process). Investigation of the obtained coating by scanning electron microscopy (SEM), X-ray diffraction (XRD), and proton elastic recoil detection analysis (ERDA) showed good quality of the Al and α-Al_2O_3 coatings on graphite. The proposed technology can be used for obtaining protective coatings in low-accessible sites of graphite articles.

The effect of TiB_2 and CrB_2 additions to the commercial self-fluxing FeNiCrBSiC eutectic alloy on the structurization of electrospark coatings was examined in [7]. The mass transfer kinetics in the electrospark deposition of FTB20 (FeNiCrBSiC + 20% TiB_2) and FCB20 (FeNiCrBSiC + 20% CrB_2) composite materials and commercial self-fluxing FeNiCrBSiC alloy coatings onto steel 45 using an Alier-52 unit was studied. When the energy parameters of electrospark deposition increased, the mass transfer coefficient became higher and the

electrospark coatings thicker and rougher.

The dielectric properties of coatings on AK6 alloy formed with a microarc oxidation method in two electric modes in alkaline-silicate electrolytes are estimated in [8-9]. It is shown that both modes, a galvanostatic mode and an arbitrarily falling power mode in alternating current circuits, make it possible to obtain coatings with a thickness of 30–60 μm, with sufficiently high electrophysical parameters: bulk specific resistance $\rho_v = 3–9 \times 10^9$ Ω m and dielectric strength E = 9–14 V/μm. It is established that higher values of ρ_v and E in the both modes can be achieved in the solutions of 1 g/L KOH + 6 g/L of liquid glass (LG) and 12 g/L of LG. In terms of absolute value, the parameters of the coatings formed in the mode of arbitrarily falling power exceed the same characteristics of the oxide layers formed under conditions of galvanostatic mode by a factor of 1.5–2.5.

Based on the analysis of literature sources, it is established that at present the technology of anode-spark coatings in general is quite well developed. However, the lack of scientifically sound recommendations for the choice of modes of technological processes and characteristics of properties in different operating conditions do not allow the widespread introduction of this technology.

The task of this work was to analyze the processes of anode-spark coatings, improve technology and study the wear resistance of samples processed by this and traditional anode technology.

Selection of technological modes of formation of anode-spark coatings

The development of technology for the application of protective coatings on valve metals in the conditions of spark discharge includes the choice of electrolyte and mode of operation of the bath: voltage, current density, hydrodynamic conditions, etc.

Currently known different types of programmable voltage changes in the bath, pulse and alternating current voltages are selected experimentally, without the necessary theoretical justification. Meanwhile, the electrical regime determines the nature and intensity of discharges and, of course, the temperature conditions on the surface of the anode. With the appropriate choice of electrolyte and electrochemical parameters of the anode-spark sludge, you can get a coating that has high hardness, wear resistance and strong adhesion to the substrate. Appropriate selection of the electrolyte and electrolysis conditions can form a coating that is equal in hardness and wear resistance of corundum and tungsten carbide. The wear of the upper layers is not due to abrasion, but due to chipping of the unevenness of the coating.

To form a coating on aluminum alloys AD31 and B95, we take the current strength range from 1800 A / m^2 to 2500 A/m^2 and the ratio of cathode current to anode 1.15. Molding is carried out at voltages from 120 V to 600 V depending on the state and concentration of the electrolyte.

The practical implementation of the anode-spark process always requires careful coordination of metal-electrolyte pairs. One of the simplest and best-known electrolytes was a dilute (2 ... 8 g/l) KOH solution, which makes it possible to obtain a high-quality anode coating on aluminum. Solutions of some acids can be used for this purpose. The first systematic study of the influence of the electrolyte on the possibility of realization of the anode-spark discharge on aluminum was carried out in [7], where the authors studied the properties of solutions of 33 different substances. The investigated electrolytes were divided into 6 groups. The first includes solutions of salts in which there is a fairly rapid dissolution of aluminum (NaCl, $NaClO_3$, NaOH, HCl, $NaNO_3$ and Na). The second group combines electrolytes that correspond to the achievement without much effort of the passive state of the metal. It includes H_3BO_3, citric and carbonic acids, as well as their salts. Lactic, adipic and oxalic acids (third group) correspond to less effective passive properties. Weak solution of metal at stationary potential is characterized by substances of the fourth group: H_2SO_4, (NH_4) $2SO_8$, Na_2SO_4. In oxalic acid and its sodium salt, sodium acetate, phosphoric acid (fifth group), the range of voltages at which the spark discharge occurs is narrow. The sixth group includes solutions of KF, NaF, disubstituted phosphate and sodium sulfite. in which the spark discharge is narrow. The sixth group includes solutions of KF, NaF, disubstituted phosphate and sodium sulfite. in which the spark discharge is narrow. The sixth group includes solutions of KF, NaF, disubstituted phosphate and sodium sulfite.

The formation of oxide films from aqueous electrolytes in the sparking mode allows to obtain a coating with much better properties than in the formation in the normal anodizing mode. Analysis of the chemical composition shows that in the composition of the anode-spark coatings, rocks with oxides of the base metal of the strip, in large quantities contain atoms that are part of the electrolyte. Other particles of oxides (iron, chromium) present in the electrolyte are also included in the structure of the coating, forming a composite structure.

Investigation of wear resistance of coatings on aluminum alloys

Samples measuring 5×5×20 mm from materials B 95 and AD 31 were used for the research. The samples must have a quality surface. Overflowing of edges on samples is not allowed.

After machining, the samples are ground on grinders with a grain size of: 400 μm, 200 μm, 80 μm. Then the anode-spark coatings were applied on the experimental setup. After coating according to the developed technological process, the samples were washed and dried with filtered paper. Samples with factory coating were additionally ground on the work surfaces with AP-3 diamond paste. The contact area is 0.25 cm^2.

Wear resistance tests were performed on a special installation. Structurally, the installation is made in two

positions, which allows you to test two samples with different load conditions at a constant sliding speed. The design of the installation implements the friction scheme of the liner shaft.

The scheme of the test setup is presented in Fig. 1. Rotation counter body 7 receives from the DC motor with adjustable speed. The speed of rotation is controlled by an electronic speed meter PIT-1 (3). The test sample 8 is fixed in the handle 9, which before starting work is balanced in relation to the strain beam 10. The handle of the sample 9 is hinged to the beam. The specified load P is created by a set of loads 12.

Before conducting experiments, the installation system is calibrated. The strain gauges are powered by the UT-4 strain amplifier. Recording of friction forces is performed by a potentiometer type KSP-4.

The body is made of hardened steel 45 (HRC 55) and has the shape of a disk with a diameter of 95 mm and a thickness of 10 mm. Surface roughness Ra = 0, 32 microns

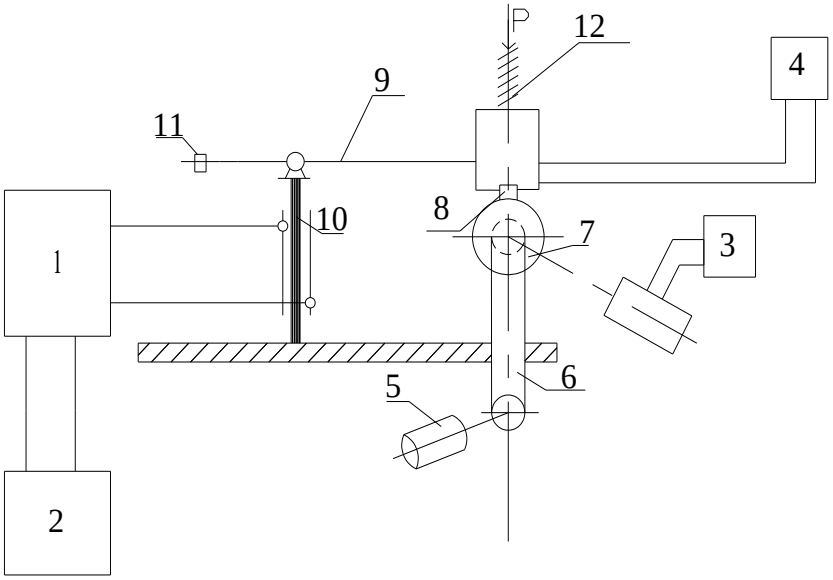

Fig. 1. Scheme of the test installation: 1 - strain amplifier UTCH-1; 2 - potentiometer PCB 4; 3 - sensor-meter of sliding speed; 4 - thermocouple temperature sensor potentiometer EPD-12; 5 - electric motor; 6 - V-belt transmission; 7 - working disk (counter body); 8 - experimental sample; 9 - sample holder; 10 - strain beam; 11 - load - balancer; 12 - loads to create the desired pressure R.

In the study of coatings under dry friction, the efficiency of the anode-spark coatings paired with hardened steel 45 is low with a predominantly abrasive type of wear. Reduced resistance of the coating is caused by brittle fracture (splitting of individual microvolumes). The coefficient of friction during operation is unstable and is measured in a wide range f = 0.3… 0.8.

The study of anode-spark coatings in the mode of ultimate lubrication was studied in the medium of oil I-20, which were saturated samples. The research was carried out before complete wear of the coating formed at different durations of molding. Data on the effect of molding duration on the wear resistance of coatings are given in table 1. The wear intensity is calculated by the formula:

$$U_w = \frac{\Delta G}{S},$$

where ΔG is the weight wear, g; S is the path of friction, mm.

Table 1

The results of studies of anode-spark coatings

Processing time, τ_{pr}, min	The weight of the sample after processing, G_1, g	Sample weight after the study, G_2, g	Weight wear, $\Delta G \cdot 10^{-4}$, g	The path of friction, $S \cdot 10^3$ m	Wear intensity, $I_W \cdot 10^{-9}$, g/m	Coefficient of friction, f
45	1.05795	1.057890	0.60	16.4	3.658	0.13
60	1.07660	1.076408	1.92	65.6	2.927	0.12
90	1.17212	1.172018	1.025	24.6	4.170	0.14

Figure 2 shows the dependence of wear intensity I_W from the duration of processing (molding) tobr. As can be seen, the optimal duration of molding should be considered up to 60 minutes The coefficient of friction is practically independent of the duration of processing and is measured in the range of 0.12…0.14.

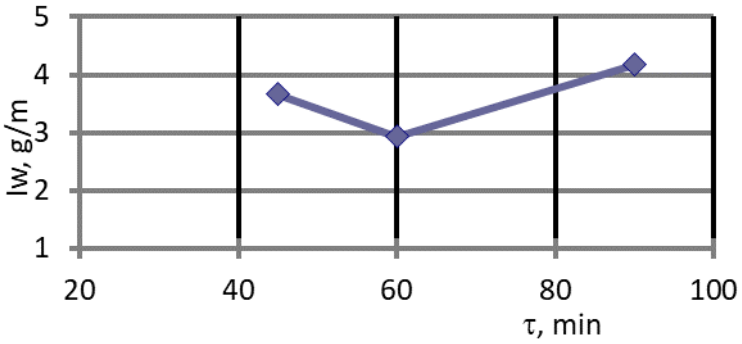

Fig. 2. Dependence of wear intensity of B-95 alloy on molding time

The results of comparative studies of wear resistance of anode-spark coatings and coatings formed by traditional oxidative anodizing technology are shown in table 2 and graphically in Fig. 3. The wear criterion was the weight wear of the samples according to the results of weight measurements before and after wear.

Table 2

Wear test results

Parameters	Meter readings, N	Friction path, $S \cdot 10^3$, m	Weight wear, $\Delta G \cdot 10^{-4}$, g	Friction force, $F_{тр} \cdot 10^{-2}$, N	Coefficient of friction, f
AC P = 0.4 MPa					
1	50	16.4	0.90	40	0.12
2	100	32.8	1.52	44	0.13
3	150	49.2	1.75	43	0.14
ASC P = 0.4 MPa					
1	50	16.4	0.5	7	0.07
2	100	32.8	0.8	9	0.09
3	150	49.2	1.0	8	0.08
ASC P = 0.8 MPa					
1	50	16.4	0.75	20	0.1
2	100	32.8	1.35	24	0.12
3	150	49.2	1.50	26	0.13

With increasing friction path, the coefficient of friction increases slightly to the appropriate value, and then stabilizes. As the load increases, the friction force and the coefficient of friction increase.

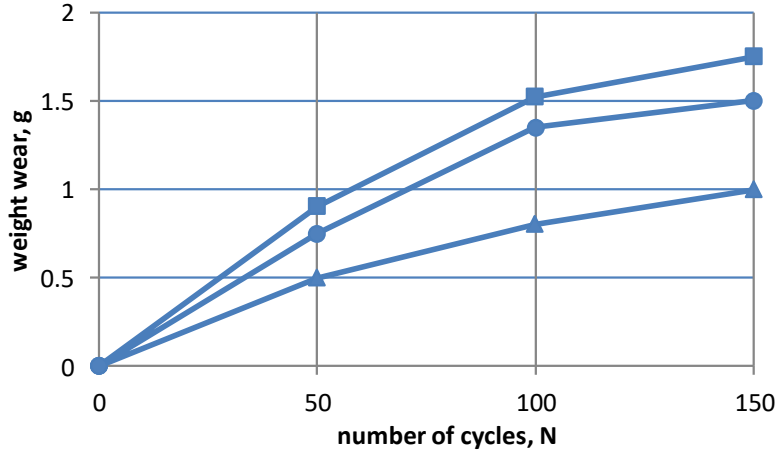

Fig. 3. Dependence of wear of coverings on duration of tests: ▲ - ASC P = 0.4 MPa; ● - ASC P = 0.8 MPa; ■ - AC = 0.4 MPa.

The analysis of the obtained results shows that the anode-spark coating is superior in its properties to the coatings obtained under oxidative anodizing conditions formed in optimal modes, but in the same electrolyte with the same concentration.

The wear resistance of anode-spark coatings in comparison with galvanic anode coatings at the same load was almost 2 times higher. The coefficient of friction of the coatings varied in the range of 0.1 ... 0.14. The optimal duration of coating formation is 60 minutes. It is also established that the wear resistance of anode-spark coatings depends not only on the duration of treatment, but also on other process parameters.

Conclusions

It is established that prolonged electrolysis in the conditions of sparking leads to the formation of anode coatings that exceed in their properties the films obtained by non-sparking oxidation.

Comparative studies of the wear resistance of anode-spark coatings and galvanic anode coatings under the same test conditions showed that the wear of anode-spark coatings is almost twice lower for the entire load range.

References

1. Subba Rao, A.N., Venkatarangaiah, V.T. Metal oxide-coated anodes in wastewater treatment. Environ Sci Pollut Res **21,** 3197–3217 (2014). https://doi.org/10.1007/s11356-013-2313-6

2. C.B. Wei, X.B. Tian, S.Q. Yang, X.B. Wang, Ricky K.Y. Fu, Paul K. Chu, Anode current effects in plasma electrolytic oxidation, Surface and Coatings Technology, Volume 201, Issues 9–11, 2007, Pages 5021-5024.

3. Bin Li, Jing Xue, Chao Han, Na Liu, Kaixuan Ma, Ruochen Zhang, Xianwen Wu, Lei Dai, Ling Wang, Zhangxing He, A hafnium oxide-coated dendrite-free zinc anode for rechargeable aqueous zinc-ion batteries, Journal of Colloid and Interface Science, Volume 599, 2021, Pages 467-475

4. L.K Xu, J.D Scantlebury, A study on the deactivation of an IrO2–Ta2O5 coated titanium anode, Corrosion Science, Volume 45, Issue 12, 2003, Pages 2729-2740.

5. Sevidova, E.K., Kononenko, V.I. Assessment of bioengineering ceramic coatings using the wetting method. J. Superhard Mater. **29,** 82–85 (2007). https://doi.org/10.3103/S1063457607020037

6. Pogrebnjak, A.D., Tyurin, Y.N. The structure and properties of Al_2O_3 and Al coatings deposited by microarc oxidation on graphite substrates. Tech. Phys. **49,** 1064–1067 (2004). https://doi.org/10.1134/1.1787669

7. Umanskyi, O., Storozhenko, M., Tarelnyk, V. et al. Electrospark Deposition of Fenicrbsic–Meb_2 Coatings on Steel. Powder Metall Met Ceram **59,** 57–67 (2020). https://doi.org/10.1007/s11106-020-00138-5

8. Markov, M.A., Bykova, A.D., Krasikov, A.V. et al. Formation of Wear- and Corrosion-Resistant Coatings by the Microarc Oxidation of Aluminum. Refract Ind Ceram **59,** 207–214 (2018). https://doi.org/10.1007/s11148-018-0207-3

9. Gutsalenko, Y.G., Sevidova, E.K. & Stepanova, I.I. Evaluation of Technological Capability to from Dielectric Coatings on AK6 Alloy, Using a Method of Microarc Oxidation. Surf. Engin. Appl.Electrochem. **55,** 602–606 (2019). https://doi.org/10.3103/S1068375519050041

Диха О.В., Бабак О.П., Маковкін О.М., Посонський С.Ф. Трибологічні властивості анодно-іскрових покрить на сплавах алюмінію.

Встановлено, що в теперешній час технологія анодно-іскрових покрить в загальному достатньо добре досліджена. Однак недостатність рекомендацій по вибору режимів технологічних процесів та трибологічних характеристик в різних умовах експлуатації обмежують широке впровадження даної технології. Задачею даної роботи був аналіз процесів нанесення анодно-іскрових покрить, вдосконалення технології та дослідження зносостійкості зразків, оброблених за вказаною і традиційною анодною технологією. Розробка технології нанесення захисних покриттів на вентильні метали в умовах іскрового розряду включала в себе вибір електроліту і режиму роботи ванни: напруга, густина струму, гідродинамічні умови та інші параметри. Випробування на зносостійкість проводилися на спеціальній установці. Конструктивно установка виконана двухпозиційною, що дозволяє одночасно випробувати два зразки з різними умовами навантаження при постійній швидкості ковзання. Конструкція установки реалізує схему тертя вал-вкладиш. Дослідження анодно-іскрових покриттів в режимі граничного змащування досліджувалось у середовищі індустріального масла. За критерій зношування приймався ваговий знос зразків по результатам вимірювань ваги до і після зношування. Встановлено, що тривалий електроліз в умовах іскріння приводить до утворення анодних покриттів, що перевищують за своїми властивостями плівки, отримані шляхом безіскрового оксидування. Порівняльні дослідження зносостійкості анодно-іскрових покрить і гальванічних анодних покрить за одакових умов випробувань показали, що знос анодно-іскрових покрить майже вдвічі нижчий для всього навантажувального діапазону. Розглянута технологія рекомендується для підвищення зносостійкості елементів приладів з алюмінієвих сплавів, що працюють в умовах корозійно-механічного зношування.

Ключьові слова: анодно-іскрові покриття, алюмінієві сплави**,** трибологічні випробування, знос, коефіцієнт тертя

Problems of Tribology, *V. 27, No 2/104-2022, 35-41*

Problems of Tribology
Website: http://tribology.khnu.km.ua/index.php/ProbTrib
E-mail: tribosenator@gmail.com

DOI: https://doi.org/10.31891/2079-1372-2022-104-2-35-41

Nanostructural glass composite coatings

S.D.Kharchenko[1], O.V.Kharchenko[2*]

[1]Institute of General Energy of the National Academy of Sciences of Ukraine
[2]National Aviation University, Ukraine
**E-mail: olena80@ukr.net*

Received: 18 March 2022: Revised: 25 April 2022: Accept: 20 May 2022

Abstract

The results of the study of glass-composite nanostructured self-lubricating coatings are presented. The developed glass composite is an antifriction material with an ultrafine structure. The structural components of these coatings significantly affect the graphitization process and provide an antifriction surface layer of α-graphite. The formation of this layer makes it possible to significantly minimize the contact parameters in the friction region.

The developed antifriction nanostructured glass-ceramic self-lubricating coatings containing magnesium carbide and structural components that promote surface graphitization do not contain expensive and scarce components, meet environmental safety requirements, and have high performance characteristics. A significant effect of aluminoborosilicate in the form of a glass phase on the tribological properties of coatings is noted. An increase in adhesive strength is achieved by forming a surface layer of glassy sodium silicate. Using X-ray phase analysis, it was found that the intercalating elements in the subsurface zone-graphite system at the initial stage of the process were Mg^{2+}, Al^{3+}, Cu^{2+} ions, which randomly penetrated into the interlayer space of the graphite matrix. At sliding speeds of more than 3.0 m/s, intercalates of binary molecular compounds of these elements with oxygen were found in the layered system of graphite. Their intercalation is accompanied by a sequence of repetitive stages, which are reversible with a change in tribological parameters and are characterized by a specific transformation of the structure and, above all, by an increase in the distance between layers due to the influence of various types of interlayer defects and the introduction of intercalants.

The presence of near-surface particles in the graphite layer does not affect the tribotechnical characteristics of the coatings. The developed glass-composite nanostructured self-lubricating coatings have high antifriction characteristics throughout the entire load-speed range.

Key words: nanostructured coatings, wear intensity, glass composite, glass phase, graphitization

Introduction

Preservation of operational characteristics limited by friction and wear, both of individual units and technical systems as a whole, can be ensured by modern surface engineering tools that implement the basic principle of minimum costs with maximum results. Structural engineering methods that use modification through the use of solid lubricants have taken a leading position in recent years in providing anti-friction contact interfaces. Coatings containing solid lubricants are among the innovative and most promising antifriction materials, the high quality of which is especially noticeable in conditions where traditional liquid lubricants are ineffective [1, 2]. They are used in various fields of technology from lubrication of precision aircraft mechanisms to preventing jamming of threaded joints [3,4].

The development of antifriction nanostructured glass-composite self-lubricating coatings meets the modern priorities of tribotechnical materials science aimed at increasing the wear resistance of friction-loaded movable interfaces and, on their basis, the development of scientific and applied solutions in the interests of improving the efficiency of using high-quality production technologies [5,6].

Objective

Ensuring high quality antifriction properties of nanostructured glass-composite self-lubricating coatings with increased adhesive strength due to the presence of aluminoborosilicate and structurally free magnesium carbide in the composition of the glass phase, as well as the selection of structural components that promote graphitization.

Materials and methods of research

As is known from the comparative characteristics of gas-thermal coatings, which are similar in their structural-phase composition, detonation-gas coatings have maximum operational properties [7]. On this basis, for the deposition of the coatings under study, the detonation method was used using nanostructured powders obtained by the mechanochemical method, the composition of SiC-Ni-Cu-Al-Si-C with a uniform distribution of the aluminoborosilicate glass phase (SiO_2-Al_2O_3-B_2O_3). According to the developed technology, structurally free magnesium nanocarbide (MgC_2) was added to the resulting nanoglass composition, after which it was mixed, ensuring its uniform distribution in the powder mixture ready for spraying. All powder materials used in the work are obtained from the mineral resource base of the country.

The antifriction properties of the coatings were evaluated during friction of the ring samples along the end scheme under conditions of distributed contact in the continuous sliding mode at a load of 10.0 MPa. The influence of the environment, speed, load, implemented during the tests, were selected taking into account the maximum approximation of the processes of physicochemical friction mechanics to the real conditions of contact interaction, in addition, the program for studying nanostructured glass-composite coatings provided for a comparative analysis of their antifriction characteristics with similar values obtained during tests of tungsten-containing coatings of the VK15 type and coatings sprayed with alloyed nichrome powder.

The study of contact interfaces, in which activation processes occur during friction, which determine the intensity of surface reactions and tribophysical phenomena, was carried out using modern methods of physical analysis, involving metallography (an optical microscope of the type Neofot-32 with an attachment), an X-ray electronic microanalyzer of the Camscan 4 DW type with a program for the distribution of chemical elements. The determination of the phase composition of the surface layers was carried out on a general-purpose X-ray diffractometer of the DRON-3 type with monochromatic CuKα radiation.

Increasing the adhesive strength, as a criterion for the performance of glass composite coatings, was carried out by preliminary deposition on the working surface of a sublayer of glassy sodium silicate $Na_2O(SiO_2)_2$. The exclusion of unproductive losses and adherence to the measurement technology using the conical pin method determined the correctness of the obtained results of the adhesion strength, which amounted to 145-150 MPa [8].

Research results

The contact interaction of surfaces is a complex sequence of cooperative influence of both external factors and internal transformations, the qualitative agreement of which reflects the commonality of quantitative patterns and determines their ordered causal relationship. According to the results of interactions of coatings under friction loading, Fig. 1 shows experimental values representing the averaged functional dependences of the wear intensity and friction coefficients, which change with time and stabilize after running in, in the field of sliding velocities at a constant load of 10.0 MPa. As can be seen from the graph, in the entire range of tests with a monotonically increasing sliding speed, the minimum values of wear rates and the corresponding friction coefficients correspond to nanostructured glass-composite coatings (curves 1 and 1'). The structure of nanoglass composites, which determines their properties, practically consists of a finely dispersed mixture representing both solid solutions and, mainly, intermetallic compounds with a significant presence of a glass phase. The invariance of the chemical composition and the constancy of the parameters of technological deposition determine the stability of the coating structure, the relative density of which was up to 99%. The cross section of the nanocomposite coating is shown in Fig.2. Metallographic analysis has established that the deposited layer has a quasi-ordered lamella-like appearance, which closely adheres to the base material, completely copying the surface topography, while accumulations of component oxides, as well as slag contamination, are practically absent, and defects in the form of pores and cracks are not detected.

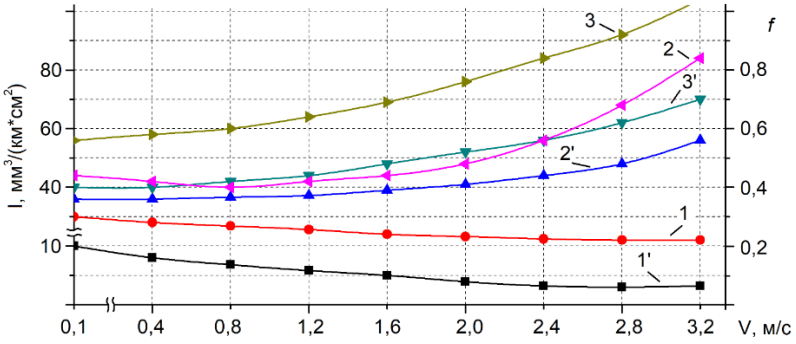

Fig.1. Dependence of wear intensity (1,2,3) and friction coefficient (1',2',3') on sliding speed of coatings SiC-Ni-Cu-Al-Si-C+glass phase+MgC2 (1,1'), WC-Co (2.2') and Ni-Cr-Al-B (3,3') on sliding speed (P=10.0 MPa).

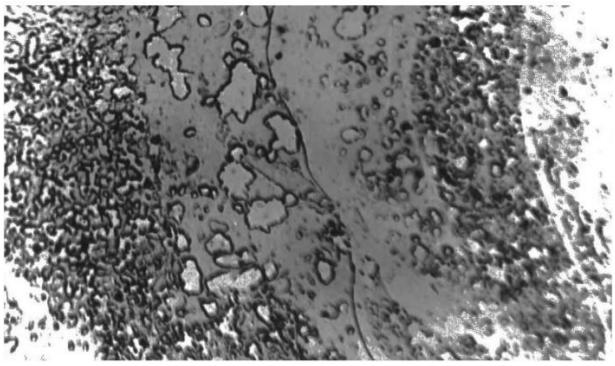

Fig.2. Coating structure (x5000)

The synthesis and study of solid solutions based on refractory compounds, in particular silicon carbide, are being carried out quite intensively, but the capabilities of the latter and its complex of tribological properties are far from the expected results. The developed glass composite is an antifriction material with an ultrafine structure. It is generally accepted that elastoplastic deformation is the main factor determining the development of the process of external friction, and in addition, in our opinion, the formation of a gradient structure is a derivative of it. It can be said that the evolution of the structure during contact interactions has pronounced scale levels, and the processes occurring at different scale levels are interdependent. The layer-by-layer picture of plastic deformation obtained by the diffraction method reveals the main regularities of the formation of a scale structure and makes it possible to establish uniform transitions from a dispersed polycrystalline fragmented structure on the surface through intermediate textured layers to the original crystalline, inherent in deep material. As can be seen from Fig. 3, in the coating under study, as it approaches the friction surface and the contact pressure increases, and the intensity of deformation, the structure is gradually replaced by an ultrafine one. In this case, high contact compressive and shear stresses create conditions for the implementation of significant plastic deformations in the near-surface layer of the coating material, which cause the formation of ultrafine structures.

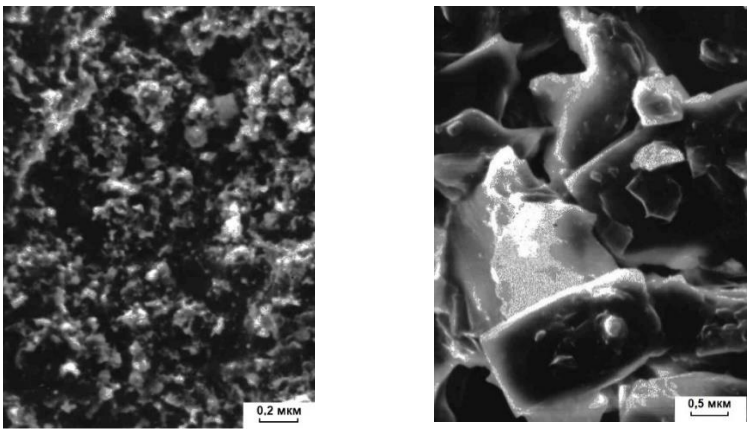

a) **b)**

Fig.3. Changes in the structure of the nanoglass-composite coating with increasing distance from the friction surface in a layer ~6 μm thick: a) near-surface zone; b) undeformed structure.

This gives grounds to single out in a structure subjected to tribotechnical loads a near-surface zone, in which deformation processes that develop inhomogeneously in microvolumes form a specific layer at the near-surface level, in which structural-thermal activation causes a complex of physico-chemical interactions that determine the concomitant and leading type of wear. The surface zone is a structurally heterogeneous finely dispersed composition.

As evidenced by the results of X-ray microanalysis (MRSA) performed on the "Camebax SX", the basis of the nanoglass composition is silicon carbide of non-stoichiometric composition, along the grain boundaries of which silicate compounds are located, among which inclusions corresponding to the composition of silicon dioxide predominate, also in the carbide structure the role of dispersion-strengthened components is performed by Al_2O_3 oxides distributed along the boundaries and intermetallic inclusions in the form of spherical nanograins. However, the high thermomechanical properties of SiC carbide are discredited by significant brittleness. We noted that the substitutional solid solution that forms Al and SiC causes a slight distortion of the crystal lattice of the carbide, since the differences in the masses of Al atoms and Si are extremely small, as a result of which the microhardness does not change, while plasticity increases. A similar effect on the composition of SiC, forming substitutional solid solutions by replacing Si atoms, is exerted by Cu and Ni. The formation of phases in the coating, as tests have shown, is determined not only by the ratio of components, temperature, dispersion, but also depends on their defectiveness and external conditions. Undoubtedly, as an axiom, tribochemical interaction takes place when the molecules receive the necessary activation energy. Endothermic reactions generally do not proceed without activation. The interaction of SiC with Mg, which is formed during the thermal decomposition of structurally free magnesium carbide under running-in conditions and depends on the process temperature, is accompanied by the formation of magnesium silicide and acetylenide magnesium, the latter, under the influence of thermomechanical action, promotes the formation of graphite through the intermediate dimagnesium tricarbide ($2SiC + 5Mg \rightarrow 2Mg_2 Si + MgC_2$, $MgC_2 \rightarrow Mg_2 C_3 \rightarrow Mg + C$). It should be noted that, under thermodynamic action, the presence of a catalyst in the form of Al promotes the decomposition of magnesium carbide. The basis of physical phenomena that initiate the mechanism of decomposition of carbide graphite are structural transformations in the solid phase, caused by thermal effects. The factors that determine the qualitative level of thermomechanical carbide graphitization include both the degree of dispersion of structural components, specific pressure, operating temperature, and temperature in the contact zone, the presence of elements that initiate decomposition processes, as well as the influence of the environment (in vacuum, the probability of the amount of graphite increases), in addition, internal factors associated with the composition of the material, its structure, the presence of defects, etc. The contact zone constituting the near-surface layer (initial scale level) separating the coating material from the antifriction film consisting of polydisperse graphite particles is a deformed zone, which, according to the results of X-ray microanalysis performed on MAR-3 (probe diameter 1 μm), represents finely dispersed heterogeneous structural -phase compounds of the components that make up the coating. Among which, the presence of Ni, as a structural component, is due to its distinctive properties, so, on actual contact spots, when a temperature of about 450-500 ^{o} C is reached, depending on the dispersion and external influences in a local high-temperature field, Ni interacts with SiC, forming nickel silicides with a predominance of metal-enriched Ni_2Si. As a result, carbon is reduced, which is transformed in the form of a solid phase of elementary polydisperse graphite colonies combined into surface structures.

However, magnesium carbide remains the main component of the antifriction surface layer, consisting of a carbonaceous product - graphite. The value of the specific wear work characteristic of the initial running-in moment, as shown by calculations, is up to 10 kJ/mm^3, which is both a necessary and sufficient condition for initiating the thermal decomposition of MgC_2, which causes the formation of carbon in the form of a solid phase.

Using the natural ability of chemical elements to graphitize through the formation of carbide graphite, a high-quality, thickened anti-friction layer was obtained, which determines the operational properties of coatings.

In the structural-phase study of glass composite coatings, the presence of intermetallic compounds based on Al and Ni such as NiAl and $Ni_2 Al_3$ was noted, while monoaluminide, being a high-temperature phase, has a significant hardness, as shown by measurements, most likely about 3.8 GPa. The presence of an ordered solid solution based on nickel monoaluminide with a reduced Al content (~20–25 wt %) was also found, which leads to increased ductility. According to the results of elemental and X-ray phase analyzes, the presence of a solid solution of Ni in Cu was noted, but their compounds were not found. Solid solutions of Ni in Si and Si in Ni, as well as their intermetallic compounds $Ni_2 Si$, $Ni_3 Si_2$, and $NiSi_2$, have been revealed. In addition, the presence of small amounts of colonies of solid solutions of Si in Cu was established, and the formation of their chemical compounds such as copper silicates is also likely, since the microhardness increases significantly. However, it was difficult to identify them accurately.

Powders of aluminoborosilicate glasses, the dispersion of which was 25–30 μm, in the process of mechanochemical treatment and thermomechanical action, being products of inorganic synthesis, caused, along with the preservation of the original components, the formation of new stable compounds, as was found, from solid solutions of $Al_2 O_3$ and SiO_2 obtained rhombic syngony, close to the structure of sillamanite, most likely it is the lowest mullite obtained by reaction as a result of the interaction of the oxidation products of the original components. From the point of view of glass-ceramic technologies, the greatest interest, in our opinion, is the

presence of components that form refractory metal oxides, primarily Al and Si oxides. The presence of B_2O_3 was also established, which, as a result of partial oxidation, formed a solid solution of Al_2O_3 - B_2O_3.

From the point of view of condensed matter physics, the addition of a glassy component affects the quality of the coating material through the structural state and, as practice shows, interest in these technical products is steadily increasing. When studying glass composites, their optimal composition was established experimentally, in which the rational use of glass structures contributes to an increase in heat resistance and chemical resistance, in addition, the manifestation of high cohesive strength, an increase in the density of nanocomponents, crack resistance with significant corrosion resistance and ensures high adhesion (more than 127 MPa) with materials different chemical nature, in addition, the formation of a silicate barrier layer prevents the mutual diffusion of structure-forming particles of the coating and substrate.

The surface zone directly adjacent to the friction surface and separating the coating material from the antifriction layer consisting of polydisperse graphite particles is the thinnest film several micrometers thick. Studies have shown that the pressure in it is uneven, and the areas of tensile and compressive stresses, which are inevitable under the conditions of deformation of heterogeneous phases, are close in structure to a conglomerate of finely dispersed (quasi-amorphous) structures, having dimensions in the range of 5-15 nm, and representing mechanical mixtures, oxygen-free and oxide compounds of structure-forming components. The influence of plastic deformation is associated not only with the dispersion of the surface zone, but also with the accumulation of defects that change its physicochemical properties, including reactivity, and affect the intensity of chemical reactions in the solid phase.

At the same time, the thermal conductivity of a finely dispersed conglomerate having an increased porosity and forming a near-surface zone is lower than that of a solid material, therefore, the heating temperature of the finely dispersed fragments of the zone is higher than the temperature of the surface areas.

The temperature factor stimulates physicochemical processes, in particular, the reactive diffusion of structure-forming particles at the atomic-molecular level, which contributes to the introduction of kinetically active components of the dispersed zone through the weakening of the bond between the polyarene planes into the interlayer space of graphite and thus the formation of intercalated graphite.

Using X-ray phase analysis, it was established that the intercalating elements in the subsurface zone-graphite system at the initial stage of the process were Mg^{2+}, Al^{3+}, Cu^{2+} ions, which randomly intruded into the interlayer space of the graphite matrix. At sliding speeds of more than 3.0 m/s, intercalates of binary molecular compounds of these elements with oxygen were found in the layered system of graphite. Their intercalation is accompanied by a sequence of repetitive stages, which are reversible with a change in tribological parameters and are characterized by a specific transformation of the structure and, above all, by an increase in the distance between layers due to the influence of various types of interlayer defects and the introduction of intercalants. Note that today there is no general intercalation model that explains the electrochemical mechanism of the synthesis of layered systems. From the energy point of view, the intercalation process, which represents reversible topo-taxial chemical reactions, can be considered as an adequate way of self-organization of surface layers in the process of structural adaptability of the friction system.

We have found that quantitative changes during the intercalation of the graphite layer, which causes a high level of antifriction, does not affect the expected degree on the qualitative values of tribological parameters during testing for related characteristics associated with the electromagnetic properties of intercalated graphite, judging by the analysis of literature data, it has a significant effect.

The developed antifriction nanostructured glass-ceramic self-lubricating coatings containing magnesium carbide and structural components that promote surface graphitization do not contain expensive and scarce components, meet environmental safety requirements, and have high performance characteristics. The most effective use of nanostructured glass-ceramic self-lubricating coatings is to improve the operational reliability of friction units during their hardening and restoration of moving parts of control mechanisms, sliding bearings, lever parts, high-speed and thermally loaded interfaces, in which the use of traditional lubricants is not desirable.

The development of nanostructured glass-ceramic self-lubricating anti-friction coatings, the substantiation of their structural components, the results of applied tests and the ability to work in production conditions can significantly expand the arsenal of achievements of modern tribotechnics.

It should be noted that the developed nanostructured glass-composite powder can be used for strengthening and restoring worn parts by any technological methods used in powder materials.

The presented work continues the cycle of research on the creation of promising nanomaterials designed to reduce the coefficient of friction and increase the wear resistance of friction units of machine and equipment parts.

Conclusions

1. By means of theoretical prerequisites and experimental studies, the optimal structural-phase composition of nanostructured glass-composite coatings of the SiC-Ni-Cu-Al-Si-C system containing a glass phase of the SiO_2-Al_2O3-B_2O_3 type and structurally free magnesium carbide was realized. To improve the adhesion strength, a sublayer of glassy sodium silicate was applied to the substrate. The role of the glass phase in the formation of glass composites is disclosed, which contributes to an increase in the cohesive component,

continuity and strength of the nanostructure, and an increase in the anticorrosion properties and chemical resistance of coatings.

2. It is noted that the assessment of the quality of the coatings under study is inextricably linked with the problem of the reproducibility of their technological process. By controlling the deposition of nanostructured glass-composite powders, it turned out to be possible to provide not only the desired chemical composition, but also to obtain a given nanostructure as a result, optimizing a set of properties that contribute to the stable manifestation of minimization of tribotechnical characteristics.

3. The physical mechanism and the main factors that determine the level of thermomechanical graphitization are considered, the nature and chemical interactions of the structural components of the friction system are noted, in ensuring high anti-friction properties of glass-composite coatings.

4. The synthesis of layered graphite compounds as a result of topo-taxial reactions has been studied. The nature of intercalants in a graphite matrix is established and it is noted that reversible topo-taxial chemical reactions in the solid phase represent one of the mechanisms of self-organization of the surface layers of a friction system under conditions of structural adaptability.

5. Fundamental ideas about the formation and structure of antifriction surface structures based on polydisperse carbide graphite were supplemented, which made it possible to expand the arsenal of achievements of modern tribotechnics.

6. Structural engineering, driven by the analysis and innovative provision of the functional properties of the developed materials, opens up promising opportunities associated with the modernization of friction surfaces.

References

1 Sahar Ghatrehsamania, SalehAkbarzadeha, M.M.Khonsari Experimentally verified prediction of friction coefficient and wear rate during running-in dry contact. // Tribology International Vol. 170 (2022). doi.org/10.1016/j.triboint.2022.107508.

2. Aleksandr V. Antsupov, Artem A. Fedulov, Alexey V. Antsupov and Victor P. Antsupov An Application of Antifriction Coatings to Increase the Lifetime of Friction Units. Mechanical Engineering. MATEC Web of Conferences 346, 03024 (2021). doi.org/101051/matecconf/202134603024.

3. I. Justin Antonyraj D. Lenin Singaravelu Tribological characterization of various solid lubricants based copper-free brake friction materials – A comprehensive study. materials today. Volume 27, Part 3 , 2020, Pages 2650-2656. doi.org/10.1016/j.matpr.2019.11.088.

4. Maciej Matuszewski, Małgorzata Słomion, Adam Mazurkiewicz and Andrzej Wojciechowski Mass wear application of cooperated elements for evaluation of friction pair components condition. mechanical engineering. MATEC Web of Conferences 351, 01006 (2021). doi.org/10.1051/matecconf/202135101006.

5. Babak, VP , Shchepetov, VV , Nedaiborshch, SD (2016). Wear resistance of nanocomposite coatings with dry lubricant under vacuum. Naukovyi Visnyk Natsionalnoho Hirnychoho Universytetuthis link is disabled , 2016, (1), nbuv.gov.ua/UJRN/Nvngu_2016_1_9.

6. Babak VP, Shchepetov VV, Harchenko SD Antifriction Nanocomposite Coatings that Contain Magnesium Carbide. J. Journal of Friction and Wear, 40 (6), Pp.593–598 (2019). doi.org/10.3103/S1068366619060035.

7. Vilhena, L.; Ferreira, F.; Oliveira, JC; Ramalho, A. Rapid and Easy Assessment of Friction and Load-Bearing Capacity in Thin Coatings. Electronics 2022, 11, 296. doi.org/10.3390/electronics11030296.

8. Zaytsev AN , Aleksandrova YP , Yagopolskiy AG Comparative Analysis of Methods for Assessing Adhesion Strength of Thermal Spray Coatings. BMSTU Journal of Mechanical Engineering. 5(734)/2021 -p48-59. DOI: 10.18698/0536-1044-2021-5-48-59 .

Харченко С.Д., Харченко О.В. Склокомпозиційні наноструктурні покриття

Наведено результати дослідження склокомпозиційних самозмащувальних наноструктурних покриттів. Розроблений склокомпозит є антифрикційним матеріалом з ультрадрібнодисперсною структурою. Структурні складові даних покриттів суттєво впливають на процес графітизації та забезпечують одержання антифрикційного поверхневого шару α-графіту. Формування даного шару дозволяє істотно мінімізувати контактні параметри у зоні тертя.

Розроблені антифрикційні самозмащувальні наноструктурні склокерамічні покриття, містять карбід магнію та структурні складові, що сприяють поверхневій графітизації, не мають у складі дорогих і дефіцитних компонентів, відповідають вимогам екологічної безпеки, мають високі робочі характеристики. Відзначено значний вплив алюмоборосилікату у вигляді склофази на триботехнічні властивості покриттів. Підвищення адгезійної міцності досягається шляхом утворення поверхневого шару зі склоподібного силікату натрію. Методом ренгенофазового аналізу встановлено, що інтеркалюючими елементами в системі підповерхнева зона-графіт, на початковому етапі процесу з'явилися іони Mg^{2+}, Al^{3+}, Cu^{2+}, що хаотично впроваджувалися в міжшаровий простір графітової матриці. При швидкостях ковзання більше 3,0 м/с виявлено у шаруватій системі графіту інтрекаляти бінарних молекулярних сполук цих елементів з киснем. Їх інтеркаляція супроводжується послідовністю повторюваних стадій, які при зміні триботехнічних параметрів є оборотними і характеризуються специфічним перетворенням структури і, насамперед, збільшенням відстані між шарами за рахунок впливу різних типів міжшарових дефектів та впровадження інтеркалантів.

Наявність у графітовому шарі частинок поверхневого шару не впливає на триботехнічні характеристики покриттів. Розроблені склокомпозиційні самозмащувальні наноструктурні покриття, мають на всьому навантажувально-швидкісному діапазоні високі антифрикційні характеристики.

Ключові слова: наноструктурні покриття, інтенсивність зношування, склокомпозит, склофаза, графітизація

***Problems of Tribology**, V. 27, No 2/104-2022, 42-48*

Problems of Tribology
Website: http://tribology.khnu.km.ua/index.php/ProbTrib
E-mail: tribosenator@gmail.com

DOI: https://doi.org/10.31891/2079-1372-2022-104-2-42-48

Estimation of tribotechnical parameters of composite polymer with metal filler

O.O. Skvortsov[1], O.O. Mikosianchyk[2*]

[1]Progresstech, Ukraine
[2]National Aviation University, Ukraine
**E-mail: oksana.mikos@ukr.net*

Received: 28 March 2022: Revised: 29 April 2022: Accept: 15 May 2022

Abstract

The use of composition material based on the polyamide (caprolon) Ertalon 4.6 as an anti-friction material in the sliding units in the aviation industry is considered. Low carbon electrotechnical sheet steel 21864 of different concentrations was used as filler of composite material. The article presents the thermal calculation of plain bearings with polymer insert in different operating modes. It is determined that the addition of a metal filler to polyamide causes a temperature decrease in the friction zone due to the effective heat exchange from the shaft to the bearing housing. The article conducts a study of tribo-technical properties of the proposed composite material on installation PT-4C under sliding conditions according to the scheme "cylinder-plane", as well as modeling of the support unit in the software complex DS SolidWorks. It has been experimentally determined that the addition of finely dispersed steel filler enhances the antifriction properties of the Ertalon 4.6 polymer and extends the temperature range of the composite insert performance. Increasing the filler concentration to 20% results in a reduction of the friction coefficient by an average of 3.6 times and an increase in the temperature range of composite material use to 100 °C. The load-bearing capacity of the composite material bushing is increased to 25 MPa at a 20% filler concentration respectively.

The practical significance of the work lies in the analysis of the antifriction properties of the polymer with metallic filler in comparison with the polymer without filler, which will prove the effectiveness of the use of such polymers in friction units instead of non-ferrous metals (bronze, babbitt).

Key words: composite material, polymer, friction coefficient, polyamides, bearing, temperature.

Introduction

For the operation of the aircraft, an important factor is the quality of its parts as well as assembly, in general. An important role in the design of the aircraft is performed by bearings, which are present in almost every structural part of the aircraft.

Bearing – a product that is part of a support or emphasis that supports a shaft, axis or other movable structure with a given stiffness. It fixes the position in space, provides rotation, rolling or linear displacement (for linear bearings) with the least resistance, senses and transfers the load from the movable unit to other parts of the structure. The scope of the bearings is huge – almost no industry is complete without the use of bearings. There are a lot of varieties of bearings, and they are used depending on the operating conditions in a particular mechanism.

In aviation, there is a specificity due to difficult operating conditions such as: high contact pressures; dynamic and vibration loads; abrasive contamination; lack of lubrication, which results in increased wear and kinematic accuracy of the conjugation.

This problem can be solved using new advanced anti-friction materials, such as polymers, in the friction assemblies of aviation equipment. Polymer materials allow to solve several technical tasks aimed at increasing the reliability and service life of the equipment, have good antifriction properties when working in friction units without lubrication. However, their wide use is constrained by the fact that they have low thermal conductivity and, because of this, low heat resistance, and with increased temperatures - low wear resistance.

To eliminate these deficiencies, it is necessary to provide heat dissipation from the friction zone. We propose to include a metal filler in the structure of the polymer plain bearing. Previously, metal frames, nets, etc., were used, which reinforced the bearing and at the same time contributed to the removal of heat from the contact zone. The drawbacks were that they were not in direct contact with the shaft, which reduced their efficiency as a heat conductor element, and the production of such bearings was complex and time-consuming.

Literature review

In the manufacture of bearings, metal (steel, bronze, aluminum, titanium, etc.) is often assumed to be the most suitable material. Depending on the type, bearings can be considered sacrificial components in an assembly. They are designed to accrue wear in a system and to be replaced when they wear out. As such, the material chosen for bearings is selected both because it will have a long life and good wear resistance, or because it will be inexpensive to manufacture and simple to replace. The composite materials provide crucial weight savings to the aircraft, and because it is not made from metallic materials, it will be very resistant to corrosion. This design also reduces the weight of the part by approximately 50% [1].

Over the past few years composites have been dominant in the emerging materials. The applications areas of composite materials have grown steadily in the various systems of Mechanical Engineering, Civil Engineering, Electrical Engineering, Medical Engineering, and Automobile Engineering. In engineering systems, failure of parts may occur due to different types of wear mechanisms. The availability of a range of fiber reinforcements, fillers, matrices, and processing techniques offers ample scope for tailoring properties in composites as required for specific applications [2].

The tribological properties of polymers and polymer matrix composites (PMCs) and the relevant mechanisms of friction and wear has been reviewed [3]. The influence of both molecular and mechanical components on friction involving polymers as well as the influence of fillers, reinforcements, and dry lubricants on the overall tribological characteristics of PMCs is evaluated. Tribological parameters include surface roughness, the mechanism of adhesion, friction and wear, and chemical interactions with dry lubricants (if present). The article reviews the main factors that influence the wear and frictional characteristics of thermoplastic and thermosetting polymers, short fiber reinforced composites and high-performance unidirectional composites. Examples of quantitative data of different pairs of polymers and PMCs with the counterface are presented.

The article [4] provides an overview of polymer materials of various buildings used as antifriction materials. The experience of using different polymer materials for manufacture of antifriction coatings is considered. The advantages of thermoset and thermoplastic polymers in comparison with metal materials have been identified. Some compositions of carbon and organoplastics developed for plain bearings are described. It is concluded about the direction of research during development new matrixes for antifriction materials.

The article [5] conducts research on influence of rotational friction process on the value of wear of polymer antifriction material, both with metal filler and without filler. The dependence of linear and weight wear of antifriction sleeve of plain bearing is revealed.

Thus, the analysis of these publications shows the relevance of the development of plain bearings with the use of polymer materials in order to increase their antifriction and wear-resistant properties, which is the main precondition for increasing the service life of the bearing.

Purpose

The purpose of the work is to study the dependence of the friction coefficient on the temperature in the contact area at various modes of operation of plain bearings with a polymer insert and to review the influence of the metal filler in the structure of the polymer plain bearing on the temperature in the contact area of the friction surfaces.

Objects of research and experimental conditions

It is proposed to introduce into the bearing structure of fine chips of material with good thermal conductivity. For this graphite, molybdenum disulfide, copper, lead, titanium, or bronze can be used. However, these expensive materials were rejected and the metal shavings of low carbon electrotechnical sheet steel 21864 were used as filler material instead. In order to increase the efficiency of the thermal conductivity of the filler during the formation of the bearing, the action is carried out by a constant magnetic field, in the process of which metal sawdust, as a ferromagnetic material, are arranged in the form of chains, because one pole of the magnet is arranged inside the sleeve, the other pole is arranged on the external side thereof. The chains come into contact with the shaft. Since the shafts are typically made of solid steel and are heat-treated, the softer materials of the filler do not wear out the shaft, but due to direct contact with it, the heat is well dissipated. The heat-conducting links shall be arranged along magnetic field lines which shall be distributed perpendicular to the axis of the sleeve [3]. The optimum metal filler content is 15... 20% by weight. A small amount of low carbon steel filler does not contribute to abrasive wear in the friction bearing, often selective transfer occurs.

Rational thickness of sleeve wall S for connection diameters d = 20... 200 mm is selected from the expression S = (0.050...0.075)d. For the antifriction sleeve we used composite material, the thickness of the bushing wall is 4 mm.

The matrix for the composite sleeve was polyamide (caprolone) Ertalon 4.6 (Mitsubishi Chemical Advanced Materials). Compared with conventional nylons, Ertalon 4.6 features a better retention of stiffness and creep resistance over a wide range of temperatures as well as superior heat aging resistance. Therefore, applications for Ertalon 4.6 are situated in the "higher temperature area" (80 - 150 °C) where stiffness, creep resistance, heat aging resistance, fatigue strength and wear resistance of PA 6, PA 66, POM and PET fall short.

Due to the metal filler in the anti-friction sleeve, one part of the heat is discharged from the friction zone through the metal shaft and the other part through the bearing housing. The temperature of the antifriction layer depends on the ratio of the amount of heat generated in the bearing by friction and the amount of heat transferred to the surrounding area.

The diagram of the bearing unit using a bushing made of filled polymer is presented in fig. 1.

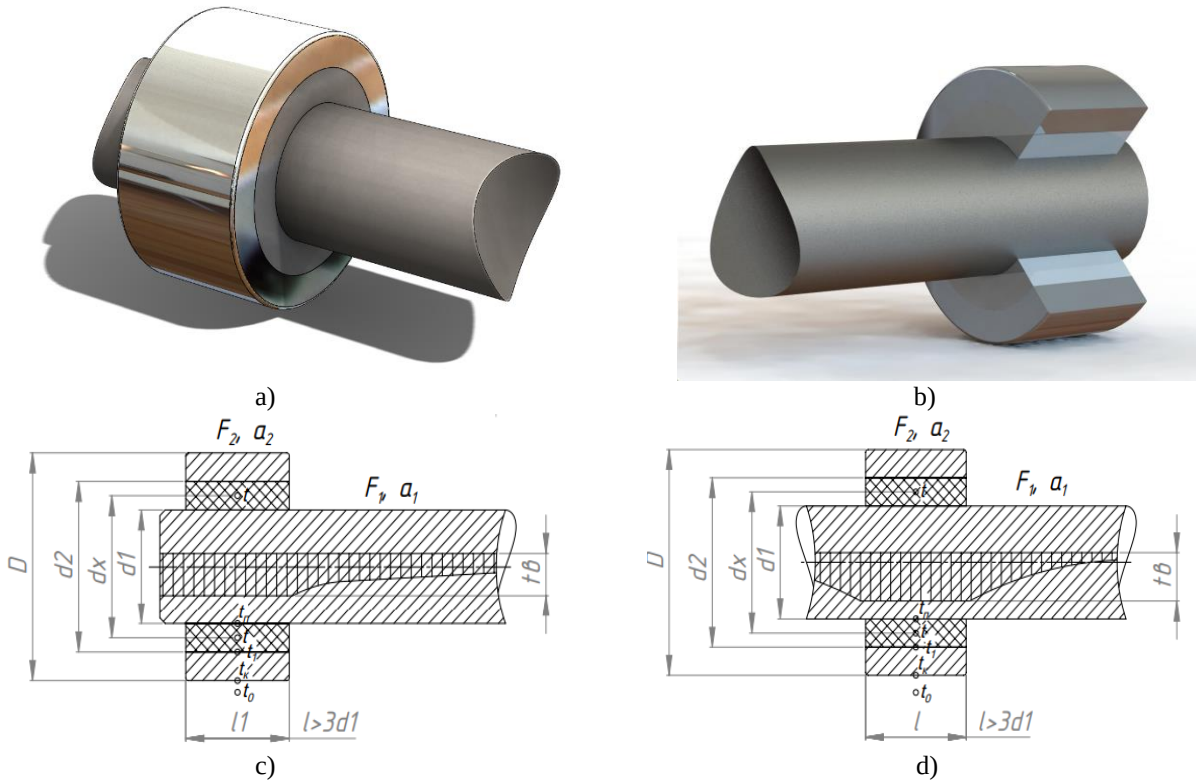

Fig. 1. Diagram of the bearing unit filled polymer: a, b – bearing units modelled using DS SolidWorks 2020; c - end bearing; d -median bearing; d_1 - shaft diameter in the friction zone; d_2 - outer diameter of bearing; D – outer bearing housing diameter; *l* - bearing length; L - length of shaft with intense heat exchange, tв – temperature distribution at shaft operation.

At the testing machine PT-4C under sliding conditions of the cylinder-plane scheme (Fig. 2), a study of the tricot technical properties of the proposed composite material was carried out. The material of the counter-sample is 40X steel (HRC 42), the material of the sample is Ertalon polyamide 4.6 without additives and a composite material based on it with the addition of fine steel 21864 chips in concentrations of 10 and 20%.

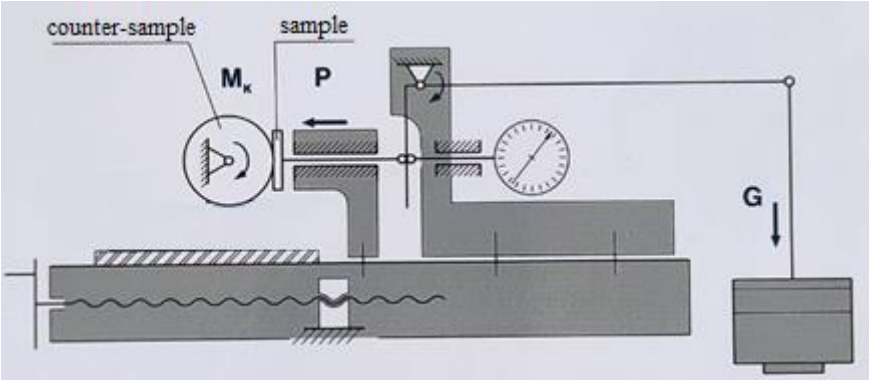

Fig. 2. Diagram of the test machine for determination of tribotechnical characteristics of materials.

The heating calculation is based on the assumption that the heat generated by friction is released into the environment through the shaft surface and partially through the bearing housing, as the thermal conductivity of the polymer (λ_2 = 0.3…0.8 W/(m ºC)) with metal filler well below the thermal conductivity of steel (λ_1 = 42...48 W/(m ºC)). In the process of friction interaction of the working surfaces of the friction unit heat is formed on the bearing support area, limited contact angle θ. Antifriction composite polymer with metal filler allows to allocate one part into the environment through the bearing housing. Lower temperature in the contact area increase the use of this composite material in plain bearings at frequent starts and stops with insufficient lubrication [2, 5].

On the surface of the friction unit the thermal source acts, the amount of heat released during the operation of the bearing is determined by the following formula:

$$Q = \frac{ldf}{427} pv, \tag{1}$$

where Q - bearing specific power, W/m^2; l - bearing length, m; d - bearing diameter, m; f - coefficient of friction; 1/427 - thermal equivalent of mechanical energy, kcal/(kg m); p - average specific pressure, N/m^2; v - slip speed, m/s.

In the process of friction interaction of the working surfaces of the unit the friction in the contact area is formed by heat. The excess temperature is discharged through the shaft in the radial and axial directions (Fig. 1). Outside the bearing support area, the temperature of the working surface decreases: the further away from the friction zone, the less [3].

When the plain bearing is operating, when the shaft rotates relative to the non-metallic layer, the surface temperature of the sleeve friction $t_п$ is some function of the distance r_x selected point from the cylinder axis and angle θ:

$$t_п = u(r_x, \theta). \tag{2}$$

The type of function (2) depends on the angle of contact of the non-metallic anti-friction layer of the sleeve with the shaft surface, the coefficient of thermal conductivity λ2 of the non-metallic layer, the thickness of the sleeve itself, the mode of operation of the friction unit, etc. factors. Since the highest temperature of the antifriction layer is observed in the contact zone of the friction surfaces, where it can be assumed to be constant at θ = 90... 120º, then the temperature distribution in the zone in question can be considered as a function only r_x [2, 6].

In this case, the temperature inside the sleeve:

$$t = t_п - \frac{t_п - t_1}{\ln\frac{d2}{d1}} \ln\frac{dx}{d1}, \tag{3}$$

where t_1 - the temperature on the external surface of the examined antifriction polymer sleeve; d_2 - external cylindrical surface of antifriction sleeve, d_2 = 2r_2; d_1 - the inner surface of the sleeve, d_1 = 2r_1;d_x- the distance of the selected point in the composite sleeve from the cylinder axis.

Since in the friction unit the outer surface of the bushing is in close contact with the metal housing of the bearing, the entire examined surface at the time of the onset of the stationary thermal mode t_1 can be considered constant due to the good thermal conductivity of the metal of the body (λ_1 = 42...48 W/(m ºC)). This value can be determined from the thermal balance:

$$Q_2 = Q_п, \tag{4}$$

where Q_2 - the amount of heat passed through the antifriction layer (in the case of polymers with metal filler) and metal bearing housing, W/m^2; $Q_п$ - the amount of heat given by the bearing housing to the environment, W/m^2.

In the established thermal mode, the temperature difference between the inner and outer surfaces of the metal bearing housing $\Delta t = t_1 - t_k$ is negligible, so it is possible to take $t_1 \sim t_k$.

The amount of heat passed through the antifriction layer of the composite polymer and metal bearing housing:

$$Q_2 = \frac{\theta\lambda_2 l}{\ln\frac{d_2}{d_1}}(t_п - t_k); \tag{5}$$

$$Q_п = \alpha_2 F_2^{'}(t_k - t_0), \tag{6}$$

where l is the length of the bearing support, m; λ2 - the coefficient of heat transfer from the bearing housing to the environment, W/(m^2 ºC); F_2' - external surface area of bearing housing, m^2; t_k- temperature of outer surface of bearing housing, º C; t_0 - ambient air temperature, ºC.

Analysis of the main results

The thermal conductivity of a polymer liner with a metal filler is determined by:

$$\lambda_2 = n_a\lambda_a + n_в\lambda_в, \tag{7}$$

where n_a and $n_в$ - volume fractions of components (steel, polymer); λ_a and $\lambda_в$ - thermal conductivity of materials (steel, polymer).

Thermal conductivity of steel λ_a = 42... 48 W/(m ºC) and thermal conductivity of polymer $\lambda_в$ = 0.3 W/(m ºC). Taking into account that the content of the metal filler does not exceed 20%, the thermal conductivity of the composite material is λ_2 = 4... 8 W/(m ºC).

After the amount of heat removed from the friction zone by the metal housing of the plain bearing has been determined, it is possible to make conclusions about the distribution of the heat flow and, consequently, about the possibility of operation of this composite antifriction material in the friction units. In a straight friction pair, a significant part of the heat is released by the rotating shaft, a smaller part is released through the bearing housing.

In order to determine the temperature on the external surface of the examined sleeve, let us substitute the expressions (5) and (6) into the equation (4), taking into account $t_1 \approx t_r$:

$$t_1 = \frac{\theta\lambda_2 l t_п + \alpha_2 F_2' \ln\frac{d_2}{d_1} t_0}{\theta\lambda_2 l + \alpha_2 F_2' \ln\frac{d_2}{d_1}}. \tag{8}$$

Having determined the temperature on the external surface of the examined polymeric sleeve with a metal filler, it is possible to determine how much heat is released by the outer surface of the plain bearing. Fig. 2 shows the temperature distribution according to the material. Composite material with metal filler (curve 2, 3) allows the heat to be dissipated through the outer surface of the plain bearing casing.

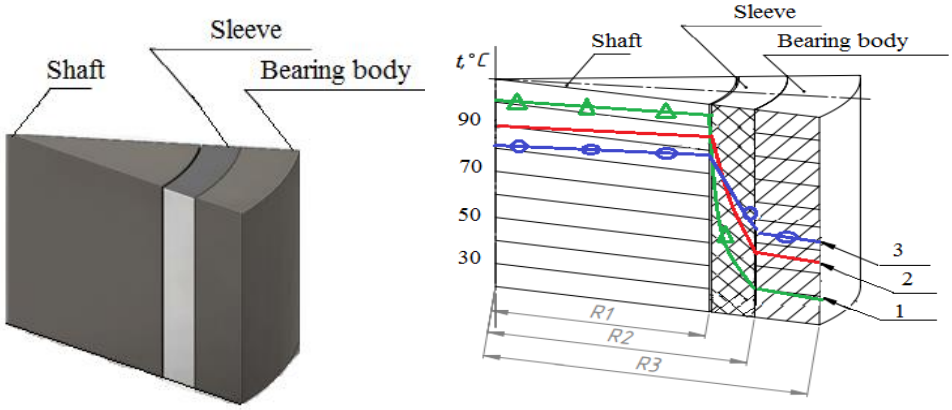

Fig. 2. Temperature distribution in the polymer sleeve bearing (S = 4 mm): 1 - pure polyamide (Ertalon 4.6); 2, 3 - polyamide filled with metal chips (steel 21864) in concentration of 10 and 20% respectively under the action of magnetic field.

By substituting the value t_1 into the expression (3), we get the formula for temperature distribution in the polymer antifriction material on the area limited by the angle θ:

$$t = t_п - \frac{t_п - t_0}{\ln\frac{d_2}{d_1} + \frac{\theta\lambda_2 l}{\alpha_2 F_2'}} \ln\frac{d_{2x}}{d_1}. \tag{9}$$

The obtained temperature of the polymeric composite material is comparable to the maximum permitted temperature [t] of the reference material: t ≤ [t]. If the condition is met - the calculation is complete, if not, it is necessary to change the size of the liner and improve the heat exchange conditions either by reducing the thickness of the antifriction layer, or by increasing the quantity of metal filler to the limit value.

It was found that the sleeve made of a polymer composite material with fine metal filler reduces the temperature on the shaft at an average of 1.15... 1.22 times depending on the concentration of the filler.

In the work, special attention was paid to the dependence of the coefficient of friction of the polyamide on the temperature (fig. 3, a). The dependance of coefficient of friction on temperature is strongly expressed in pure Ertalon 4.6, in composite material with metal filler this dependence is less obvious. The addition of fine steel filler significantly increases the antifriction properties of the Ertalon 4.6 polymer and extends the temperature range of the composite bushing. For example, adding a 10% concentration of the filler reduces the friction

coefficient at an average working temperature of up to 80 °C. Increasing the concentration of the filler to 20% reduces the friction coefficient by 3,6 times and extend the temperature range of the use of composite material to 100 °C.

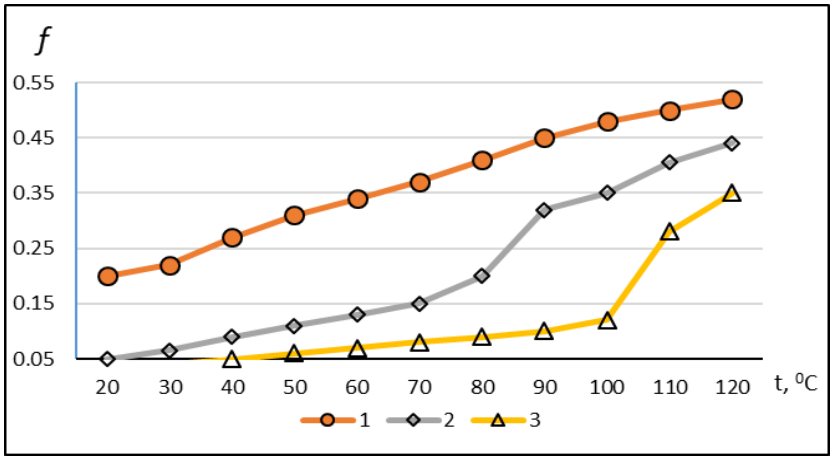

a)

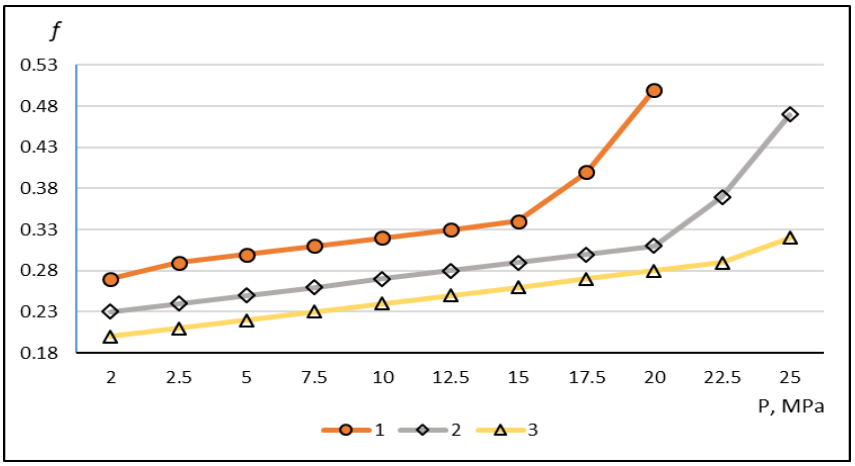

b)

Fig. 3. Dependence of coefficient of friction on temperature at contact load of 7,5 MPa (a) and on the specific load on plain bearing (V = 0,78 m/s; Δ= 0,3 mm, *t* = 50 ^{0}C) (b): 1 - pure polyamide (Ertalon 4.6); 2, 3 - polyamide filled with metal chips (steel 21864) in concentration of 10 and 20% respectively under the action of magnetic field.

Fig. 3, b shows the dependence of the friction coefficient on contact load. It is observed that the working capacity of the sleeve made from pure Ertalon 4.6 polymer reaches contact load of 15 MPa, further increase of contact load leads to sharp increase of coefficient of friction and destruction of the polymer. Adding a fine-dispersion steel filler increases the bearing capacity of the composite sleeve to 20 and 25 MPa at a concentration of 10 and 20% filling respectively.

Thus, the reduction of temperature in the zone of friction contact of plain bearing due to the use of a composite sleeve causes increase of antifriction properties and increase of carrying capacity of a composite, which is a promising direction for introduction of polymeric materials in the aircraft units under the harsh operational conditions.

Conclusions

It was shown that addition of the metal filler in the structure of the polymer plain bearing leads to increased heat dissipation from the bearing contact area and consequently to decrease of the friction coefficient.

Analysis of the laboratory studies shows that the polymer with metal filler has high antifriction properties compared to polymer without filler and in some cases can replace in bearings non-ferrous metals (bronze, babbit).

The use of composite meterial in friction units will extend the service life and reduce the cost of manufacturing such friction units.

References

1. Use of Composites in Bearings,19 February 2001, https://kaman-kargo.com/use-of-composites-in-bearings/.

2. P. Gohil Piyush, H. Parikh Hiral, Composites as TRIBO materials in engineering systems: significance and applicatios. In: Advances in Chemical and Materials Engineering (ACME) Book Series: Processing Techniques and Tribological Behavior of Composite Materials. USA: IGI Publisher, 2015, pp. 168–191.

3. Gordana Bogoeva-Gaceva, Dimko Dimeski, Vineta Srebrenkoska, Friction mechanism of polymers and their composites, Macedonian Journal of Chemistry and Chemical Engineering, Vol. 37, No. 1, pp. 1–11 (2018).

4. Buznik V. M., Yurkov G. Y. Primenenie ftorpolimernyh materialov v tribologii: sostoyanie i perspektivy. – Voprosy materialovedeniya, 2012, № 4(72), s. 133–149.

5. Posharnikov F.V., Serebryanskij A.I., Usikov A.V. Issledovanie vrashchatel'nogo processa treniya v podshipnikah skol'zheniya lesoobrabatyvayushchego oborudovaniya // Lesotekhn. zhurn. 2011. № 2(2). S. 92–95.

6. Posharnikov F.V., Usikov A.V. Snizhenie temperaturnoj napryazhennosti v podshipnikah skol'zheniya s polimernymi antifrikcionnymi materialami // Uchen. zapiski PetrGU. Ser. «Estestv. i tekhn. nauki». 2010. № 8 (113). S. 76–78.

Скворцов О.О., Мікосянчик О.О. Оцінка триботехнічних параметрів композиційного полімеру з металевим наповнювачем

Розглянуто використання композиційного матеріалу на основі поліаміду (капролону) Ertalon 4.6 як антифрикційного матеріалу в вузлах ковзання в авіаційній промисловості. В якості наповнювача композиційного матеріалу використовувалась дрібнодисперсна добавка низьковуглецевої електротехнічної листової сталі 21864 в різних концентраціях. У роботі представлено тепловий розрахунок підшипників ковзання з полімерною вставкою при різних режимах роботи. Визначено, що додавання металевого наповнювача в поліамід обумовлює зниження температури в зоні тертя за рахунок ефективного відведення тепла від валу до корпусу підшипника. Дослідження триботехнічних властивостей запропонованого композиційного матеріалу проводились на установці ПТ-4Ц в умовах ковзання за схемою циліндр – площина, також було проведено моделювання підшипникового вузла у програмному комплексі DS SolidWorks. Експериментально встановлено, що добавка дрібнодисперсного сталевого наповнювача підвищує антифрикційні властивості поліаміду Ertalon 4.6 та розширює температурний діапазон роботоздатності втулки з композитного матеріалу. Підвищення концентрації наповнювача до 20% призводить до зниження коефіцієнту тертя, в середньому, в 3,6 разів та розширення температурного діапазону використання композиційного матеріалу до 100 ^{0}C. Встановлено підвищення несучої здатності втулки з композиційного матеріалу до 25 МПа при концентрації наповнювача 20% відповідно.

Практична значимість роботи полягає в аналізі антифрикційних властивостей полімеру з металевим наповнювачем порівняно з полімером без наповнювача, що дозволить довести ефективність використання таких полімерів у вузлах тертя замість кольорових металів (бронза, бабіт).

Ключові слова: композиційний матеріал, полімер, коефіцієнт тертя, поліамід, підшипник, температура

***Problems of Tribology**, V. 27, No 2/104-2022, 49-54*

Problems of Tribology
Website: http://tribology.khnu.km.ua/index.php/ProbTrib
E-mail: tribosenator@gmail.com

DOI: https://doi.org/10.31891/2079-1372-2022-104-2-49-54

Effect of fullerene-like nanoparticles at low concentrations on the anti-wear properties of motor fuels

V.S. Pyliavsky[1], Y.V. Polunkin[1], O.O. Haidai[1*], O.B. Yanchenko[2]

[1] V.P. Kukhar Institute of Bioorganic Chemistry and Petrochemistry. National Academy of Sciences of Ukraine
[2] Vinnytsia National Technical University, Ukraine
**E-mail: gaidaj@ukr.net*

Received: 04 April 2022: Revised: 29 April 2022: Accept: 22 May 2022

Abstract

Motor fuels are the source of energy for internal combustion engines, and also a lubricant for friction units of the fuel equipment of automobile, aircraft and ship engines. The reliability and service life of the entire mechanism depend on the antiwear properties of fuels. Traditional anti-wear additives containing sulfur, phosphorus, chlorine, etc., are not applicable in motor fuels due to restrictions on emissions of toxic compounds. To improve the antiwear properties of lubricants, it is possible to use a new class of spatial carbon compounds - fullerene-like nanoparticles (FLNs).

This work shows that modification of liquid hydrocarbon motor fuels with fullerene-like nanoparticles (FLNs) increases the antiwear properties of fuels.

Key words: tribological characteristics of lubricants, motor fuels, antiwear additives, bearing capacity, fullerenes and fullerene-like nanoparticles

Introduction

Liquid motor fuels, a source of energy for internal combustion engines, are also a lubricant in the friction units of the fuel equipment of power mechanisms. The reliability of automobile, aircraft, and ship engines depends on the antiwear properties of such fuels [1].

The antiwear properties of lubricants can be improved by using surfactants, as well as unsaturated, aromatic or polycyclic hydrocarbons [2]. However, with a significant content of such components in fuels, their performance characteristics (viscosity, combustion efficiency, corrosivity, filterability, varnish deposits and carbon formation) deteriorate significantly.

Currently, special antiwear additives are added to lubricants to improve antiwear properties, which form chemical secondary structures on metal surfaces with high compressive resistance and reduced shear resistance. A wide range of compounds containing sulfur, phosphorus, chlorine, boron, and other heteroatoms are used as such antiwear additives [3, 4]. However, these additives cannot be used in motor fuels due to environmental restrictions on engine emissions [5]. Moreover, motor fuels are fundamentally different from oils in terms of the implementation of both lubricating effects. The oil is constantly (or for quite a long time) in the zone of frictional contact. The fuel passes through the friction zones of the fuel supply equipment in portions - once and for a short time (pieces of millisecond). For such periods of time, the chemical processes of the interaction of the components of the lubricant with metal surfaces cannot be fully realized.

New spatial nanostructures based on carbon are currently being considered as promising antiwear additives for lubricants. According to the recommendation of the International Union of Pure and Applied Chemistry (IUPAC), single- and multilayer closed spherical polyhedra consisting of carbon pentagonal and hexagonal faces (resembling a soccer ball in structure) are classified as fullerenes (or fullerene-like nanoparticles) [6].

The mechanism of action of fullerene-like nanoparticles on the tribological characteristics of lubricants is explained by the precipitation of fullerenes from the liquid phase on the contact surfaces during friction. It is assumed that a layer of ball-like fullerene nanoparticles formed on the friction surfaces transforms sliding

friction into rolling friction with a decrease in the friction coefficient and minimization of wear out [7]. The role of the lubricating fluid in this case is reduced only to the delivery of fullerenes to the friction zone.

In accordance with such ideas, it should be expected that the positive effect of these additives on the tribological characteristics should increase as the contact surfaces are filled with fullerene particles. In turn, the precipitation of fullerenes accelerates with an increase in their concentration in the solution.

However, fullerene-like nanoparticles are very slightly soluble in hydrocarbon liquids based on alkanes [8]. The literature presents mainly the results of studies of the effect of C_{60} fullerene additives (at concentrations of 1–5 wt %) on the tribological properties of high-viscosity lubricants and oils, where sufficient stability of the compositions is ensured [9, 10].

Even in motor oils, which, for reasons of necessary thermal stability, are based on linear saturated hydrocarbons, fullerenes are poorly dispersed. The solubility of such compounds in aromatic solvents and vegetable oils with a high content of oleic acid is somewhat higher. Therefore, to improve the stability of fullerene components in motor oils, it is proposed to pre-disperse fullerenes in high-oleic vegetable oils, and then add these compositions to mineral oils. This technique was used, for example, during the project [10], where the optimal antiwear properties of lubricating oil were observed at the following ratio of components:

– 1% wt. fullerene C_{60};

– 10% wt. vegetable rapeseed oil;

– 89% wt. mineral motor oil M-10G2k.

But for motor fuels, such methods of fullerene dispersion are unsuitable because of the deterioration of the filterability of fuels.

Up to this moment, in terms of scientific substantiation of the use of fullerene additives in fuels, a contradictory situation has developed:

- on the one hand, they should not settle on filters and precision surfaces of fuel equipment when fuel is supplied to the combustion chambers of engines;

– on the other hand, it is assumed that it is as a result of the deposition of fullerenes that their positive antiwear effect can be realized.

This contradiction prevents the use of fullerene-like nanoparticles in low-viscosity fuels with a predominance of saturated hydrocarbons (gasoline, diesel and aviation fuels). However, advertising materials recommend them as multifunctional additives, for example, to diesel fuels without justifying the permissible concentration limits.

In low-viscosity hydrocarbon fuels, solutions of fullerene-like nanoparticles are stable only when the content of these additives is up to dozens of ppm. Previously, in [11, 12], we showed that the addition of LPF even in the amount of several ppm to gasoline and diesel fuels significantly affects the energy efficiency of fuel combustion. When working with such additives, the engine efficiency increases up to 10-15% and, accordingly, fuel consumption per unit of useful power is reduced by 10-15%.

In the present work, the following questions are studied.

- Do the minimum concentrations of fullerene-like nanoparticles in hydrocarbon liquid motor fuels affect their anti-wear properties?

- If such an influence takes place, is it due to the deposition of fullerene particles on the friction surfaces or is there another mechanism of their action?

The clarification of these issues will make it possible to substantiate the strategy for the use of FLNs in low-viscosity motor fuels.

Materials and methods of experiment

Aviation turbine fuel Jet A-1 was used as the object of study. Some characteristics of the fuel taken for research are given below.

Physical and chemical parameters of aviation fuel Jet A-1.

Fractional composition:

- ✓ distillation start temperature, °C... 150
- ✓ 10% is distilled off at a temperature, °C, not higher... 165
- ✓ 50% is distilled off at a temperature, °C, not higher than ... 195
- ✓ 90% is distilled off at a temperature, °C, not higher than ... 230
- ✓ 98% is distilled off at a temperature, ° C, not higher than ... 250

Kinematic viscosity, mm^2/s: at 20 °C, not less than ... 1.3

Mass fraction of aromatic hydrocarbons, %, not more than ... 22

Concentration of actual resins, mg per 100 cm^3 of fuel, no more than... 3

Mass fraction of total sulfur, %, no more than ... 0.2

During the tests, fuel samples were used in a volume of 25 ml; samples were taken from one batch of fuel. Samples of fuels with additives of fullerene nanoparticles were prepared as follows. Fullerene-like nanoparticles were obtained by high-frequency discharge-pulse synthesis using a light hydrocarbon fraction of propane-butane as

a feedstock [13]. To increase the stability of hydrocarbon solutions of FLNs, the resulting product was brominated in excess liquid bromine at room temperature for 72 hours. Residual bromine was distilled off in vacuum at 20°C.

The isolation of fullerene nanoparticles from the synthesis product and their size fractionation were carried out by extraction in absolute ethanol. The average size of isolated nanoparticles, according to estimates made by electron and atomic force microscopy, was 10–15 nm [11].

Solutions of fullerene nanoparticles in fuel were prepared using an ultrasonic low-frequency (22 kHz ± 10% kHz) disperser. From the resulting stable solution with the maximum concentration of FLNs, solutions with a lower concentration required for the study were prepared by adding calculated amounts of fuel.

The possible effect of the addition of fullerene nanoparticles on the antiwear properties of the fuel was assessed by the change in two tribological characteristics:

- wear indicator (registered by the diameter of the wear spot of mating steel balls);
- bearing capacity (registered by the value of the critical load to scuffing).

The bearing capacity of the fuel and the wear index were determined on a four-ball friction machine according to the method ASTM D2783 [14]. When choosing this method of tribological tests, we were guided by the following considerations. On this machine in the friction unit, the conditions of pure sliding with point contact are reproduced. On such an installation, the constancy of the initial conditions for individual measurements is ensured (the same physical, chemical and geometric characteristics of the frictional interface in the form of balls made of steel SH15 with a diameter of 12.7 mm with equal roughness parameters). Therefore, this method provides high reproducibility of results.

The wear index (diameter of wear spots of mating balls) was measured by the method of fixed loads with a normalized load of 100 N at a rotation frequency of 1500 min^{-1}. The wear scar diameters of the balls were measured at three different trial durations of 2, 3, and 5 min. After each measurement, the balls in the friction assembly were replaced with new ones.

The bearing capacity of fuels was determined by the value of the critical load to scuffing at the temperature of 20 °C, similarly to the ASTM D2596 method.

Characteristics of prototypes

Used alloying compositions of the following composition:

1 - Cr-B4C-Mo-C - 2% chromium, 1% boron carbide, 0.5% molybdenum and 0.4% carbon;
2 - Cr-Mo-V-C - 5% chromium, 1% molybdenum, 1% vanadium, 0.8% carbon;
3 - Cr-Mo-V-C - 10% chromium, 1% molybdenum, 1% vanadium, 0.8% carbon.

Visible defects, micro- and macrocracks are absent for the deposited layers.

From the above data on the chemical composition of the components it is clear that the main alloying elements are chromium with the addition of vanadium, molybdenum or boron carbide in the presence of carbon.

Results of research and discussion

According to those results of tribological tests shown in Fig. 1 and 2, the modification of liquid hydrocarbon fuels with low concentrations of FLNs improves the antiwear properties of fuels.

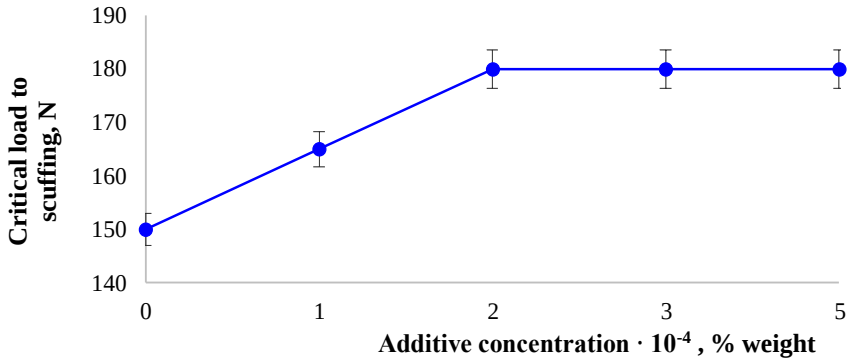

Fig. 1. Dependence of the bearing capacity of turbine fuel Jet A-1 on the concentration of the FLNs additive

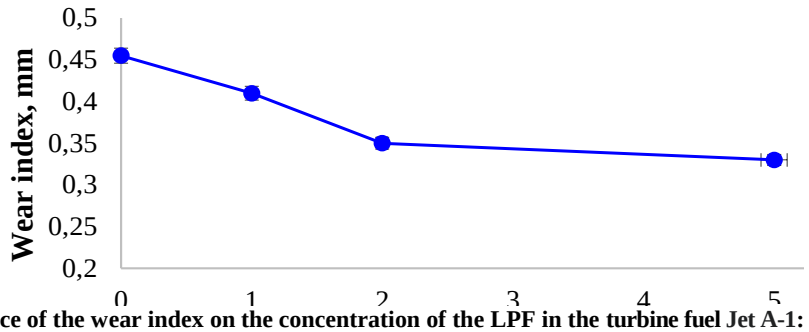

Fig. 2. Dependence of the wear index on the concentration of the LPF in the turbine fuel Jet A-1: the duration of the tribological tests is 5 min

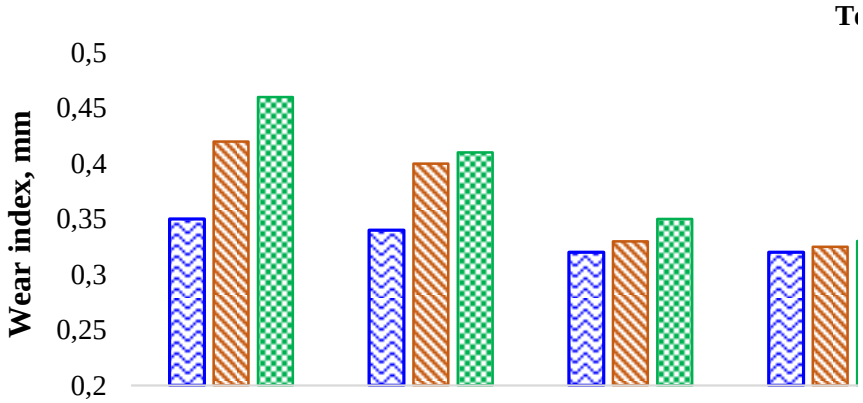

Fig. 3. Change in the wear index with an increase in the duration of the friction process in the turbine fuel Jet A-1: without additive (0) and at three different concentrations of FLNs (1, 2 and $5 \cdot 10^{-4}$, % wt.)

In the presence of fullerenes in the composition of the fuel, the bearing capacity increases and the wear index decreases. As the additive concentration increases, both of these tribological characteristics change no monotonically.

The bearing capacity increases most sharply in the initial range of the investigated additive concentrations, and then stabilizes. The optimal value of the FLNs concentration in terms of increasing the carrying capacity of the fuel was observed at $2 \cdot 10^{-4}$ % wt., with a further increase in the FLNs concentration, this characteristic practically does not change.

The dependence of the wear index (wear scar diameter) on the additive concentration in the fuel is non-linear. As can be seen from the diagrams in Fig. 2, this indicator also decreases most sharply in comparison with tests in fuel without additives at FLNs concentrations in the region up to $2 \cdot 10^{-4}$ % wt. At an additive concentration above this value, a decrease in the wear index is also observed (in contrast to the bearing capacity, which plateaued at this concentration), but this change is very weak.

The dependence of the wear index on the duration of the testing process is interesting (Fig. 3). This dependence is different for different concentrations of the FLNs additive in the fuel. In the absence of FLNs additives in the fuel and at their low concentrations, the wear indicator noticeably increases with an increase in the duration of tribological tests. At additive concentrations of 2 ppm and more, the amount of wear changes slightly with an increase in the duration of the friction process.

The results obtained can be explained as follows.

There is currently no generally accepted point of view on the mechanisms and processes underlying the various effects of ultra-low doses of additives on the behavior and properties of bulk phases (both liquid and solid). As a rule, the explanation of such effects can be reduced to one of two hypotheses.

According to one of these hypotheses, the effect of additives in micro quantities is caused by the concentration of the active ingredient in certain local volumes. As a result, the amount of a substance in such micro volumes can be several orders of magnitude higher than the initial average concentration in the solution, and the course of processes in these volumes is determined by the properties and behavior of the group of particles.

In the framework of another hypothesis, the influence of micro quantities of additional substances is associated with their coordinating (controlling) effect on the particles of the medium and the restructuring of the structural organization of these particles throughout the volume.

Based on such general ideas, it should be assumed that the effect of small doses of fullerenes on the antiwear properties of fuel can be due to the superposition of two different effects:

– Concentration of the additive substance in the most loaded areas of the friction surface due to the deposition of fullerenes.

– The coordinating effect of fullerenes on the molecules of the liquid phase with the rearrangement of the supramolecular structure of the fuel in the volume.

It is possible to single out the influence of these two effects on the basis of the fact that their action should be reflected differently on different tribological characteristics.

Indeed, the bearing capacity is a characteristic of the instantaneous state of the tribosystem. When measuring this characteristic, tribological tests are short-term (test time is 10 s). Therefore, this characteristic should not be affected by the rather inertial process of deposition of fullerene particles from the liquid phase onto the contact surfaces. Changes in this tribological characteristic of fuel in the presence of fullerenes in it are mainly due to processes occurring in the liquid phase, and not on the surface of solids.

When determining the wear indicator (wear scar diameter), the process of tribological testing is relatively long (from several minutes to 1 hour). Therefore, this indicator can depend both on processes in the liquid phase and on the slow-in-time phenomenon of deposition of fullerene nanoparticles from solution onto solid surfaces.

The obtained results of the study indicate that the change in tribological characteristics when FLNs is added to the fuel is indeed due to the superposition of two effects.

An increase in the fuel carrying capacity is observed only with an increase in the concentration of fullerenes up to 2 ppm. With an increase in the concentration of FLNs in the solution above 2 ppm, this tribological characteristic practically does not change.

Apparently, this effect can be associated with the formation of the domain structure of solvent molecules around the center-forming nanoparticles of the additive [18, 19]. At the additive concentration limit of 2 ppm, saturation is reached, i.e. filling the entire volume of the solution with such domain formations. In the region of an increased concentration of the additive (exceeding 2 ppm), clustering of the particles of the additive between themselves is possible, which is accompanied by a decrease in the effectiveness of the effect of such associates on the properties of the solution compared to the efficiency of individual nanoparticles [14].

However, the wear indicator continues to decrease somewhat with an increase in the content of fullerenes in the solution above 2 ppm. The change in the wear index in this concentration range can apparently be explained by the deposition of fullerene nanoparticles on the friction surface. However, the influence of this effect on the antiwear properties of the fuel under the given conditions of tribological testing is less significant than the effect of nanoparticles on the change in the structure of the liquid phase.

Conclusions

1. Modification of liquid hydrocarbon motor fuels with fullerene-like nanoparticles (FLNs) increases the antiwear properties of fuels.

2. The effect of low concentrations of FLNs on the antiwear properties of liquid hydrocarbon fuels is mainly associated with the effect on the structure of the liquid phase and, to a lesser extent, with the deposition of fullerene nanoparticles on the friction surface.

3. Based on the obtained results, a strategy for the use of FLNs in hydrocarbon liquid motor fuels is substantiated. In such petroleum products, additives based on fullerene-like nanoparticles are advisable to use at concentrations of several ppm. A further increase in the concentration of the additive does not lead to a significant increase in antiwear properties, but may impair the efficiency of engines due to deposits on filters and on working surfaces.

References

1. Hsieh P.Y., Bruno T.J. A perspective on the origin of lubricity in petroleum distillate motor Fuels. *Fuel Processing Technology*. 2015. V. 129. P. 52–60.

2. Likhterova N.M., Seleznev M.V., Goryunova A.K. Tribologicheskiye kharakteristiki sovremennykh aviatsionnykh kerosinov. Neftepererabotka i neftekhimiya. 2019. № 7. S. 35–40.

3. Zhang J., Spikes H. On the Mechanism of ZDDP Antiwear Film Formation. *Tribol. Lett.* 2016. V. 63. P. 3–27.

4. Rastogi R.B., Maurya J.L., Jaiswal V. Phosphorous free antiwear formulations: zinc thiosemicarbazones–borate ester mixtures. *Proc. IMechE, Part J: J Engineering Tribology.* 2012. V. 227. P. 220–233.

5. The technical regulations for automobile gasoline, diesel, ship and boiler fuels. Cabinet of Ministers of Ukraine, 2013, 22p.

6. Lyubchuk T.V. Fulereny ta inshi aromatychni poverkhni (struktura, stabil'nist', shlyakhy utvorennya). K.: Vydavnycho-polihrafichnyy tsentr “Kyyivs'kyy universytet”. 2005. 322 s.

7. Tuktarov A.R., Khuzin A.A., Dzhemilev U.M. Fullerenosoderzhashchiye smazochnyye materialy: dostizheniya i perspektivy (obzor). Neftekhimiya. 2020. T. 60, № 1. S. 125–147.

8. Yeletskiy A.V. Fullereny v rastvorakh. Teplofizika vysokikh temperatur. 1996. T. 34, № 2. S. 308–323.

9. Ginzburg B.M., Baydakova M.V., Kireyenko O.F., Tochil'nikov D.G., Shepelevskiy A.A. Vliyaniye fullerena C60, fullerenovykh sazh i drugikh uglerodnykh materialov na granichnoye treniye skol'zheniya metallov. Zhurnal tekhnicheskoy fiziki. 2000. T. 70, Vyp. 12. S. 87–97.

10. Kravtsov A.G. Modelirovaniye formirovaniya maslyanoy plenki na poverkhnosti treniya pri nalichii fullerenovykh dobavok v smazochnom materiale i yeye vliyaniye na skorost' iznashivaniya tribosistem. Problems of Tribology. 2018. № 1. S. 69–77.

11. Polunkin YE.V., Pylyavs'kyy V.S., Bereznyts'kyy YA.O., Kamenyeva T.M., Levterov A.M., Avramenko A.M. Pokrashchennya khimmotolohichnykh vlastyvostey dyzel'noho palyva mikrodobavkoyu vuhletsevykh sferoyidal'nykh nanochastok. Kataliz ta naftokhimiya. 2020. №. 29. S. 59–64.

12. Increasing surface wear resistance of engines by nanosized carbohydrate clusters when using ethanol motor fuels / O.O. Haiday, V.S. Pyliavsky, Y.V. Polunkin, Y.O. Bereznytsky, O.B. Yanchenko, A. Smolarz, P. Droździel, S. Amirgaliyeva, and S. Rakhmetullina. *Mechatronic Systems 1*. London, 2021. P.89-99. URL: https://doi.org/10.1201/9781003224136-8

13. Rud' A.D., Kuskova N.I., Boguslavskiy L.Z., Kir'yan I.M., Zelinskaya G.M., Belyy N.M. Strukturno-energeticheskiye aspekty sinteza uglerodnykh nanomaterialov vysokovol'tnymi elektrorazryadnymi metodami. Khimiya i khimicheskaya tekhnologiya. 2013. T. 56, Vyp. 7. S. 99–104.

14. Yadav G., Tiwari S., Jain M.L. Tribological analysis of extreme pressure and anti-wear properties of engine lubricating oil using four ball tester. *Materials Today*. 2018. V. 5, No. 1. Part 1. P. 248–253.

Пилявський В.С., Полункін Є.В., Гайдай О.О., Янченко О.Б. Вплив фулереноподібних наночастинок у малих концентраціях на протизносні властивості моторних палив

Моторні палива є джерелом енергії для двигунів внутрішнього згоряння, а також мастилом для вузлів тертя паливної апаратури автомобільних, авіаційних і суднових двигунів. Від протизносних властивостей палив залежить надійність і термін служби всього механізму. Традиційні протизносні присадки, що містять сірку, фосфор, хлор тощо, не застосовуються в моторних паливах через обмеження на викиди токсичних сполук. Для покращення протизносних властивостей мастильних матеріалів можливе використання нового класу просторових вуглецевих сполук – фулереноподібних наночастинок (ФНЧ).

У даній роботі показано, що модифікація рідких вуглеводневих моторних палив фулереноподібними наночастинками (ФНЧ) підвищує протизносні властивості палива.

Ключові слова: трибологічні характеристики мастильних матеріалів, моторні палива, протизносні присадки, несуча здатність, фулерени та фулереноподібні наночастинки

***Problems of Tribology**, V. 27, No 2/104-2022, 55-63*

Problems of Tribology
Website: http://tribology.khnu.km.ua/index.php/ProbTrib
E-mail: tribosenator@gmail.com

DOI: https://doi.org/10.31891/2079-1372-2022-104-2-55-63

Thermodynamic substantiation of the direction of nonequilibrium processes in triadconjugations of machine parts based on the principles of maximum and minimum entropy

V.V. Aulin*, S.V. Lysenko, A.V. Hrynkiv , D.V. Holub

Central Ukrainian National Technical University , Ukraine
** E-mail: AulinVV @ gmail.com*

Received: 05 April 2022: Revised: 05 May 2022: Accept: 27 May 2022

Abstract

The article gives a thermodynamic substantiation of the direction of nonequilibrium processes in tribocouples of machine parts, in tribosystems, based on the principles of maximum and minimum entropy. It is clarified how nonequilibrium processes can be substantiated on the basis of the minimum and maximum function of entropy production: linear and nonlinear nonequilibrium processes and their different thermodynamics. The entropy production function is considered as a function of thermodynamic force flows and thermodynamic flows.

The theory of nonequilibrium processes is based on the Liouville equation for classical tribosystems, taking into account external influences or perturbations. It is shown that in thermodynamic processes in tribosystems the principle of entropy maximization is realized as the second principle of synergetics.

Key words: triadconjugation of details, nonequilibrium processes, thermodynamics, synergetics, entropy, thermodynamic flow

Introduction

The essence of the principle of maximum entropy production G. Ziegler is that the evolution of the nonequilibrium tribosystem develops in the direction of maximizing the production of entropy in it under given external constraints. The second law of thermodynamics in the language of entropy production is formulated as follows: entropy production $\sigma_S \geq 0$ not only has a positive value, but also goes to the maximum.

Given the statistical interpretation of entropy and the work of Boltzmann and Gibbs, entropy, and consequently its production, tends to increase to the maximum level assumed by the constraints imposed on tribosystems. The final equilibrium state of the tribosystem is the most probable and is described by the maximum number of microstates. Such a statistical interpretation allows us to consider the principle of maximum entropy production as a natural generalization of its Clausius-Boltzmann-Gibbs formulation, and in some cases as a consequence.

Literature review

The peculiarity of nonequilibrium thermodynamics in tribosystems is initially based on the equations of balance of entropy, momentum energy and matter and on the first two laws of thermodynamics [1,2] .

Compared with the principle of I. Prigogine [4] , the principle of G. Ziegler [5] describes a wider range in the evolution of nonequilibrium tribosystems and is a more generalized approach in their study and study of the relationship of characteristics and properties with entropy (entropy production) [3] . G. Ziegler's principle makes it possible to constructively construct both linear and nonlinear thermodynamics. It follows that Onsager's variational principle is valid only for linear nonequilibrium thermodynamics of tribosystems [4,6] . At that time, the principle of Onsager-Diarmati, as a partial statement, is valid for stationary processes, in the presence of free forces. From it follows the principle of I. Prigogine [7-9]. If given thermodynamic forces (flows), then, based on

the principle of G. Ziegler, the tribo system will adjust its thermodynamic flows (forces) to $\sigma_S \Rightarrow \max$ [10-12]. If σ_s it is a quadratic function, then the relationship between flows and forces in the tribosystem is adjusted as a result. If the system is in a stationary weakly nonequilibrium state, but part of the thermodynamic forces remains free, then the currents generated by Ziegler will begin to reduce the thermodynamic forces, and those in turn - thermodynamic flows. As a result, the production of entropy is minimized: $\sigma_S \Rightarrow \min$ [4].

It is possible to substantiate nonequilibrium processes in tribosystems by the methods of general statistical theory [13-15]. Classical kinetic theory is not suitable for relatively dense tribosystems with a strong interaction between their elements and particles. The problem is to create a nonequilibrium microscopic theory that can describe such systems. This is primarily to obtain the equations of energy transfer, momentum, mass and calculation of kinetic coefficients directly from the equations of classical and quantum mechanics. Such a statistical theory began to develop intensively from the middle of the twentieth century [16,17]. L. Onsager stated: the temporal evolution of the function of a given physical quantity in the equilibrium system occurs on average by the same laws as the change of the corresponding macroscopic variable in the nonequilibrium system [1,2,10,18].

Being in an unbalanced state, the tribosystem does not feel how it got into it - due to fluctuations or due to external influences, and therefore its next reaction must be the same. As a result of relaxation of the nonequilibrium tribosystem near the state of equilibrium and resorption of fluctuations will occur according to the same laws [19,20].

Purpose

The aim of this work is a thermodynamic substantiation based on the maximum entropy of the direction of nonequilibrium processes occurring in the triad conjugations of machine parts.

Results

If the tribosystem, the conjugation of machine parts, is in some nonequilibrium state, then after some time (relaxation time) it will come to an equilibrium state from the set of possible states for which the entropy will be maximum. The change in entropy during this period of time will be the maximum among the possible, and therefore the maximum becomes the production of entropy. The variational principle gives possible relations of linear nonequilibrium thermodynamics:

$$J_i = \sum_k L_{ik} X_k \; ; \qquad L_{ik} = L_{ki}, \tag{1}$$

where L_{ik} – the matrix of kinetic coefficients independent of J_i and X_k.

The system of equations (1) makes it possible to describe the transfer of entropy, momentum, mass. The above equations (1) are valid for relatively small thermodynamic forces, when the relationship between forces and flows is almost linear. This is L. Onsager's first deductive formulation of linear nonequilibrium thermodynamics. If the values of irreversible forces are given X_i, then the true flows J_i maximize the expression $[\sigma_S(X_i, J_k) - \Phi(J_i, J_k)]$. The variation in flow J at constant *X* is equal to:

$$\delta_J [\sigma_S(X_i, J_k) - \Phi(J_i, J_k)]_X = 0; \tag{2}$$

$$\Phi(J_i, J_k) = \frac{1}{2} \sum_{i,k} R_{ik} J_i J_k \; , \tag{3}$$

where Φ – the scattering potential ($\Phi > 0$); R_{ik} – coefficient matrix, inverse matrix L_{ik}, matrix R_{ik} – can be considered a system tensor, which should be considered as the sum of symmetric S_{ik} and antisymmetric A_{ik} tensors:

$$\Phi = \frac{1}{2} \sum_{i,k} \left(S_{ik} J_i J_k + A_{ik} J_i J_k \right). \tag{4}$$

Because for the antisymmetric tensor $A_{ii} = 0$ and $A_{ik} = -A_{ki}$, the antisymmetric part of the tensor R_{ik} in equation (3) does not contribute to the scattering potential Φ and the tensor R_{ik} becomes symmetric

$R_{ik} = R_{ki}$. Substituting the expression $\sigma_S = \sum_i X_i J_i$ into equation (2), as well as transforming (3) by replacing the variation derivative over the corresponding flows, we obtain:

$$\frac{\partial}{\partial J_i}\left[\sum_i X_i J_i - \frac{1}{2}\sum_{i,k} R_{ik} J_i J_k\right]_{x=const} = 0. \tag{5}$$

The equation for thermodynamic force after differentiation will look like:

$$X_i = \frac{1}{2}\sum_k (R_{jk} + R_{kj}) J_k = \sum_k R_{kj} J_k . \tag{6}$$

Since the flow function is nonnegative $\Phi \geq 0$, the solution of equation (6) with respect to unknown flows is equal to:

$$J_j = \sum_k R_{jk}^{-1} X_k = \sum_k L_{jk} X_k , \tag{7}$$

where $R_{jk}^{-1} = L_{jk}$. In this case R_{jk} – a symmetric matrix, it is R_{jk}^{-1} also symmetric.

This suggests that the expression $[\sigma_S(X_i, J_k) - \Phi(J_i, J_k)]$ in equation (2) has one extreme point X_i, J_k, which is described by expressions (6) and (7). Because the flow function Φ is a homogeneous quadratic positive function, this point is the point of maximum.

Note that the Onsager variation principle is formulated for thermodynamic flows in the tribosystem. For the space of forces in the tribosystem, according to I. Diarmati, if the values of thermodynamic flows are given J_i, then the irreversible existing forces X_i maximize the expressions $\sigma_S(X_i, J_i) - Y(X_i, X_k)$, ie we have:

$$\delta_X [\sigma_S(X_i, J_i) - Y(X_i, X_k)]_J = 0; \tag{8}$$

$$Y(X_i, X_k) = \frac{1}{2}\sum_{i,k} L_{ik} X_i X_k , \tag{9}$$

where $Y(X_i, X_k) > 0$ is the scattering potential in the force space of the tribosystem.

Analysis of entropy production shows that its function is a symmetric bilinear form. Then according to the principle of Diarmati equation (2); (3) and (8), (9) are equivalent.

The principle of minimum entropy production, formulated by I. Prigogine, against the background of the apparatus of nonequilibrium thermodynamics also describes various nonequilibrium processes supported by constant applications of irreversible forces $X_i, i = \overline{1, j}$ where $j \leq n$, *n* is the number of forces in the system and entropy production is minimal $i = j+1,..., n$, disappear.

Prigogine's principle is a simple consequence of the Onsager-Diarmati principle. The theory of linear nonequilibrium thermodynamics is widely used in tribosystems:

– it becomes possible to solve the system of equations of mass transfer, momentum and energy, because the number of equations is equal to the number of unknowns;

– using non-diagonal coefficients L_{ik}, it becomes possible to describe cross-flows in chemical, electrical and other kinetic processes;

– it is possible to obtain additional information about the values of kinetic coefficients;

– the presence of entropy production values σ_s that have extreme values in the nonequilibrium state allows to obtain additional information about the characteristics and properties of the tribosystem.

Note that linear nonequilibrium thermodynamics in tribosystems describes thermodynamic forces of small magnitude. Linear nonequilibrium thermodynamics cannot explain and describe the fundamental problems of self-organization, oscillatory processes, etc. Onsager's linear thermodynamics in thermodynamic theory is generalized to the nonlinear case on the basis of the maximum entropy production (G. Ziegler's principle). In the flow space $\{J_k\}$ we have:

$$\sigma_S(J_i) = \sum_k X_k(J_i) J_k . \tag{10}$$

To find the functional dependence $X_k(J_k)$, G. Ziegler proposed the principle of maximum entropy production σ_S: if an irreversible thermodynamic force X_i is given, then the true flow J_i that satisfies the equation $\sigma_S(J_i) = \sum_i X_i J_i$ contributes to the maximum entropy production. σ_S [5] .

This principle can be widely used in the theory of plasticity in the form of the principle of maximum rate of dissipation of mechanical energy (Mises principle): the rate of dissipation of mechanical energy per unit volume during plastic deformation has maximum value for the actual stress state among all stress states. plasticity. The strain rate is considered fixed. This principle of the theory of plasticity is in fact generalized to all nonequilibrium thermodynamics.

For nonequilibrium processes described by linear nonequilibrium thermodynamics, in the tribosystem at a given complex of forces there is always a maximization of the $\sigma_s(J_i) \Rightarrow \max$ entropy production function, ie from the Ziegler principle we can obtain the Onsager principle. G. Ziegler's principle is realized in the system of equations:

$$\begin{cases} \dfrac{\partial}{\partial j_i}\left[\sum_{i,k} R_{ik} J_i J_k - \mu\left(\sum_{i,k} R_{ik} J_i J_k - \sum_i X_i J_i\right)\right]_{X,\mu=const} = 0 \\ \sum_{i,k} R_{ik} J_i J_k = \sum_i X_i J_i \end{cases}. \qquad (11)$$

Where the space of thermodynamic forces is determined by the expression:

$$X_i = \frac{2\cdot(\mu-1)}{\mu}\sum_k R_{ik} J_k \ . \qquad (12)$$

Substituting the last expression for the thermodynamic force in the second equation of system (11), we obtain: $2\cdot\left(\dfrac{\mu-1}{\mu}\right) = 1$ ie $\mu = 2$.

Given this, we have:

$$\delta_J \cdot \left[\sum_{i,k} R_{ik} J_i J_k - 2\cdot\left(\sum_{i,k} R_{ik} J_i J_k - \sum_i X_i J_i\right)\right]_{X=const} = 0 . \qquad (13)$$

Taking into account equation (10) and making some transformations, we obtain:

$$\delta_J\left[\sigma_S - \frac{1}{2}\sum_{i,k} R_{ik} J_i J_k\right]_{X=const} = 0 \text{, or } \partial_J\left[\sigma_S(X_i, J_k) - \Phi(J_i, J_k)\right]_{X=const} = 0 . \qquad (14)$$

The latter indicates that the principle of G. Ziegler follows the variational principle of Onsager.

The research shows that the function of entropy production, as a function of flows, is convex, and G. Ziegler's principle proves a mutually unambiguous correspondence between flows and forces and triadconjugations of details. This is confirmed by the geometric interpretation of the function $\sigma_S(J_i)$: it $\sigma_S(J_i)$ tries to go to zero when $J_i \to 0$, and the whole surface $\sigma_S(J_i)$ is sign-defined. When $\sigma_S(J_i) \le 0$, for arbitrary values of forces, the line of intersection of the surface $\sigma_S(J_i)$ and the plane $\sum_i X_i J_i$ will lie in the negative region and $\sigma_S \Rightarrow \max$ corresponds to this line.

Based on the principle of G. Ziegler, it can be argued that there can never be physically realized states of tribosystems with negative entropy production, ie always $\sigma_s \ge 0$. In the variational construction of nonequilibrium thermodynamics, a particular species σ_s is postulated, J_i and X_i there is some freedom in expression.

If in the tribosystem there are two thermodynamic forces X_1 and X_2, which are known functions of flows J_1 and J_2. The entropy production in this case is equal to:

$$\sigma_S(J_1, J_2) = X_1(J_1, J_2)J_1 + X_2(J_1, J_2)J_1. \tag{15}$$

The orthogonality condition is:

$$X_k^* = \frac{\partial \sigma_S}{\partial J_k}; k = \overline{1,n}; \tag{16}$$

$$\lambda = \sigma_S \left(\sum_{k=1}^{2} \frac{\partial \sigma_S}{\partial J_k} J_k \right)^{-1}. \tag{17}$$

Converting (16) and (17), taking into account (15), we obtain:

$$X_1^* = X_1 + \Delta / J_1 ,, \qquad X_2^* = X_2 - \Delta / J_2 -$$

where Δ is the deviation from the orthogonality condition, which is finally in these conditions equal to:

$$\Delta = -\frac{\lambda J_1 J_2}{\sigma_S} \left(X_1 J_1 \frac{\partial X_1}{\partial J_1} - X_2 J_2 \frac{\partial X_2}{\partial J_2} + X_1 J_2 \frac{\partial X_2}{\partial J_2} - X_2 J_1 \frac{\partial X_1}{\partial J_1} \right). \tag{18}$$

Assuming that $\Delta \to 0$, we have:

$$X_2(J_1, J_2) \frac{\partial \sigma_S(J_1, J_2)}{\partial J_1} = X_1(J_1, J_2) \frac{\partial \sigma_S(J_1, J_2)}{\partial J_2}. \tag{19}$$

Equation (19) defines a class of functions σ_s for which thermodynamic forces are determined. It is valid for the quadratic function σ_S (15) if the Onsager reciprocity relations are valid.

If we assume that the fluctuation of quantities a_i near the equilibrium state occurs according to a linear law (proportional to X_i) and that they are ergodic, we can obtain reciprocity and give kinetic coefficients L_{ij} through time correlation functions to quickly change $\dot{a}_i$ the corresponding values:

$$L_{ij} \cong \int_0^\infty \overline{\dot{a}_i(t)\dot{a}_j(o)} dt, \tag{20}$$

where $\overline{\dot{a}_i(t)\dot{a}_j(o)}$ is the averaging over the equilibrium ensemble of functions $\dot{a}_i(t)$ with the distribution function $P(a)$:

$$P(\vec{a}) \cong \exp\left(-\frac{\Delta S(a)}{k_B} \right), \tag{21}$$

where k_B – the Boltzmann constant; $\Delta S(a)$ – change of entropy at fluctuation $\Delta S(a) = S_{eq} - S$; S_{eq} – entropy system in equilibrium; $\vec{a}(a_e ... a_i ... a_j)$ – a set of values that characterize the system.

The physical meaning of expression (20) is as follows: the longer the fluctuation, ie, the slower the attenuation of the correlation function, the greater the canonical coefficient.

Let the tribosystem at the moment t_0 be in an unbalanced state with entropy S_0. Until the next time *t*, when the difference $t - t_0$ is significantly longer than the duration of one interaction, but less than the relaxation time, the system can go to one of the states with entropy $S_1 \ldots S_N$ ($S_1 < \ldots < S_N$) . Due to the fact that the ongoing process in the tribosystem is spontaneous, the entropy S_i, will be greater than S_0. According to Onsager's approach, the transition to the state with entropy S_N will be the most probable. Each of the states S_1.. S_N can be considered as a fluctuation, the probability of which is greater the greater the entropy of the equilibrium state $S_{eq} - S_N \Rightarrow \min$. As a result, the value $\frac{S_N - S_0}{t - t_0}$ will be maximum possible and the system evolves according to the principle of maximum entropy production $\sigma_S \Rightarrow \max$.

Modern theory of nonequilibrium processes is characterized by a great variety of approaches, but the main ideas are quite close to each other [21,22]. The Liouville equations [23,24] for classical tribosystems are taken as a basis:

$$\frac{\partial \rho_q}{\partial t} + i_y L_l \rho_q = 0, \tag{22}$$

where $\rho_q(q, p, t)$ is the phase function of the particle distribution of the triboelement material; q , p – coordinates and momentum in $6N$ – dimensional space; t – time; i_y – imaginary unit; L_l *is* a linear Liouville operator.

$$iL_l\varphi = \{\varphi, H\} = \sum_k \left(\frac{\partial \rho}{\partial q_k}\frac{\partial H_r}{\partial P_k} - \frac{\partial \varphi}{\partial P_k}\frac{\partial H_r}{\partial q_k} \right), \tag{23}$$

where φ is a function; H_r is the Hamiltonian of the system, $H_r = H_r(q,p,t)$.

We believe that the nonequilibrium macroscopic state is described by a set of observed quantities $\overline{P_m}^t$, which is the average value of the corresponding basic dynamic variables P_m (energy, momentum, number of particles). Since $\overline{P_m}^t$ it does not unambiguously define the distribution $\rho(t)$, we choose the one that corresponds to the principle of max information entropy. Finally get the quasi-equilibrium distribution ρ_q:

$$\rho_q(t) = \exp(-\Phi(t) - \sum_m F_m(t) P_m), \tag{24}$$

where

$$\Phi(t) = \ln\left(\int \exp\left\{ -\sum_m F_m(t) P_m \right\} d\Gamma \right) - \tag{25}$$

the Masier-Planck function, which is determined from the rationing condition, and the Lagrangian factors $F_m(t)$ are selected from the self-matching condition:

$$\overline{P_m}^t = \overline{P_m}_q^t = \int \rho_q P_m d\Gamma, \tag{26}$$

where $d\Gamma = dqdp/(N! h_p^{3N})$, N – the number of particles of the material of the tribosystem element, h_p – the Planck constant.

Based on equality (26), the average values on the quasi-equilibrium ensemble (24) coincide with the true value of the macroscopic quantities.

Let at some point in time t' we have:

$$\rho(t') = \rho_q(t'), \tag{27}$$

Then the solution of Liouville's equation (22) is a function [44,45]:

$$\rho(t) = \exp(-i(t-t')L)\rho_q(t'). \tag{28}$$

It is determined that due to the significant infinity of classical phase trajectories, the behavior of the macrosystem at considerable time intervals should not depend on the microscopic characteristics of the initial conditions. Evolution with equal probability can begin with any state $\rho_q(t')$ in the time interval from t_0 to t and the distribution takes the form:

$$\rho(t) = \frac{1}{t - t_0} \int_{t_0}^{t} \exp(-i(t-t')L)\rho_q(t')dt'. \tag{29}$$

After some transformations of equation (16) we have:

$$\rho(t) = \lim_{\varepsilon \to +0} \varepsilon \int_{-\infty}^{t} \exp(-\varepsilon(t-t'))\exp(-i(t-t')L)\rho_q(t')dt'. \tag{30}$$

Note that the preboundary statistical distribution satisfies the Liouville equation with an infinitesimal source on the right:

$$\frac{\partial \rho}{\partial t} + iL\rho = -\varepsilon\{\rho(t) - \rho_q(t)\}. \tag{31}$$

When $\varepsilon \to 0$, the source selects the "delayed solution" of this equation and describes the irreversible evolution of the system.

Correlations (30, 31) form the basis of the method of nonequilibrium statistical operator, which can be used to obtain kinetic, hydrodynamic or relaxation equations that describe the evolution of the nonequilibrium system at different time scales [1-3,9]. Note that the idea of the method is similar to the ideas and results of other existing approaches to building a general theory of nonequilibrium processes from the first principles.

If the effect or perturbations that disturb the equilibrium of the tribosystem are weak enough, then the given equations can be simplified by leaving linear perturbation corrections to the equilibrium values according to the theory of linear reactions.

Let the perturbation be represented as an expression $\sum_j H_j B_j$, where H_j are some stationary external fields; B_j – conjugate dynamic variables. The stationary equations of the reaction parameters of the system F_m for this perturbation has the form:

$$\psi_m = \sum_n D_{mn} F_n , \tag{32}$$

where $D_{mn} = \overline{(P_m; \dot{P}_n)}_{i\varepsilon}$ – generalized transition probability; $\psi_m = \sum_j \overline{(P_m; \dot{B}_j)}_{i\varepsilon} H_j$ – drift member.

Variational principle can be used to solve equations (32). The test set of reaction parameters of the system satisfies the condition:

$$\sum_m F'_m \psi_m = \sum_{mn} F'_m D_{mn} F_n . \tag{33}$$

Based on this, we can formulate and prove the following principle: the response parameters of the tribosystem, which is the solution (32), maximize among all functions $\{F'_m\}$, subject to condition (33), the entropy production of the system is equal $\sum_j H_j \overline{B}_j^t$ to the positive constant factor. According to this principle, there is a selection of flows (response parameters) that maximize the production of entropy at given forces. A similar generalization was made by H. Nakano, who pointed not only to the maximum entropy production σ_s, but also to the maximization of the transfer coefficients determined by the linear reaction theory. Given the universality of the principle of maximizing information entropy G. Hacken, considers the second beginning of synergetics [13,25].

If the external production of entropy is equal $\sigma_{Se} = \sum_i X_i I_i$, then the internal production of entropy $\sigma_i(\Theta)$, where Θ the microscopic parameters describing the internal state of the elements of the tribosystem of the system. If the thermodynamic forces X_i are fixed and maintain the state of the tribosystem, which evolves from some initial state to stationary with parameters Θ^* with the relaxation time of the system τ, then to produce the entropy of any stationary nonequilibrium state internal and external σ_s must be equal $\sigma_i(\Theta^*) = \sum_i X_i J_i(\Theta)$.

Conclusions

1. There is some hierarchy of processes developing in tribosystems: at short intervals the system maximizes the production of entropy $\sigma_s \Rightarrow \max$ at given fixed forces at the observed time, and as a result linear relations will be valid (1); on a large scale, the system varies with free thermodynamic forces to reduce entropy production $\sigma_s \Rightarrow \min$. This indicates that the speed of the tribosystem's attempt to reach the state with maximum entropy is the highest.

2. The system at each time so selects its thermodynamic flows at fixed thermodynamic forces, so that the change in entropy was maximum and, accordingly, the movement of the tribosystem to the final state is the fastest. This occurs continuously or abruptly (at bifurcation points), depending on the specifics of the system. In the latter case, several forces can correspond to one force at the same time, from which the one that satisfies the Ziegler principle is selected, because the relationship between flows and forces is ambiguous.

3. To construct nonequilibrium statistical mechanics of tribosystems based on the Liouville equation, it is necessary to obtain time-irreversible transfer equations. The transition to the irreversibility of processes in tribosystems is due to the rejection of a complete description of the distribution function to a brief description of their nonequilibrium states and states of elements.

References

1. Aulin VV (2014). Fizychni osnovy protsesiv i staniv samoorhanizatsii v trybotekhnichnykh systemakh: monohrafiia [Kirovohrad: TOV "KOD"] 369 c.

2. Aulin VV (2015). Trybofizychni osnovy pidvyshchennia zosostiikosti detalei ta robochykh orhaniv silskohospodarskoi tekhniky [dys. ... Dr. Tech. Science: 05.02.04] 360 p.

3. Aulin V.V. (2016). Rol pryntsypiv maksymumu ta minimumu vyrobnytstva entropii v evoliutsiinomu rozvytku staniv trybosystem [Problems of tribology. №2] S.6-14.

4. Prigozhin I. (1960). Vvedenie v termodinamIku neravnovesnyih protsesov [M.: Izdatelstvo inostrannoy literaturyi] 127s.

5. Tsigler G. (1966) Ekstremalnyie printsipyi termodinamiki neobratimyih protsessov i mehanika sploshnoy sredyi [M.: Mir] 134s.

6. Bershadskiy L.I. (1990). Strukturnaya termodinamIka tribosistem [K:Znanie] 30s.

7. Martyushev L.M. (2010). Proizvodstvo entropii i morfologicheskiy perehodyi pri neravnovesnyih protsessah [avtoref. Dr. fiz.-mat. nauk spets: 01.04.14] 32s.

8. Martyushev L.M., Seleznev V.D. Printsip maksimalnosti proizvodstva entropii v fizike i smezhnyih oblastyah [Ekaterinburg: GOU VPO UGTU-UPI] 83 s.

9. Martyushev L., Seleznev V. (2006). Maximum entropy production principle in physics, chemistry and biology [Physics Reports. Vol. 426, Issue 1] P. 1-45.

10. Delas N.I. (2014). Printsip maksimalnosti proizvodstva entropii v evolyutsii makrosistem: nekotoryie novyie rezultatyi [Vostochno-Evropeyskiy zhurnal peredovyih tehnologiy. T.6, №4 (72)] S.16-23.

11. Dewar R.C. (2005) Maximum entropy production and the fluctuation teorem [Journal of Physics A: Mathematical and General. Vol. 38, lssue 21] P.L371-L.381.

12. Niven R.K. (2009) Steady state of a dissipative flow-controlled system and the maximum entropy production principle [Physical Review E. Vol. 80, lssue 2] P.021113.

13. Groot S., Mazur P. (1964). Neravnovesnaya termodinamIka [M.: Mir] 456 s.

14. Niven R. K. (2009). Steady state of a dissipative flow–controlled system and the maximum entropy production principle [Physical Review E. Vol. 80, Issue 2] P. 021113.

15. Dewar, R. C. (2005). Maximum entropy production and the fluctuation theorem [Journal of Physics A: Mathematical and General. Vol. 38, Issue 21] P. L371–L381.

16. Simak V., Sumbera M., Zborovsky I. (1988). Entropy in Multiparticle Production and Ultimate Multiplicity Scaling [Phys. Lett. B. V.206] P. 159-162.

17. HuberP.J. Robast Statistics (1981). [N.Y.: Wiley]

18. Barrodale I., Erikson R. E. (1980). Algorithms for Least Square Linear Prediction and Maximum Entropy Spectral Analysis [Geophysics. V.5, No.3] P. 420.

19. Ozawa H., Ohmura A., Lorenz R. D., Pujol T. (2003). The second law of thermodynamicsand the global climate system: A review of the maximum entropy production principle [Reviews of Geophysics. Vol. 41, Issue 4] P. 1–24.

20. Kleidon A., Lorenz R.D. (2005). Non-equilibrium Thermodynamics and the Production of Entropy: Life, Earth and Beyond, Springer Verlag, Heidelberg principle [Reviews of Geophysics. Vol. 41] P. 1018–1041.

21. Cejnar P., Jolie J. (1998). Wave-Function Entropy and Dynamical Symmetry Breaking in Interacting Boson Model [Phys. Rev. E. V.58, No. 1] P. 387-399.

22. Cejnar P., Jolie J. (1998). Dynamical-Symmetry Content of Transitional IBM-I Hamiltonian [Phys. Lett. B. V.420] P. 241-247.

23. Jaynes E. T., Levine R. D., Tribus M. (1979). Where do we Stand on Maximum Entropy?' in The Maximum Entropy Formalism [M.I.T. Press, Cambridge] 105 p.

24. Vilson A.Dzh. (1978). Entropiynyie metodyi modelirovaniya slozhnyih sistem [M.: Nauka].

25. Budanov V.G. (2006). O metodologi sinergetiki [Voprosyi filosofii. №5] S.79-94.

Аулін В.В., Лисенко С.В., Гриньків А.В., Голуб Д.В. Термодинамічне обґрунтування спрямованості нерівноважних процесів в трибоспряженнях деталей машин на основі принципів максимуму і мінімуму ентропії

В статті дано термодинамічне обґрунтування спрямованості нерівноважних процесів в трибоспряженнях деталей машин, в трибосистемах, на основі принципів максимуму і мінімуму ентропії. З'ясовано, як нерівноважні процеси можливо обґрунтувати на основі мінімуму та максимуму функції виробництва ентропії: лінійні та нелінійні нерівноважні процеси й різні їх термодинаміки. Функцію виробництва ентропії розглянуто як функцію потоків термодинамічних сил і термодинамічних потоків.

В основу розгляду теорії нерівноважних процесів покладено рівняння Ліувілля для класичних трибосистем з урахуванням зовнішнього впливу або збуреннння. Показано, що в термодинамічних процесах в трибосистемах принцип максимізації ентропії реалізується, як другий початок синергетики.

Ключові слова: трибоспряження деталей, нерівноважні процеси, термодинаміка, синергетика, ентропія, термодинамічний потік

Problems of Tribology, *V. 27, No 2/104-2022, 64-70*

Problems of Tribology
Website: http://tribology.khnu.km.ua/index.php/ProbTrib
E-mail: tribosenator@gmail.com

DOI: https://doi.org/10.31891/2079-1372-2022-104-2-64-70

The influence of the chemical composition of the hardened auger on its wear during dehydration process of municipal solid waste in the garbage truck

O.V. Bereziuk[1*], V.I. Savulyak[1], V.O. Kharzhevskyi[2]

[1]Vinnitsa National Technical University, Ukraine
[2]Khmelnytskyi National University, Ukraine
**E-mail: berezyukoleg@i.ua*

Received: 09 April 2022: Revised: 15 May 2022: Accept: 02 June 2022

Abstract

The article is dedicated to the study of the influence of the chemical composition of the hardened auger by the chromium on its wear during dehydration of solid waste in the garbage truck. Using the rotatable central composition planning of the experiment of the second order by means of the Box-Wilson method, the dependencies of auger wear depending on the chemical composition of the hardened steel and friction path are determined. The responce surfaces of the objective functions are shown – the wearing of the hardened steel and energy consumption of the dehydration process by the hardened auger press of the mixed municipal solid waste according to the influense parameters. It is established that on the friction path s = 56850 m, during the dehydration process of solid waste in the garbage truck, the simultanuous incresing of the carbon content from 0.45% to 2.1%, and the chromium content – from 0.25% to 12%, at the optimum content of the manganese as 0.527% in the hardened steel of the auger, enable to decrease the energy consumption of the dehydration process of solid waste by 25.7 kWh/tons, or 10.7%. Therefore, it tends to cheaper the process of dehydration in the garbage truck. It is established the expediency of further research for the determination the rational composition and the structural state of the auger material and the ways to increase its wear resistance.

Key words: wear, chemical composition, hardening, auger press, garbage truck, dehydration, solid waste, regression analysis

Introduction

Among the important tasks of municipal engineering, one of the leading task is increasing of wear resistance and reliability of the machine parts. One of the promising technologies for primary processing of municipal solid waste (MSW), aimed at reducing both the cost of transportation of solid waste and the negative impact on the environment is their dehydration, accompanied by pre-compaction and partial grinding. Dehydration of solid waste in the garbage truck is performed using a conical screw, the surface of which due to the existing friction wears out intensively. This is due to the fact that solid waste contains small metal parts, glass, ceramics, stones, bones, polymeric materials, which have abrasive properties. Besides, the presence of moisture 39-92% by weight in MSW creates an aggressive corrosive environment. For the manufacturing of the augers, the alloyed steels are widely used. The usage of steels and cast irons that are alloyed by chromium and manganese is well-grounded. Such alloys hardened well and have high resistance to corrosion and abrasive wear. Therefore, the study of the influence of the chemical composition of the hardened steel of the auger on its wear during dehydration of municipal solid waste in the garbage truck is a topical task.

Literature review

In the paper [3], the results that were obtained in the operating conditions of extruders while processing of feed grain, with impurities of saponite mineral are presented. The results of experimental studies of wear resistance of different auger materials with different thermal and chemical-thermal treatment in corrosive-abrasive medium on special friction machines are included.

The authors found that the wear resistance of materials in a corrosive-abrasive environment at elevated temperatures depends not only on the hardness of the friction surface, but also on its structure and phase composition and changes in the hardness gradient along the depth of the hardened layer. To ensure high wear resistance of extruders in the manufacture of animal compound feed with impurities of the mineral saponite, it is recommended to use for the manufacture of parts of the extrusion unit steel X12, hardened by nitro-hardening technology.

In the paper [1] the influence of structure, phase composition and properties on abrasive wear resistance of chromium-manganese cast irons in the cast state was investigated. It is shown that the abrasion resistance of chromium-manganese cast irons is due to the microhardness of the matrix and austenitic carbide eutectic based on Me_7C_3 carbide, determined by the degree of alloying and shape parameter of eutectic carbide, and depends on deformation-phase transformations that occur in the process of testing for abrasive wear.

The article [4] shows the prospects of obtaining cost-effective alloyed manganese and chromium-manganese deposited metal that can be applied by surfacing on low-carbon steel without preheating. This is important for the industrial use of developed surfacing materials. It was also found that the highest wear resistance in different types of wear has a deposited metal with martensitic-austenitic and austenitic structures, and the presence of ferrite in the structure of the deposited metal reduces wear resistance.

By the authors of the the article [5], it was established a mathematical model for calculating the wear rate of triboelements in a tribosystem operating in conditions of corrosion and abrasive wear was developed. The input factors were: active acidity, abrasiveness, roughness, load and sliding speed. Theoretically, the degree of influence of the above factors on the wear rate is established. It was found that abrasiveness is the most important factor, followed by the degree of decline – the level of active acidity and load**.**

In the article [6], a new design of the auger with a sectional elastic surface, which is designed to reduce the degree of damage to the grain material during its transportation. The theoretical calculation of the interaction of the grain with the elastic section of the auger is carried out. A dynamic model has been developed to determine the influence of structural, kinematic and technological parameters of the elastic auger on the time and path of free movement of bulk material particles during their movement between sections, as well as to exclude the possibility of grain material interaction with the non-working surface of the auger working body to reduce the possibility of its damage.

The authors of the paper [7] determined that restoration of the auger requires surfacing or spraying a layer of a certain thickness on the end part of the coil of the auger, while the width of the restored layer is usually a few millimeters. An algorithm for selecting the optimal composite powder material for plasma spraying in order to increase the wear resistance of the working surfaces of machine parts, in particular the auger, is described. Plasma spraying of composite powder materials, according to the authors, will increase the durability of the auger by 2-3 times, which will reduce repair costs by tens of times.

In the article [8], the influence of geometrical parameters on productivity and design of the briquetting machine using the model of pressure, based on the theory of piston flow is investigated. An analytical model that uses a pressure model was also developed based on Archard wear law to study the wear of augers of biomass briquetting machines. The developed model satisfactorily predicted the wear of the auger and showed that the greatest influence on it have the speed of rotation and the choice of material. The amount of wear increases exponentially to the end of the auger, where the pressure is the highest. Changing the design of the auger to select the optimal geometry and speed with the appropriate choice of material can increase the life of the auger and the productivity of the machine for briquetting biomass.

The resulls of the analysis of the process of screw briquetting of plant materials into fuel and feed is investigated in the work [9]. Regularities of this process are the basis for determining the rational parameters of the working bodies. When designing briquette presses it is necessary to consider deformation of biomass taking into account change of physical and rheological properties at the moment of interaction with the working surfaces of the auger.

The materials of the article [10] contains the research of the wearing of a twin-auger extruder of rigid PVC resins is investigated. The pressures around the cylinder when extruding two rigid PVC resins in a laboratory extruder with a diameter of 55 mm were measured and the forces acting on the auger core were determined. Numerical simulation of the flow was performed using the power parameters of the viscosity of the resins.

The pericularities of the process of pressing wood chips in auger machines was investigated in the work [11]. The processes occurring in different parts of the auger are established, formulas are defined that allow to calculate the loads acting on the auger coils, as well as to determine the power required for pressing. The specific energy consumption and the degree of heating of raw materials during pressing are determined.

Based on the planning of the experiment using the Box-Wilson method, the results of experimental research of the process of dehydration of municipal solid waste (MSW) in the garbage truck are shown in the

article [12]. Quadratic regression equations with the 1st order interaction effects were obtained using rotatable central composite planning for such objective functions as humidity and density of pre-compacted and dehydrated MSW, maximum drive motor power, energy consumption of solid waste dehydration. This allowed to determine the optimal parameters of equipment for dehydration by the criterion of minimizing the energy consumption of the process (auger speed, the ratio of the radial gap between the auger and the body, and the ratio of the auger core diameter to the outer diameter of the auger on the last coil) for both mixed and "wet".

In the paper [13] the improved mathematical model of work of the dehydration drive of MSW in the garbage truck is suggested that takes into account wear of the auger, which allowed to research numerically the dynamics of this drive during the start-up, and to define that with the increase of wear of the auger pressure of working liquid on the speed of the auger it is significantly reduced.

The power regularities of change of the nominal values of pressures at the inlet of the hydraulic motor, angular speed and frequency of rotation of the auger from values of its wear are defined, the last of which describes detuning from optimum frequency of rotation of the auger in the course of its wear. It is established that the wear of the auger by 1000 μm leads to an increase in the energy consumption of solid dehydration by 11.6%, and, consequently, to an increase in the cost of the process of their dehydration in the garbage truck and accelerate the wear process.

In the paper [14], the influence of chromium alloying of the auger material on its wear during dehydration of solid waste in the garbage truck was investigated by means of the regression analysis method. It was also found that during operation and the wearing process of the auger on the path s = 56850 m during dehydration of solid waste in the garbage truck, the increase of the chromium content in the hardened material of the auger from 0.25% to 12% leads to a decrease the speed of the wearing an energy consumption of solid waste dehydration from 12.2% to 3.1%, and, consequently, to reduce the cost of dehydration in the garbage truck.

Purpose

Researching the influence of chemical cmposition of the of the hardened steel of auger on its wear during dehydration of solid waste in a garbage truck.

Methods

The determination of the regularity of the wear of the screw depending on its chemical composition of the hardened steel and the friction path was carried out by means of a rotatable central composite planning experiment of a second order by the Box-Wilson method. The required coefficients were determined using the developed computer program "PlanExp" that is protected by a copyright registration certificate.

For the determination of the energy consumption of MSW dehydration, taking into account the auger wear, the following dependencies were used [13]:

$$\begin{aligned} E = {} & 1504 - 15.92 w_0 + 0.3214 \rho_0 - 1.069 n(u) - 2061 (\Delta_{aug} + u)/(D_{\min} - 2u) - 1947 (d_{\min} - \\ & -2u)/(D_{\min} - 2u) + 9.118 \cdot 10^{-4} w_0 \rho_0 + 0.002142 w_0 n(u) + 18.12 w_0 (\Delta_{aug} + u)/(D_{\min} - 2u) - \\ & -2.115 w_0 (d_{\min} - 2u)/(D_{\min} - 2u) + 4.392 \cdot 10^{-4} \rho_0 n(u) - 2.005 \rho_0 (\Delta_{aug} + u)/(D_{\min} - 2u) + \\ & +0.3361 \rho_0 (d_{\min} - 2u)/(D_{\min} - 2u) + 0.09031 w_0^2 - 7.923 \cdot 10^{-4} \rho_0^2 + 0.008241 n(u)^2 + \\ & +104172 [(\Delta_{aug} + u)/(D_{\min} - 2u)]^2 + 1318 [(d_{\min} - 2u)/(D_{\min} - 2u)]^2 \ [\text{kWh/tons}]; \end{aligned} \quad (1)$$

$$n = 52.43 - 1.276 \cdot 10^{-3} u^{1,5} \ [\text{rpm}], \quad (2)$$

where E – is the energy consumption of solid waste dehydration, kW·h/tons; ρ_0 – initial density of solid waste, kg/m^3; w_0 – initial relative humidity of solid waste, %; n – the nominal speed of the auger, rpm; u - auger wear, m; Δ_{aug} - radial clearance between auger and housing, m; d_{min} – outer diameter of the auger on the last coil, m; D_{min} is the diameter of the auger core on the last coil, m.

Results

Preliminary analysis [13, 14] of the results of experimental studies [3] showed that the wear of a hardened screw is a function of such 4 main parameters:

$$u = f(C_C, C_{Cr}, C_{Mn}, s), \quad (3)$$

where u – value of wear, μm; C_C, C_{Cr}, C_{Mn} – content of the carbon, chromium, manganese in the material of auger, consequently, in %; s – friction path, m.

The research of the influence of the mentioned factors on the wear of the hardened auger during the processing of the results of the single factor experiment by means of the regression analysis method, has

significant difficulties and large volume of calculations. Thus, in our opinion, it is better to conduct a multifactor experiment to obtain a regression equation for the response function – wear of the hardened auger by planning a multifactor experiment by the Box-Wilson method [15].

The values of the wear of the auger for a different chemical composition of hardened steel and the friction path are shown in the Table 1 [3].

Table 1

The wear of the auger for a different chemical composition of hardened steel and the friction path [3]

№	Material of the auger	Content in the auger material, %			Wear, μm, for the friction path, m			
		carbon	chromium	manganese	3000	6000	9000	12000
1	Steel 45	0.45	0.25	0.65	53	103	153	203
2	Steel У8	0.8	0.2	0.25	48	91	134	177
3	Steel ШХ15	1	1.5	0.3	43	80	116	152
4	Steel Х12	2.1	12	0.3	39	72	105	138

Based on the data shown in the Table 1, using rotatable central compositional planning of the second order of the experiment, using the developed software, protected by the copyright certificate, after discarding insignificant factors and effects of interactions by the Student's criterion, the regularity of screw wear depending on the chemical composition of its hardened steel and the friction path is determined:

$$u = 95 - 7.467C_C - 72.39C_{Cr} - 1782C_{Mn} + 0.0344s - 0.02148C_C s + \\ +0.00214C_{Cr} s - 0.01323C_{Mn} s + 352.5C_C^2 - 3.065C_{Cr}^2 + 2405C_{Mn}^2. \quad (4)$$

In the Fig. 1 it is shown the response surfaces of the objective function – the wear of the hardened auger u and its two-dimensional cross-sections in the planes of the impact parameters, plotted using regularity (4) that allow us to determine this relationship.

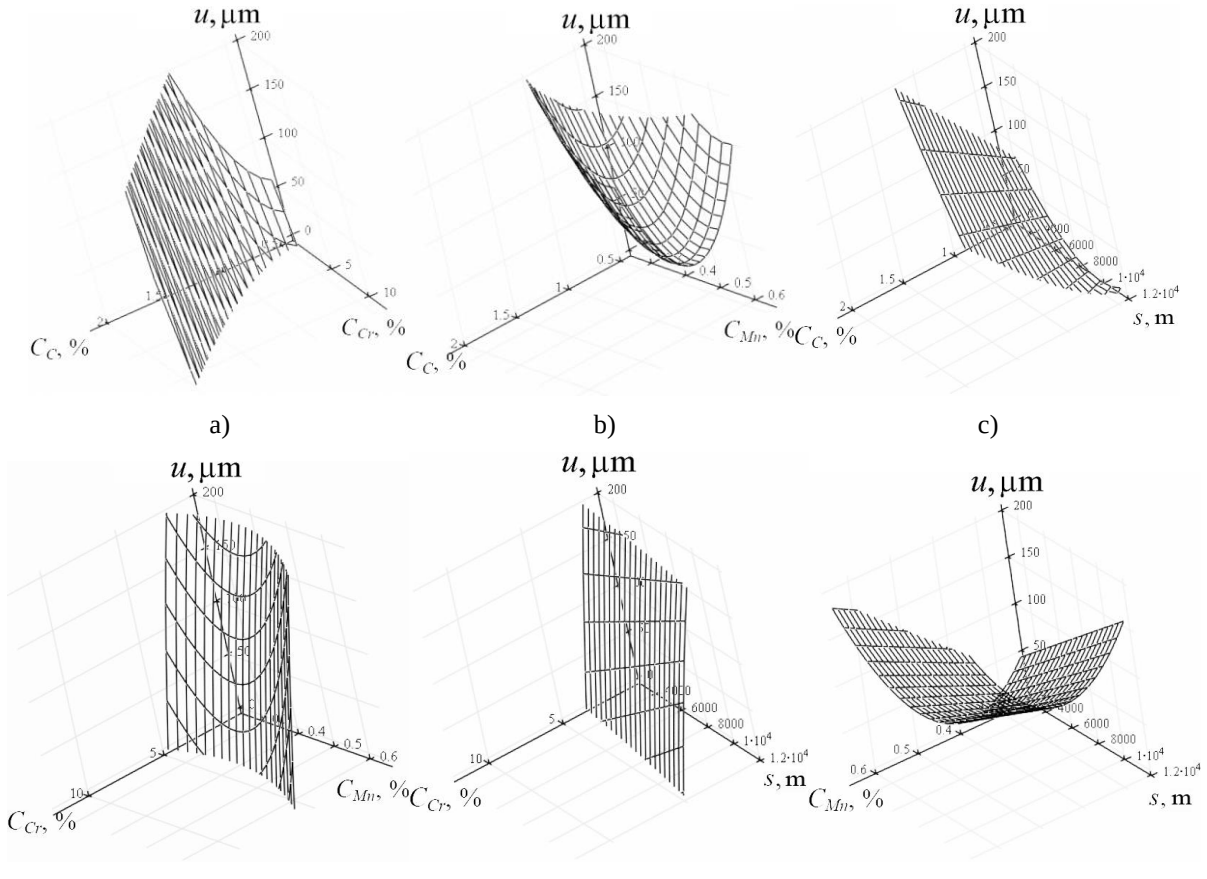

Fig. 1. The response surfaces of the objective function - wear of the hardened auger u in the planes of the impact parameters (a) – $u = f(C_C, C_{Cr})$, (b) – $u = f(C_C, C_{Mn})$, (c) – $u = f(C_C, s)$, (d) – $u = f(C_{Cr}, C_{Mn})$, (e) – $u = f(C_{Cr}, s)$, (f) – $u = f(C_{Mn}, s)$

It is established that according to Fisher's criterion the hypothesis about the adequacy of the regression model (4) can be considered correct with 95% reliability. The coefficient of multiple correlation was R = 0.999994 that indicates the high accuracy of the results.

According to Student's criterion, it was found that among the researched factors of influence (chemical composition of hardened steel) the most affected on the wear of the screw is the carbon content, and the least – the manganese content.

In the Fig. 2 the response surfaces of objective function – energy consumption of the process of dehydration by the hardened screw press of mixed municipal solid waste (when it wears during the way s = 56850 m [14]) and its two-dimensional cross sections in the planes of impact parameters (chemical composition of its hardened steel), that are plotted by means of regularities (1, 2, 4) and allow to illustrate the specified dependence are shown.

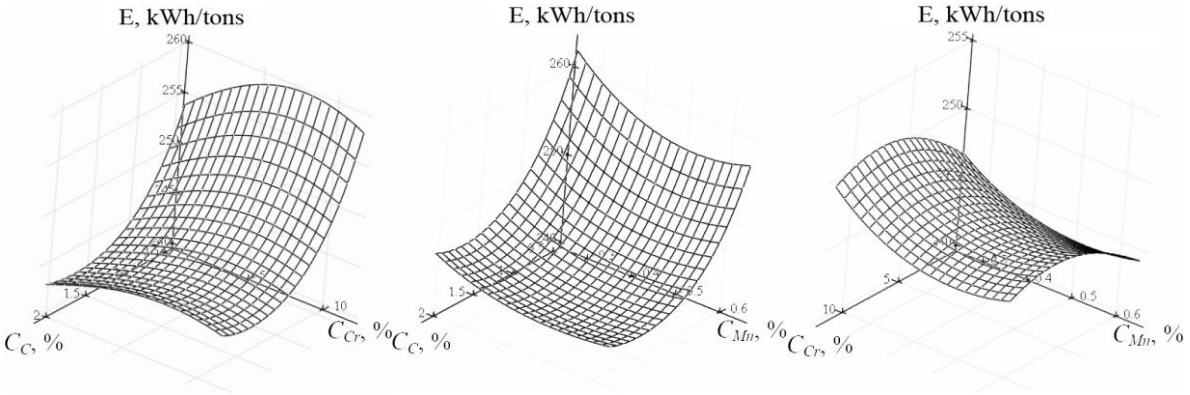

a) b) c)

Fig. 2. Response surfaces of the objective function - energy consumption E of the process of dehydration of the hardened screw press of mixed solid household waste in the planes of the parameters of impact after its operation and wear on the way s = 56850 m (a) – $E = f(C_C, C_{Cr})$, (b) – $E = f(C_C, C_{Mn})$, (c) – $E = f(C_{Cr}, C_{Mn})$

As shown on the Fig. 2, after operation and wear on the path s = 56850 m during dehydration of MSW in the garbage truck, the simultaneous increase the content of carbon from 0.45% to 2.1%, and chromuim from 0.25% to 12%, at optimal content of magnasese as 0.527% in the hardened steel of the auger leads to reduced energy consumption by 25.7 kWh/tons or 19.7% and to cheap the process of dehydration of MSW in the garbage truck, which indicates the importance of determining the rational composition and structural state of the material of the friction surfaces of the auger and the ways to increase its wear resistance.

Conclusions

According to Fisher's criterion, the regularity of auger wear from the chemical composition of its hardened steel and the friction path is determined. It is also established that according to Student's criterion, among the studied factors of influence (chemical composition of hardened steel), the most important effect on the wear of the auger is the carbon content, and the least – the manganese content.

The response surfaces of the objective functions – wear of hardened auger and energy consumption of the process of dehydration by the hardened auger press of mixed solid waste, and their two-dimensional cross sections in the planes of impact parameters that illustrate the dependence of these objective functions on individual impact parameters.

It is established that on the friction way s = 56850 m of the auger during dehydration of MSW in the garbage truck, the simultaneous increase the content of carbon from 0.45% to 2.1%, chromuim from 0.25% to 12%, at optimal content of magnasese as 0.527% in the hardened steel of the auger enable to reduce energy consumption by 25.7 kWh/tons or 19.7% and, therefore, to cheap the process of dehydration of MSW in the garbage truck. Thus, the importance of determining the rational composition and structural state of the material of the friction surfaces of the auger and the ways to increase its wear resistance needs to conduct the further researches.

References

1. Kutsova V.Z., Kindrachuk M.V., Kovzel M.A., Tisov O.V., Hrebevieva A.V., Shets P. Yu. (2016). Vplyv struktury, fazovoho skladu ta vlastyvostei na abrazyvnu znosostiikist khromomarhantsevykh chavuniv u lytomu stani [Influence of structure, phase composition and properties on abrasive wear resistance of chromium-manganese cast irons in cast state]. Problems of Friction and Wear, 2, 78-85.

2. Dykha O.V. (2018) Rozrakhunkovo-eksperymentalni metody keruvannya protsesamy hranychnoho zmashchuvannya tekhnichnykh trybosystem: monohrafiya. [Computational and experimental methods for

controlling the processes of maximum lubrication of technical tribosystems: a monograph.] Khmelnyts′kyi: KHNU.

3. Kaplun V.H., Honchar V.A, Matviishin P.V (2013) Pidvyshchennya znosostiykosti shneka ta ekstrudera pry vyhotovlenni kormiv dlya tvaryn iz domishkamy mineralnoho saponitu. [Improving the wear resistance of the auger and extruder cylinder in the manufacture of animal feed with impurities of the mineral saponite]. Visnyk of Khmelnytsky National University, 5, 7-11.

4. Malinov V.L. (2011) Vliyanie soderzhaniya marganca i rezhimov otpuska na strukturu i iznosostojkost' hromomargancevogo naplavlennogo metalla [Influence of manganese content and tempering regimes on the structure and wear resistance of chromium-manganese deposited metal]. Zakhyst metalurhiinykh mashyn vid polomok: collection of scientific works, 13, 247-254.

5. Cymbal B.M. (2017) Pidvyshchennya znosostiykosti shnekovykh ekstruderiv dlya vyrobnytstva palyvnykh bryketiv u kyslotnykh ta luzhnykh seredovyshchakh [Increasing the wear resistance of auger extruders for the production of fuel briquettes in acidic and alkaline environments]: abstract dis. … cand. tech. sciences: 05.02.04 – Friction and wear in machines, Kharkiv, 20.

6. Hevko R.B., Zalutskyi S.Z., Hladyo Y.B., Tkachenko I.G., Lyashuk O.L., Pavlova O.M., ... & Dobizha N.V. (2019). Determination of interaction parameters and grain material flow motion on screw conveyor elastic section surface. INMATEH-Agricultural Engineering, 57(1).

7. Zhachkin S.Y., Trifonov G.I. (2017) Vplyv plazmovoho napylennya kompozytsiynykh poroshkovykh materialiv na znosostiykist′ detaley mashyn [Influence of plasma spraying of composite powder materials on the wear resistance of machine parts]. Master's Journal, № 1, 30-36.

8. Orisaleye J.I., Ojolo S.J., Ajiboye J. S. (2019) Pressure build-up and wear analysis of tapered screw extruder biomass briquetting machines. Agricultural Engineering International: CIGR Journal, 21(1), 122-133.

9. Eremenko O.I., Vasilenkov V.E., Rudenko D.T. (2020) Doslidzhennya protsesu bryketuvannya biomasy shnekovym mekhanizmom [Investigation of the process of biomass briquetting by auger mechanism]. Inzheneriya pryrodokorystuvannya, 3 (17), 15-22.

10. Demirci A., Teke I., Polychronopoulos N. D., Vlachopoulos J. (2021) The Role of Calender Gap in Barrel and Screw Wear in Counterrotating Twin Screw Extruders. Polymers, 13(7), 990.

11. Tataryants M.C., Zavynskyy C.S., Troshyn A.D. (2015). Rozrobka metodyky rozrakhunku navantazhen′ na shnek i enerhovytrat shnekovykh presiv [Development of a method for calculating auger loads and energy consumption of auger presses]. ScienceRise, 6 (2), 80-84.

12. Berezyuk O.V. (2018) Eksperymental′ne doslidzhennya protsesiv znevodnennya tverdykh pobutovykh vidkhodiv shnekovym presom [Experimental study of solid waste dehydration processes by auger press]. Visnyk Vinnyts′koho politekhnichnoho instytutu, № 5, 18-2413.

13. Bereziuk O.V., Savulyak V.I., Kharzhevskyi V.O. (2021) The influence of auger wear on the parameters of the dehydration process of solid waste in the garbage truck. Problems of Tribology, No 26(2/100), 79-86.

14. Bereziuk O.V., Savulyak V.I., Kharzhevskyi V.O. (2022) The influence of the alloying of the auger by the chromium on its wear during dehydration process of municipal solid waste in the garbage truck. Problems of Tribology, 27(1/103), 50-57.

15. Andersson O. (2012). Experiment!: planning, implementing and interpreting. John Wiley & Sons.

Березюк О.В., Савуляк В.І., Харжевський В.О. Вплив хімічного складу гартованого шнека на його знос під час зневоднення у сміттєвозі твердих побутових відходів

Анотація

Стаття присвячена дослідженню впливу хімічного складу гартованого шнека на його знос під час зневоднення твердих побутових відходів у сміттєвозі. За допомогою використання ротатабельного центрального композиційного планування експерименту другого порядку методом Бокса-Уілсона визначено закономірність зносу шнека залежно від хімічного складу його гартованої сталі та шляху тертя. Показано поверхні відгуків цільових функцій – зносу гартованого шнека та енергоємності процесу зневоднення гартованим шнековим пресом змішаних твердих побутових відходів в площинах параметрів впливу. Встановлено, що на шляху зношування шнека s = 56850 м під час зневоднення твердих побутових відходів у сміттєвозі одночасне збільшення вмісту вуглецю з 0,45% до 2,1%, хрому з 0,25% до 12% при оптимальному вмісті марганцю 0,527% в гартованій сталі шнека дозволяє зменшити енергоємність зневоднення твердих побутових відходів на 25,7 кВт·год/т або 10,7%, а, отже, і до здешевлення процесу їхнього зневоднення у сміттєвозі. Виявлено доцільність проведення подальших досліджень з визначення раціонального складу і структурного стану матеріалу шнека та шляхів підвищення його зносостійкості.

Ключові слова: знос, хімічний склад, гартування, шнековий прес, сміттєвоз, зневоднення, тверді побутові відходи, планування експерименту.

Problems of Tribology, V. 27, No 2/104-2022, 71-79

Problems of Tribology
Website: http://tribology.khnu.km.ua/index.php/ProbTrib
E-mail: tribosenator@gmail.com

DOI: https://doi.org/10.31891/2079-1372-2022-104-2-71-79

Influence of high-modulus filler content on critical load on tribocouples made of microheterophase polymer composite materials

V.V. Aulin[1*], S.V. Lysenko[1], A.V. Hrynkiv[1], O. D. Derkach[2], D.O. Makarenko[2]

[1] *Central Ukrainian National Technical University , Ukraine*
[2] *Dnipro State Agrarian And Economic University, Ukraine*
** E-mail: AulinVV @ gmail.com*

Received: 10 April 2022: Revised: 15 May 2022: Accept: 05 June 2022

Abstract

The influence of the content of high-modulus filler on the assessment of the critical load on the conjugation of polymeric composite materials is theoretically substantiated from the tribological point of view. Various cases of destruction of polymeric composite materials are considered. The conditions under which the setting of polymeric composite materials is observed, as well as the conditions of their destruction are formulated. Both viscous and brittle fracture of polymeric composite materials are considered. The main focus is on critical loads and stresses depending on the content of high-modulus filler, taking into account the modulus of elasticity of the polymer matrix and filler and the nature of their destruction.

Key words: polymer composite material, microheterophase composite, high modulus filler, triad coupling of parts, critical load, setting, failure

Introduction

When the influence of the structure and composition of polymer composite materials (PCM) on the value of the critical pressure should be considered in the contacts of different types of microheterophase composites. In this case, the size of the structural components of PCM is much smaller than the size of the contact spot, and therefore we can consider the contact of two PCM as the contact of homogeneous materials [1]. In such PCM, the physico-mechanical and tribological properties of the friction surfaces depend on a number of factors. Conditions for efficient operation of triad couplings of parts with PCM at a critical setting load depend on the following factors [2]:

– volume content of high-modulus filler of conjugated PCM of the same phase composition and with the same volume content;

– differences in the volumetric content of the high-modulus filler when contacting conjugate parts with PCM of the same phase composition;

– physical-mechanical and tribological properties of structural components of PCM conjugations with the same volume content of fillers;

– physical-mechanical and tribological properties of structural components of PCM conjugations at different volume content of fillers;

– bond strength of filler particles with the matrix in PCM;

– particle size of fillers.

Consideration of these factors will make it possible to design the PCM in accordance with the operating conditions of the moving couplings of machine parts, without reaching the critical values of the load and the observation of setting and failure.

Literature review

By introducing particles of brittle high-modulus fillers into the plastic polymer matrix, the nature of deformation and destruction of PCM with increasing their bulk content c_f will change [1,2]. The low content (concentration) of high-modulus filler particles indicates that the yield strength σ_T PCM increases with c_f increase, and elongation at destruction ε_R – decreases. As the yield strength of PCM in contact increases, the critical σ_T setting pressure p_c for a single microroughness on the conjugate surfaces of the parts increases in accordance with the equation I.V. Kragelsky [3-6]:

$$p_c = C_u \sigma_T . \tag{1}$$

Since the geometry of roughness slightly depends on the properties of PCM [7-9] at low roughness of friction surfaces of conjugation of parts, it can be assumed that the geometry of their contact with increasing volume fraction of filler c_f remains unchanged.

With increasing c_f plastic properties of ε_R PCM decrease according to equation [10]:

$$N_{M_1-M_2} + \sum_{j=1}^{m} N_{j_{M_1-M_2}} = N \tag{2}$$

It was found that c_f > 0.15 value ε_R changes c_f slightly with increasing. In this regard, for PCM with c_f >0.15 the ability of the irregularities of the conjugate surfaces of the parts to plastic deformation can be assumed to be almost the same [11,12]. The diameter of the contact spot for such PCM is about 1...5 μm. This indicates that the dislocation processes will not change dramatically with the change in the diameter of the contact spot. For PCM with c_f >0.15 the value of the coefficient of proportionality C_u can be assumed to be constant and in accordance with the recommendations of I.V. Kragelsky at a value equal to 3...4. The value of the critical pressure p_c in tribocouples with microheterophase PCM will mainly depend on the value of the yield strength of the material σ_T.

When strengthening polymeric materials with spherical incoherent filler particles, the yield strength is equal to:

$$\sigma_T = \sigma_{PM} + \gamma_{PCM} c_f^{1/n}, \tag{3}$$

where $n = \overline{1,6}$; γ_{PCM} – coefficient that takes into account the shear modulus and Burgers vector of the polymer matrix, as well as the size and shape of the filler particles in PCM [13,14].

For PCM with a small value c_f when contacting irregularities of the same composition, the critical pressure in the triad couplings of the parts is:

$$p_c = C_u \left(\sigma_{PM} + \gamma_{PCM} c_f^{1/n} \right). \tag{4}$$

From the last equation it follows that at n>1 the increase in critical pressure p_c with increasing c_f gradually slows down. Note that the slowdown occurs the faster the value of n [15]. Despite the decrease in PCM elongation with increasing c_f, such composites have a viscous nature of fracture, and therefore setting when reaching the pressure in tribocouples p_c will occur mainly by the mechanism of active centers [16-18]. The destruction of the micro-irregularities of the conjugate surfaces of the gripping parts, when shifting one of them relative to the other will be cohesive in nature with the formation of growths on one of the surfaces, which in some cases can scratch or plow another surface. Note that the formation of such growths is possible with equal probability on both contacting directed surfaces of the parts and there are also traces of the process of plowing on the surfaces of the triad.

Purpose

The aim of this work is tribophysical theoretical substantiation of the influence of changes in the content of high modulus filler in polymer composite material on the magnitude and nature of changes in the critical pressure on the tribocoupling of materials and their critical stress when varying the modulus of elasticity of

polymer matrix and filler.

Results

As the filler content c_f in the polymer matrix of the material of the tribocouple parts with the considered type of contact of their working surfaces increases, the critical setting pressure will increase, and the wear at pressures close to p_c will decrease slightly. The latter suggests that with increasing value, the c_f efficiency of tribocoupling of parts with PCM should increase, which indicates an increase in their tribological efficiency .

It is possible to predict that in PCM there is such a filler content when the value of its yield strength exceeds the value of the yield strength. In this case, the viscous nature of the destruction of PCM will turn into brittle fracture fracture [13]. In this case, equation (1) will change and take the form:

$$p_c = B\sigma_c, \tag{5}$$

where B – the coefficient that for fragile materials takes into account the same parameters as the coefficient C_u; σ_c – tensile strength of PCM.

Since for this class of materials with a change in the c_f value of B is likely to change slightly, the value of p_c, as in the previous case, will mainly be determined by the value σ_c.

The dependence σ_c on c_f for PCM can be represented by the Kramer-Griffiths-Orovan equation:

$$\sigma_c^2 = AE_p\left(1-c_f\right)+k_r, \tag{6}$$

where E_{pM} – the modulus of elasticity of the polymeric material (PM), A and k_r are the coefficients characterizing the structural and phase state of PCM.

At high contents of the filler ($c_f \geq 0.6$), taking into account the data [10-12] with a high probability we can assume that the modulus of elasticity of PCM can be estimated by the formula:

$$E_p = \beta E_f c_f, \tag{7}$$

where β – the coefficient experimentally determined for PCM or calculated from condition (2) for the lower limit, at c_f =0,6:

$$E_{pM}H_M((1-c_f)E_{pM}+C_fE_{pM}) \leq E_p \leq (1-c_f)E_{pM}+c_fE_{pM}. \tag{8}$$

It is also possible to write the following equations:

$$\sigma_c^2 = \beta AE_{pf}c_f\left(1-c_f\right)+k_r; \tag{9}$$

$$p_c = B\left[\beta AE_{pf}c_f\left(1-c_f\right)+k_r\right]^{\frac{1}{2}}. \tag{10}$$

From equation (10) it follows that with increasing the c_f value of p_c critical pressure in the tribocouples of parts should decrease.

The moment of transition from the viscous nature of the destruction of PCM to brittle with increasing content of filler theoretically can not be estimated. At the same time, the value of p_c with increasing c_f passes through the maximum. This gives grounds to introduce the criterion of maximum bearing capacity of triad couplings of parts made of PCM. At the optimal value of the filler content c_{fopt}, at which $\sigma_T = \sigma_c$, and the value $C_u = B$.

Equating the right parts of equations (4) and (10), we obtain:

$$\left(\sigma_T + \lambda c_{fopt}^{1/n}\right) = [\beta AE_{popt}(1-c_{fopt})+k_r]^{1/2}. \tag{11}$$

Hence we can find c_{fopt} at which p_c has a conditional maximum value of $p_{c.opt}$. Since the c_{fopt} values in σ_T the environment σ_B change smoothly, the value *of* p_c will also change smoothly and the effective performance of PCM in triad couplings of parts can be realized in some interval c_{fopt}. At friction of microroughness of conjugate surfaces of details can be in the conditions of comprehensive uneven compression that promotes manifestation of plasticity and effective values c_f should be a little more than c_{fopt}. Depending on the composition and particle size of the filler should be effective PCM with c_f =0.6...0.9. With a relatively high content of brittle filler on conjugate surfaces, it is possible to observe cracks, and with less – traces of setting.

When contacting PCM with different contents of the same filler, as for single-phase materials, the value of p_c will depend on the nature of deformation and destruction of contacting PCM, as well as their modulus of elasticity. When contacting PCM with $c_f > c_{fopt}$ value of p_c will be determined by the strength of the more fragile PCM and the ratio of their modulus of elasticity. At these values of p_c, the modulus of elasticity of PCM, with increasing c_f, increases in dependence close to rectilinear, and σ_c decreases along a smooth curve. In the case of a small increase in the filler content c_f compared to c_{fopt} can be expected to even increase the value of p_c. In this case, the probability of setting by the mechanism of active centers with increasing E_M of one of the materials of the parts will decrease, and the strength will decrease slightly. This is especially observed in conditions when the micro-irregularities of the conjugate surfaces of the parts are in uneven all-round compression, ie at small values of equilibrium roughness. In cases where the material of one of the parts c_f is much more c_{fopt} and p_c will be lower than the pressure when the PCM has c_{fopt}.

When contacting PCM conjugate parts with $c_f < c_{fopt}$ in case of increase c_f in one of the materials of the part, the value of p_c will increase in all cases, because the values of the modulus of elasticity E_p and σ_T PCM with large c_f will be higher, and accordingly will be lower and the probability of setting materials.

In tribocouple contacts of parts in which one of the PCM has $c_f > c_{fopt}$ and conjugate – $c_f < c_{fopt}$, the value of p_c for tribocoupling will be determined by the same conditions as in the contacts of brittle single-phase polymeric material with plastic material. Since the values σ_T in σ_B these PCMs are higher than in the polymer matrix and the brittle filler, respectively, the p_c in such contacts will be higher than in the contact of the filler with the matrix. In addition, high values of the modulus of elasticity E_p PCM at $c_f > c_{fopt}$ will reduce the probability of setting on the mechanism of active centers. Since the number of active centers increases with increasing c_f PCM under the condition $c_f > c_{fopt}$, the values of p_c will be higher the higher the content of filler c_f in this PCM. However, in PCM under the condition $c_f < c_{fopt}$ we have: with increasing c_f the resistance of the dislocations will increase, and the number of dislocations in the cluster before the boundary of the contact surfaces will decrease. The maximum value of p_c in this type of contact will be when the value c_f in one of the conjugations of parts with PCM is slightly smaller, and in the other – slightly larger c_{fopt}.

Analyzing the results of the dependence of p_c on the content of high-modulus filler c_f in different materials of the tribocouple parts, it can be noted that the highest values of p_c should be expected when contacting them, provided that conjugate PCM have different filler content c_f. Moreover, in one of the PCM the value c_f should be close to c_{fopt}, and in the second - should be greater c_{fopt} by a value at which the effect of increasing the modulus of elasticity E_p in the tribocontact prevails over the effect of reduction σ_c. Approximately can be c_f taken equal to half the range of effective values when contacting PCM of the same composition (c_f = 0.75...0.85).

Mechanical and tribological properties of matrix and filler materials, other things being equal, will also affect the value of p_c. In such PCMs, according to the Kramer-Griffiths-Orovan equation , the values of the modulus of elasticity and the σ_c PCM as a whole increase as the modulus of elasticity of the filler E_{pf} increases. The value of p_c will also increase with increasing E_{pf}. The maximum value of p_c will be in the PCM contacts, in which the same c_f modulus of elasticity of the filler is maximum. Contacts of two conjugate PCMs with a low

value of E_{pf} will be the least efficient.

When the PCM is strengthened by the Ansell and Lenel mechanism [3,13,16-18] , the value σ_c of the three-coupled parts increases with increasing shear modulus of the reinforcing phase and the volume fraction of filler particles in this phase. Under conditions of uneven comprehensive compression PCM with small values of constant elasticity of the filler E_f will be more prone to setting. To reduce the adhesion of conjugate PCM it is necessary to increase c_f in both PCM; in contacts with such PCM the value of p_c with increasing c_f outside c_{fopt} will increase to large values c_f than in PCM with large modulus of elasticity of the filler E_{pf}. Values p_c for contacts in which one of the PCM has a filler content with a higher, and in the other – with a lower value of the modulus of elasticity E_{pf}, ie should acquire intermediate values.

For this type of PCM contacts with a smaller modulus of elasticity, the values σ_c are smaller and to increase the efficiency of these PCM contacts with a smaller modulus of elasticity, the filler content should be closer to c_{fopt}. In the case of PCM with a large modulus of elasticity E_p can be taken with both smaller and larger c_{fopt}. Due to the fact that the probability of adhesion by the mechanism of active centers with increasing E_p decreases, it is more appropriate in such contacts in PCM with large E_{pf} should take the value $c_f > c_{fopt}$. The limit value c_f in these contacts may be greater than in the contacts of two conjugate PCM with a larger E_p. With a large difference between E_{p2} and E_{p1} for PCM with large E_p effective are the following values of filler c_f =0.95...0.98.

Assuming that basically, the setting of the friction surfaces is determined by the mechanism of formation of the general step of microroughnesses, the value of p_c can be estimated by equations of the type:

$$\sigma_c = 2\overline{\sigma}\left(\frac{l_\partial}{l_c}\right)^{1/2}\left(\frac{3B_T\varepsilon rT}{V}\right)^{1/2}\exp(U_0/3rT)+\left(\frac{3B^f\varepsilon rT}{V^f}\right)^{1/2}\exp(U_0'/3rT)\left(1-2\left(\frac{l_\partial}{l_c}\right)^{1/2}\right). \quad (12)$$

Taking p_c proportional $\overline{\sigma}$, we have:

$$p_c = C_u\overline{\sigma} = 2C_u\left(\frac{l_\partial}{l_c}\right)^{1/2}\left(\frac{3B_T\varepsilon rT}{V}\right)^{1/2}\exp(U_0/3rT)-C_u\left(\frac{3B^f\varepsilon rT}{V^f}\right)^{1/2}\exp(U_0'/3rT)\left(1-2\left(\frac{l_\partial}{l_c}\right)^{1/2}\right). \quad (13)$$

Lack of data on the value of C_u, l_∂, B, U_0 i U_0^f impossible to determine a specific value p_c. However, it is known that the value p_c is greater the greater U_0 and U_0^f .

If we take into account the results of the study of the evolution of the structure of multiphase PCM, we can conclude that the deformation processes during friction PCM with fillers with low and medium modulus of elasticity more accurately describes the Ansell-Lenel mechanism [4-6]. Knowing the values of the average PCM stresses and fillers by the equations:

$$\overline{\sigma} = \sigma_T = \sigma_{TM} + \left(\frac{G_M G_f b}{2L_p c_p}\right)^{1/2}; \qquad \sigma_f = \sigma_T^f = \sigma_{TM}^f + \left(\frac{G_M^f G_f^f b^f}{2L_p c_p}\right)^{1/2}, \quad (14)$$

you can estimate the value of p_c when contacting two conjugate PCM:

$$p_c = B^f\sigma_c = 2B^f\left(\frac{l_d}{l_c}\right)^{1/2}\left(G_{TM}+\left(\frac{G_M^f G_f b}{2L_p c_p}\right)^{1/2}\right)+\left(1-2\left(\frac{l_d}{l_c}\right)^{1/2}\right)B^f\left(G_{TM}^f+\left(\frac{G_M^f G_f^f b^f}{2L_p c_p}\right)^{1/2}\right). \quad (15)$$

From equation (15) it follows that to increase p_c tribocoupled parts with PCM it is necessary to choose matrices with high σ_{TM} and shear modules G_M , and fillers – with high modulus of elasticity and such content that the distance between particles l_p close to its minimum value , in which the Ansell-Lenel mechanism still works. The value of l_p equal to 1.5...2.5·10^{-2} μm, at d_p = 0.5...2 μm, is observed if the volume fraction of binding is 1...5% .

For tribocouples of parts made of PCM with a fragile matrix, the amount of stress can be estimated by the formula:

$$\overline{\sigma_n} = \left(\frac{3B\dot{\varepsilon}kT}{V \exp\left(\frac{U_0 k_B}{3T} \right)} \right)^{1/2} . \quad (16)$$

In this case:

$$\sigma_f = \sigma_{TM} + \left(\frac{G_M G_f b_B}{2 l_p c_p} \right)^{1/2} . \quad (17)$$

Then the value of the critical filler can be estimated by the equation:

$$p_c = B^f \sigma_c = 2B^f \left(\frac{l_d}{l_c} \right) \left(\frac{3B\dot{\varepsilon}kT}{V} \right)^{1/2} \exp\left(\frac{U_0}{3k_B T} \right) + \left(1 - 2\left(\frac{l_d}{l_c} \right) \right) B^f \left(\sigma_{TM} + \left(\frac{G_M G_f b_B}{2 l_p c_p} \right)^{1/2} \right). \quad (18)$$

From equation (18) it follows that in triad couplings of parts with PCM with a fragile matrix must have a high value of U_0, and the filler is a high modulus of elasticity, ie high modulus. The volume fraction of binding should strive for its minimum allowable value (1...5%). At high values of U_0, the given tribocouples of parts with PCM on the value of the critical setting load may be more effective than tribocouples with a metal matrix. But by the criterion of fragile destruction, they will be inferior to tribocouples with a metal matrix.

The strength of PCM is significantly influenced by the strength of the interfacial boundaries. As noted, the destruction of the interfacial boundary leads to the development of cracks or chipping PCM, the formation of micropores, followed by their fusion in viscous fracture. During friction, due to the presence of sliding conjugate surfaces, the role of the boundaries will depend on the depth of the filler particles in the surface layer of the PCM material. All particles that do not come to the surface of the contact spot will perform the same role as under the volumetric load of PCM. The filler particles coming to the surface of the contact spot during friction will specifically affect the behavior of the material in the contact spot. In the case where the destruction of the interfacial boundaries leads to the appearance of cracking cracks, a network of microcracks will develop on the surface of the contact spot and the bearing capacity of PCM surfaces will be determined by brittle fracture rather than setting, which will reduce p_c.

If micropores are formed during the destruction of the interfacial boundary, then at $d_p \approx 1$ μm they can positively affect the process of friction of the conjugation of parts. The newly formed pores serve as reservoirs for lubrication, which improves the regeneration of the lubricating distribution film on the friction surfaces, reduce the coefficients of friction and heat release in the contact zone, and, accordingly, reduce the likelihood of setting materials of conjugated parts. In this regard, weak interfacial boundaries can be allowed in cases where the destruction of the boundaries do not develop cracking cracks, ie only when using plastic matrices and with such a content of filler particles, when contacts between them are absent. This structure of the material at $d_p \approx 1$μm can be provided in the manufacture of PCM with $c_f < c_{fopt}$.

In addition to improving the lubrication, in case of loss of filler particles, their strengthening effect will be reduced and there will be a positive gradient of shear resistance, which will improve the performance of triad coupling parts with PCM. When using such PCM filler particles with a high modulus of elasticity in the event of loss of most particles from the surface layer on a high modulus substrate, a plastic coating with a thickness of 1 μm is formed, which reduces friction and improves the performance of three-coupled parts. The value of p_c in this case should not be greatly reduced, because the presence of a solid substrate in PCM will limit the ability of Frank-Reed sources and generate dislocations in a thin surface layer, and, accordingly, removing filler particles from the surface layer In order to prevent setting on the mechanism of formation of the general step, from such PCM it is necessary to make only one detail of tribocoupling, and the second – with the high-modulus filler with strong interphase borders.

If we limit ourselves to the effect of improving the lubrication of surfaces due to the formation of micropores on them when the filler particles fall, it is more appropriate to create a combined PCM, when one part has strong interfacial boundaries and the other - weak. In such a PCM, particles with a strong interfacial boundary must have a high modulus of elasticity, and particles with a fragile boundary can have any value of the modulus of elasticity. This expands the number of materials that can be used as filler particles with weak interfacial boundaries and allows you to enter such particles not in one part, but in both conjugate parts, because the development of the setting process by both mechanisms will prevent filler particles with high modulus and elasticity high strength of interfacial boundaries.

The role of the size and shape of the filler particles can be determined by two factors [10-12]: cracking of

particles and their ability to inhibit the movement of dislocations. It was previously shown that on the spots of actual contact, larger filler particles crack at smaller values σ. However, the mechanism of hardening Orovana at $c_f < c_{fopt}$ and at the same time c_f more effectively increase the size σ_T of the smaller filler particles. Therefore, from the position of cracking and setting at $c_f < c_{fopt}$ more effective should be PCM with smaller reinforcing particles. However, due to the facilitation of the possibility of transverse sliding of the dislocation with decreasing r_p, with r_p slightly larger size of the dislocation nucleus r_0, too small particles will be an inefficient barrier to dislocation and will develop plastic deformation of irregularities on conjugate surfaces, and with it the probability of setting.

Since $r_0 = 4b$ [15,18], the lower value of r_h should be of the order of $5 \cdot 10^{-3}$ μm. Such particles are very difficult to obtain, so we can assume c_{fopt} that c_f with a decrease in the particle size of the filler, the critical setting load will often increase in the case of modern technological methods.

In PCM, the c_f value σ_c increases c_{fopt} when the plastic deformation that develops at the crack tip covers a large volume, ie with a large particle size of the filler. But here the value of r_p has its limits. When r_p increases to a certain value, the crack does not bypass this particle in the plastic phase, but goes through the body of a large particle of brittle material. As a result γ_p, the Griffiths-Orovan equation decreases and the value σ_c decreases. The maximum particle diameter of the filler should be at the level of 10...50 μm. From this analysis it follows that to increase the value of p_c in PCM with $c_f < c_{fopt}$ particle size should be reduced, and in PCM with $c_f > c_{fopt}$ – increase to 1...2 μm. With large diameters of filler particles, the nature of contacting the surfaces changes, so the critical setting pressure will be subject to other laws close to the laws inherent in single-phase materials.

All of the above applies to PCM with a plastic matrix. Further, the possibility of increasing the value of p_c in contacts involving PCM with a brittle matrix should be analyzed, because at close values of the coefficient of thermal expansion of the matrix and filler, not very large difference E_p (not more than 5 times), low temperatures PCM, small diameter filler particles (about 3.5...11 μm) and their small content (c_f <0.3) can increase the strength of PCM.

Conclusions

1 . Thus, based on the strength of the interfacial boundaries, the most effective should be considered three-coupled parts that are made of PCM with high-modulus filler particles with strong interfacial boundaries. When using filler particles with weak interfacial boundaries, good results can be expected in the case of using high-modulus filler particles or a mixture of high-modulus particles and particles with a small modulus of elasticity.

2. It was found that PCM of microheterophase type based on brittle matrices have a strength close to the strength of single-phase brittle materials. The critical setting pressure depends on the same parameters on which the critical pressure of single-phase brittle materials considered for different types of contacts depends.

3. According to the criterion of critical setting pressure, the most effective should be considered triad-coupling of parts in which PCM one of the working surfaces has $c_f > c_{fopt}$ and the size of the filler particles approaching the upper limit of the size of the reinforcing particles, and the other PCM has $c_f < c_{fopt}$ and the particle size the size of the reinforcing particles of the filler.

4. The role and forms of particles of high-modulus filler, as well as its content in the polymer matrix in the formation of the value of the critical load on the moving conjugation of parts are theoretically substantiated.

References

1. Aulin, VV (2014). Fizychni osnovy protsesiv i staniv samoorhanizatsii v trybotekhnichnykh systemakh: monohrafiia [Kirovohrad: TOV "KOD"] 369 c.

2. Aulin VV (2015). Trybofizychni osnovy pidvyshchennia zosostiikosti detalei ta robochykh orhaniv silskohospodarskoi tekhniky [dys. ... Dr. Tech. Science: 05.02.04] 360 p.

3. Aulin VV, Derkach OD, Makarenko DO, Hrynkiv AV (2018). Vplyv rezhymiv ekspluatatsii na znoshuvannia detalei, vyhotovlenykh z polimerno-kompozytnoho materialu [Problems of tribology. №4] - P.65-69.

4 . Kabat, O., Sytar, V., Derkach, O., Sukhyy, K. (2021). Polymeric composite materials of tribotechnical purpose with a high level of physical, mechanical and thermal properties [Chemistry and Chemical Technology, 15 (4)] pp. 543-550.

5. Kabat, O., Makarenko, D., Derkach, O., Muranov, Y. (2021). Determining the influence of the filler on

the properties of structural thermalresistant polymeric materials based on phenylone C1 [Eastern-European Journal of Enterprise Technologies, 5 (6-113)] pp. 24-29.

6. Dudin, V., Makarenko, D., Derkach, O., Muranov, Y. (2021). Determining the effect of a filler on the properties of composite materials based on polytetrafluoroethylene for tribological conjugations in machines and mechanisms [Eastern-European Journal of Enterprise Technologies, 4 (12-112)] pp. 61-70.

7. Kobets, AS, Derkach, OD, Kabat, OS, Volovyk, IA, Kovalenko, VL, Kotok, VA, Verbitskiy, VV (2020). Investigation friction and wear of constructional plastics based on aromatic polyamide [ARPN Journal of Engineering and Applied Sciences, 15 (10)] pp. 1189-1195.

8. Kobets, AS, Derkach, OD, Kabat, OS, Kovalenko, VL, Kotok, VA (2019) . Recycling of constructional plastics with additives of exhausted polyethylene [ARPN Journal of Engineering and Applied Sciences, 14 (13)] pp. 2397-2406.

9. Kabat, OS, Kharchenko, BG, Derkach, OD, Artemchuk, VV, Babenko, VG (2019). Polymer composites based on fluoroplastic and method for the production thereof (2019) . [Voprosy Khimii i Khimicheskoi Tekhnologii (3)] pp. 116-122.

10. Aulin VV (2006). Pole napruzhen v kompozytsiinomu materiali ta kompozytsiinomu pokrytti v umovakh tertia kovzannia. [Coll. science. prats LNAU. Series: Technical Sciences. №.65 (88)] P.13-20.

11. Aulin VV (2004). Vyznachennia obiemnoho vmistu napovniuvacha v antyfryktsiinomu kompozytsiinomu pokrytti. [Mashynoznavstvo №7 (85)] pp. 49-53.

12. Aulin VV (2006). Vplyv kharakterystyk komponentiv kontaktuiuchykh kompozytsiinykh materialiv i pokryttiv na parametry ta vlastyvosti zony tertia [Problems of tribology. Khmelnytskyi. KhNU, №4 (42)] pp. 110-112.

13. Aulin VV, Hrynkiv AV, Smal VV, Lysenko SV ta in. (2021). Basic approaches and requirements for the design of tribological polymer composite materials with high-modulus fillers [Problems of Tribology, V. 26, No 4 / 102-2021] P. 51-60.

14. Aulin VV, Derkach OD, Hrynkiv AV, Makarenko DO (2021) Vyznachennia robochoi temperatury kompozytnykh elementiv rukhomykh ziednan v zoni tertia [Naukovyi visnyk Tavriiskoho derzhavnoho ahrotekhnolohichnoho universytetu: Vronnekove . 11, vol. 1, stattia21] .

1 5. Aulin V., Derkach O., Makarenko D., Khrynkiv A., Krutous D., Muranov E. (2020). Development of a system for diagnosing bearing assemblies with polymer parts during operation [Technology audit and production reserves № 5/1 (55)] pp.18-20.

16. Aulin V., Derkach O., Makarenko D., Hrynkiv A. and in. (2019). Analysis of tribological efficiency of movable junctions "polymeric-composite materials - steel" [Eastern-European Journal of Enterprise Technologies. Vol. 4 (12-100)] P. 6-15.

17. Aulin VV , Derkach OD, Kabat OS, Makarenko DO, Hrynkiv AV, Krutous DI (2020). Application of polymer composites in the design of agricultural machines for tillage [Problems of Tribology, V. 25, No 2 / 96-2020] - P. 49-58.

18. Aulin V., Kobets A., Derkach O., Makarenko D., Hrynkiv A. and in. (2020). Design of mated parts using polymeric materials with enhanced tribotechnical characteristics [Eastern-European Journal of Enterprise Technologies. Vol.5 (12-107)] P. 49-57.

19. Aulin VV (2016). Trybofizychni osnovy pidvyshchennia nadiinosti mobilnoi silskohospodarskoi ta avtotransportnoi tekhniky tekhnolohiiamy trybotekhnichnoho vidnovlennia: monohrafiia [Kropyvnytskyi: Lysenko VF] 303 s.

Аулін В.В., Лисенко С.В., Гриньків А.В., Деркач О.Д., Макаренко Д.О. Вплив вмісту високомодульного наповнювача на критичне навантаження на трибоспряження з мікрогетерофазних полімерних композиційних матеріалів

В роботі теоретично з трибологічної точки зору обґрунтовано вплив вмісту високомодульного наповнювача на оцінку критичного навантаження на спряження полімерних композитних матеріалів. При цьому розглядаються різні випадки руйнування полімерних композитних матеріалів. Сформульовані умови, при яких спостерігаються схоплювання полімерних композитних матеріалів, а також умови їх руйнування. Розглядається як в'язке, так і крихке руйнування полімерних композитних матеріалів. Основна увага зосереджена на критичних навантаженні і напруження в залежності від вмісту високомодульного наповнювача з урахуванням модулів пружності полімерної матриці і наповнювача та характеру їх руйнування.

Ключові слова: полімерний композитний матеріал, мікрогетерофазний композит, високомодульний наповнювач, трибоспряження деталей, критичне навантаження, схоплювання, руйнування.

***Problems of Tribology**, V. 27, No 2/104-2022, 80-86*

Problems of Tribology
Website: http://tribology.khnu.km.ua/index.php/ProbTrib
E-mail: tribosenator@gmail.com

DOI: https://doi.org/10.31891/2079-1372-2022-104-2-80-86

Properties of coatings obtained by electric arc spraing for renovation of parts of machines and vehicle mechanisms

A. Lopata[1*], M. Holovashchuk[2], L. Lopata[3], E. Solovuch[4], S. Katerinich[4]

[1]National Technical University of Ukraine "Igor Sikorsky, Polytechnic Institute", Ukraine
[2]National Transport University, Kyiv. Ukraine
[3] G. S. Pisarenko. Institute for Problems of Strength of the National Academy of Sciences of Ukraine
[4]Central Ukrainian National Technical Universityi, Ukraine
E-mail: beryuza @ukr.net

Received: 20 April 2022: Revised: 20 May 2022: Accept: 07 June 2022

Abstract

The robots present the results of investigating the power of coatings, excluding electric arc (EAS) filings, and their comparison with the powers of coatings, excluding gas-flame filings. The porosity of the coating, taken from electric arc filings, was in the range of 8-10%. the adhesion strength was 80…100 MPa. The results of the investigations show the advantages and purpose of using electric arc sawing to improve and move the capacity of machine parts and transport mechanisms. In the work, the following factors are added to the process of electric arc sawing: storage of fuel sum, distance of sawing, dispersion of sawing and other. on authority cover. In the course of the investigation, the increase in resistance, adhesive strength, coating thickness, the term for the coating thickness, was determined by the parameters of the electric arc filing. The robots have considered the possibility of securing the necessary authorities influencing the surface with the method of advancing the resource of machine parts by way of regulation by the factors of EAS. Regulating the smoothness and temperature of the stream of transporting gas and particles, you can change the diameter of the droplet, increase the width and reduce the oxidation of the coating. The results of comparative analysis of the properties of coatings applied by electric arc spraying (EAS) using the products of combustion of propane-air mixture and gas-flame spraying (**FSP**) using gas-air mixture are presented. Under optimal conditions of the spraying process, the porosity of the coatings obtained by electric arc spraying is much lower compared to gas-flame spraying: 8-10% and 20-30%, respectively. Adhesion strength of coatings obtained by electric arc spraying increased by 1.8-2.2 times (from 30-40 MPa in gas-flame spraying to 100 MPa in electric arc), wear resistance increased by 2-2yu5 times.

Key words: electric arc spraying, coating**,** flame spraying, porosity, adhesion strength, wear resistance, corrosion resistance, thickness coating, gas permeability

Introduction

The service life of vehicles is inextricably linked with the problem of increasing the wear resistance of its parts. Cam - and crank-shafts are the most responsible and expensive engine parts. During operation, alternative loads on the shaft promote the following phenomena:

- friction and wear of its necks;
- fatigue failures in the neck-to-web passages and at the oil channel outlets;
- bending and twisting owing to its bending, torsion and axial vibrations [1-3].

The shaft neck - bearing coupling operates under conditions of hydrodynamic lubrication. However, the stability of conditions of hydrodynamic friction is frequently broken and semiliquid and sometimes semidry frictions arise, for example, at the start moment or other short-time overloading of the engine. Under such conditions, the wear rate of shaft and bearing surfaces increases [1-3]. However, the behavior of shaft, the webs of which have been recovered via deposition of a coating, is different. Pores in a coating are filled with the oil which flows out of pores due to the shaft rotation. The oil immediately forms a protective film located around the

shaft neck. Moreover, resulted from abrasion metallic particles are pressed into pores moving away from the friction region.

Techniques for prolongation of the service life of crankshafts, which are the most expensive parts of transport means, have been studied well enough and are still being improved. As a rule, inserts and bushes, which form triboconjuctions with crankshafts, wear sooner. In most cases, they are not renewed and instead replaced with new ones. Traditionally, the working layers of inserts and bushes are made from low-friction materials on the basis of copper, tin, aluminum and their alloys. Herein scarce and expensive nonferrous metal is spent uneconomically. Increase in the service life and reduction in expenses for manufacture and maintenance of friction pair parts (crankshafts, inserts, bushes et al.) of transport machinery is one of the most important problems to be solved by scientific researchers, technologists and constructors.

The carried out researches works have shown that one of the most efficient ways to the solution of this problem is the use of electric arc spraying (EAS) for deposition of coatings. The shortage of spare parts has become a major problem in the efficient use of vehicles. The development of international cooperation leads to continuous rise in application of transport means produced abroad, whose maintenance requires steady increase in the quantity of various spare parts. Under the conditions of the broken economic ties and increasing international cooperation, the development of modern technologies for strengthening and protection of new parts against corrosion and renewal of worn ones will make it possible to improve the reliability and longevity of transport means as well as to significantly weaken the dependence on foreign providers of important expensive metal-consuming scarce parts. Herein selection of techniques for strengthening, corrosion protection and reconstruction of parts, which must provide ecologically conscious production, long service life of parts and be universal enough, simple and available, is of great importance. Methods for plasma and detonation spraying, which have been counted on in prolongation of the service life of parts for transport means, require bigger expenses because of expensive equipment and gases. In the current world engineering which deals with the development and application of techniques for deposition of protective coatings and renewal of parts using thermal spraying, more and more attention is paid to electric arc spraying. Nowadays this method is widely applied, especially in the European countries and steadily replays the traditional gas flame method thanks to many advantages as follows [1 -5]:

- the required equipment is produced and is simple and cheap;
- the developed equipment for EAS permits deposition of coatings, the quality of which does not yield coatings obtained by plasma and denotation methods;
- increased thermal effectiveness up to 57 % as compared to 13 and 17 % for gas flame and plasma spraying, respectively;
- high efficiency, which is 3-4 times higher than that for gas flame spraying;
- the absence of need in scare gases;
- availability of power sources for metal melting;
- possibilities of mechanization and automation;
- manufacture of better coatings with higher adhesion strength as compared to gas flame spraying.

The tendency to replace a gas flame rod spraying with EAS has appeared lately. However in the beginning, EAS was only aimed at corrosion protection of welded metallic constructions, and properties of electric arc coatings for other purposes have not been studied properly yet. Therefore implementation in industry of EAS in order to prolong the service life of parts and renew them for provision of transport enterprises with spare parts is an actual task.

The purpose of the work

The purpose of the work was to investigate properties of EAS-derived coatings designed for prolongation of the service life and renewal of friction pair parts (crankshafts, inserts, bushes et al.) of transport machinery.

Properties of coatings obtained by electric arc spraying

The main physicomechanical properties of EAS coatings affecting their operation characteristics are the adhesion strength and porosity. The physical and mechanical properties of experimental samples of coatings made of steel 40Kh13 by arc metallization on an EAS installation were studied [6, 7]. As a result of the conducted experiments, the dependences of the adhesion strength, porosity and gas permeability of coatings on the spraying process parameters such as the current and voltage of arc, spraying distance, speed of spraying apparatus movement relative to the base surface, pressure of the compressed air or combustion products in the distributor head of the electric arc apparatus as well as on the surface pretreatment have been established. The base surface was prepared for spraying using bead blasting treatment. The roughness of the prepared surface (R_Z) fell in the range 5-60 mcm. Before spraying samples were fixed in a special device located in the holder of the lathe. Arc spraying apparatuses were placed on the support of the lathe. The speed of the apparatus movement relative to the sample surface and the spraying distance could be governed by varying the revolution number of the spindle and the support-spindle distance.

The EAS unit was a modern universal system which combined advantages of electric arc and high-rate spraying. Its chief distinctive feature is the presence of a small high-efficiency chamber for combustion of propane-air mixture, whose ultrasonic jet left the chamber with a speed of 1500 m/s at 2200 K. The flow strength, determined by the ratio of the kinetic energy to the gas volume and characterizing the force acting on a particle in the flow, was equal to 234 kPa. The latter permitted melted metal particles to speed up to 500 m/s and to form a coating with doubled adhesion strength compared to flame spraying and sufficient for operation under extreme conditions including the presence of shock-abrasion wear.

The use of the products of propane-air mixture combustion as a spraying gas significantly decreased oxidation of sprayed metal and burning-out of alloying elements. For example, at the fuel combustion coefficient b=0.4 the carbon amount in the coating made from 40Kh13 rods practically did not differ from that in the initial rod. However at equal amounts of air and propane the carbon content in coating was lower than that in the initial material by two times, whereas in spraying by pure air the carbon content decreased by three times.

The conditions of formation and transport of particles as well as of coating formation, which differ from other methods, lead to formation of different structures in the coating material. The small amount of brittle oxides, high content of intermetallic compounds along with formation of hardening structures and high enough plasticity of the deposited layer create favorable background for application of this method for strengthening and renovation of parts of transport means and essentially widen the nomenclature of parts that can be renewed. Moreover, under high-rate spraying conditions, the coefficient of material concentration in the jet increases as the divergence angle of two-phase supersonic jet is smaller as compared to undersonic jets and is equal to 5-7°. As a result, the diameter of deposited spot decreases and the coefficient of material consumption increase.

For EAS it reaches 0.85 against 0.75 for flame spraying. As a material for spraying, a wire from any commercial material (zinc, aluminum, copper, brass, bronze, nichrome, carbon and stainless steels, etc.) can be used as well as a powdered wire or combination of any two wires. The porosity of steel coatings is within 2-4 %; density of aluminum wires is close to that of cast material. This factor is particularly important in production of anticorrosion coatings as herein significant saving of spraying material is attained at the expense of decrease in the coating thickness required for closing of through porosity, and thus the service life of coatings increases. For spraying, 2.0 mm 40Kh13 wires (GOST 5632-72) were used. The process conditions were as follows: arc voltage 32 V, spraying distance 50 - 200 mm, arc current 100-400 A, compressed air consumption 80 m^3/h, pressure 0.65 MPa; when the apparatus EDN was used, propane-butane consumption was 0.011 kg/h, pressure 0.4MPa.

Technique for researching the properties of coatings

The porosity of coatings was determined via hydrostatic weighing according to GOST 18893-73. In order to study distribution of pores through a coating and to determine their size and shape, the system of texture analysis of images Leitz TAS" (Germany) was used composed of a microscope “Ortoplan” with a TV camera, a unit for processing of TV signals and a display. The system operates under the control of a computer designed on the basis of microprocessor LS1 - II/2. To examine coatings, metallographic samples were prepared according to the standard techniques [8]. To determine gas permeability of coatings from steel 40Kh13, samples were made in the form of a bush with a hole and a conic end pin from steel 20. Before spraying, the end surface of the tin was subjected to jet-abrasion treatment for modeling of surface roughness followed by heating in air to 700-760 K for 3-5 min. In such a way, a thick oxide film was formed which prevent from the evolution of chemical interaction between the materials of coating and base. The pin was inserted into the bush, and spraying started to the achievement of required thickness of coating. Then the pin was carefully separated from the coating and taken out the bush hole. The coated sample was put into a unit for measurement of gas permeability.

The coating thickness was measured with a micrometer; the area was determined on the basis of the bush hole before spraying. The adhesion coating-part strength was estimated using a glue method [8]. Metallographic examination was performed on an optic microscope MIM - 8 with the magnification 90-200 and a SEM microscope "MSV-2" (firm "Akasi") with the magnifications 100 and 200. Samples for metallography were prepared using standard techniques [8]. Roughness of the surfaces of base and coating was estimated on a profilograph-profiler of type 201.

Results of experimental studies

The analysis of the structure of coatings produced using electric arc and flame spraying revealed that the latter provides particle sizes which are 5-6 times smaller compared to traditional spraying. Consequently, the sizes and quantity of pores in EAS coatings decreased by 2-3 times.

Gas permeability is a structure-sensitive characteristic of coating, and there is a distinct enough dependence of it on open porosity [8]. Under optimal spraying conditions, the porosity of EAS coatings is much lower than in the case of liquid metal spraying with cold air (2-4% and 9-11%, respectively), and the gas permeability is lower by approximately 30-40 times. This may be related to the essential decrease in the sizes of pore channels in coatings. Fig. 1 demonstrates the curves of pore size distribution for coatings obtained by electric arc and flame spraying.

The analysis showed that for EAS the number of pores is much smaller. Herein the minimal porosity and gas permeability are attained at spraying distances within 50-60 mm. In case of high-efficiency spraying, that is, at currents of 400 A and higher, high enough apparatus movement speed (relative to the base) is required. There was observed different dependences of the porosity (P) on the spraying distance (L_s) for coatings obtained by electric arc and flame spraying.

The porosity of EAS coatings obtained at the minimal apparatus speed, that is, after a one-run deposition, decreased with shortening the spraying distance to 100 mm, but then it increases to the values characteristic for EAS coatings. The speed increase results in decreasing porosity in coatings obtained at small distances (L_s < 80-90 mm). Slight decrease in porosity is observed in flame spraying (FSP) coatings as well. The weak effect of the spraying apparatus speed on the coating porosity at distances L_s > 80-90 mm is caused by weakening of the aerodynamic effect of the reflected plane jet and cooling of d_p<1 mcm particles to temperatures, at which they do not adhere onto base asperities.

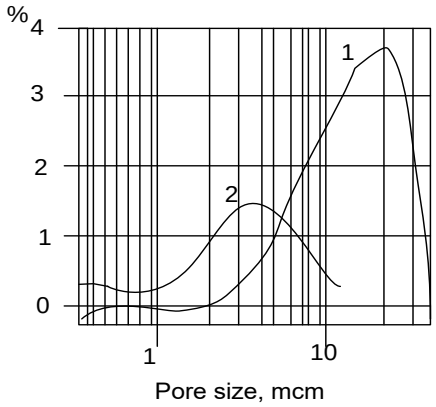

Fig. 1. Pore size distribution: (1) flame spraying FSP; (2) electric arc spraying EAS

The peculiarities of the effect of the arc current (I_a) on the coating porosity are worth noticing. Whereas at big arc currents an increase in the spraying apparatus speed (V_M) markedly decreases porosity, spraying at small currents practically does not affect it. This may be prescribed to small both spraying efficiency and mass-average particle temperature at small arc currents [8, 9].

Properties of anticorrosion electric arc coatings depend on not only the value but also the type of porosity. The authors [8, 9] have proposed to divide porosity into a volume and a surface one as at a layer thickness commensurable with the average microasperity height a drastic change in porosity occurs, which, in its turn, is accompanied by a drastic change in structure-sensitive characteristics of coating, for example, gas permeability.

The investigation of the effect of the thickness of coating on its porosity has shown that the EAS method provides a decrease in the porosity (Fig. 2a). The profilograph indicate the fact of decrease in the surface roughness of a EAS -derived coating. The average microasperity height of the 0.1 mm thick steel coating deposited on a polished base surface at a spraying distance of 100 mm was 5-10 and 30-50 mcm for EAS and FSP, respectively.

Such a marked decrease in the EAS coating porosity (for example, at a coating thickness of 0.05 mm the porosity of coatings under the comparison differ by almost an order of magnitude (Fig. 2, a) inevitably causes still greater difference in the gas permeability (Fig. 2, b). For FSP, reduction in the coating thickness, h <0.1 mm, leads to rapid decrease in the gas permeability.

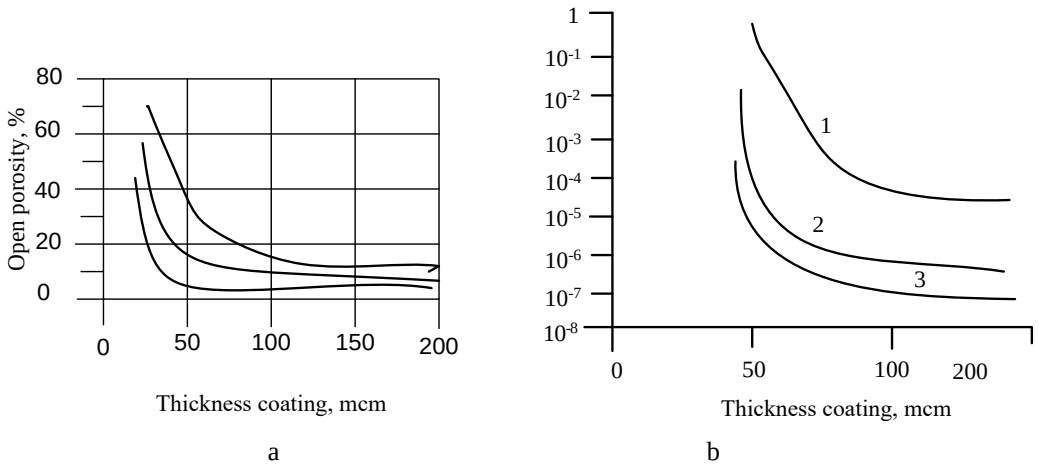

a b

Fig. 2.The effect of the coating thickness on (a) the open porosity and (b) gas permeability: (1) FSP; (2,3) EAS at a coating thickness of (1,3) 100 mm and (2) 50 mm

The reduction in surface roughness of the EAS coating is connected with the particle size decrease and may be the main reason for lower coating open porosity at small thicknesses due to decrease in the surface component of porosity due to bigger surface roughness.

Similar picture is observed in case of EAS, but only beginning with h = 0.05 mm. The sharp rise in the gas permeability may be related to the appearance of a through porosity [8, 9]. Hence, the gas permeability of steel coatings made using the EAS method is lower than that of FSP coatings by 1-2 orders of magnitude. h = 0.05-0.1 mm this difference reaches 4-5 orders of magnitude.

To reach required adhesion strength, which is determined by mechanical or physicochemical bonds depending on the materials of the "coating-base" pair [8, 9], the base surface pretreatment is conducted. The most used technique is jet-abrasive treatment, which purifies the surface and destroys its equilibrium state with the medium by release of interaction forces of surface atoms, that is, chemically activates the base. Unfortunately, the base activity rapidly decreases because of chemical adsorption of air gases and oxidation. It is therefore desirable to shorten the time between the pretreatment and spraying as much as possible. The pretreatment makes the surface rough, which raises the temperature in the contact zone under sprayed particles on microasperity and increases the total surface of spots for welding.

The area of a rough surface is larger than that of a smooth surface, which also results in adhesion strength increasing. The rise of R_z is accompanied with increase in the adhesion coating-base strength (σ_{ad}) (Fig. 3, a). However, it is not high enough as could be expected taking into account the high particle velocity, which reaches 500 m/s. This may be related to the action of the following main factors:

- increase in the particle velocity increases the relative area of the physical particle-base contact [8, 9], which leads to an increase in the adhesion strength;
- reduction in the average particle size in EAS by 4-7 times reduces the particle crystallization time, lowers both the particle-base contact temperature and completeness of chemical interaction, which can reduce the adhesion strength. .

Thanks to the action of these factors, the adhesion strength of EAS coatings is higher by 1.8-2.2 times.

However, in manufacture of anticorrosion coatings, whose thickness is usually small (0.04-0.2 mm), the problem of the right choice of roughness becomes principal as in this case, the layer thickness can be commensurate with the height of microasperity. Insufficient roughness accompanied with big thickness of coating may cause the detachment of coating, whereas a rough surface accompanied with small thickness may become the reason of early corrosion.

As shown in Fig. 3, b, with increasing the height of base surface microasperities, the gas permeability ($K_в$) increases for coatings deposited by any method of arc spraying. However, the most marked effect of R_z on $K_в$ is observed on the coating made using an EAS. The different degree of the influence of the base roughness on $K_в$ is due to the bigger particle size in the case of compressed air spraying, when the first layer of coarse particles is jammed into pits between microasperities so that they cannot affect the coating formation process. The stronger dependence of the gas permeability of EAS coating on R_z is the result of significant inclination of this method towards formation of porous "bumps". Conditions for this become more favorable with increasing the base roughness. It should be mentioned that in case of FSP with increasing the coating thickness the effect of R_z on $K_в$ is negligible, whereas for EAS coatings with h<0.2 mm, this effect only diminishes depending on the spraying distance.

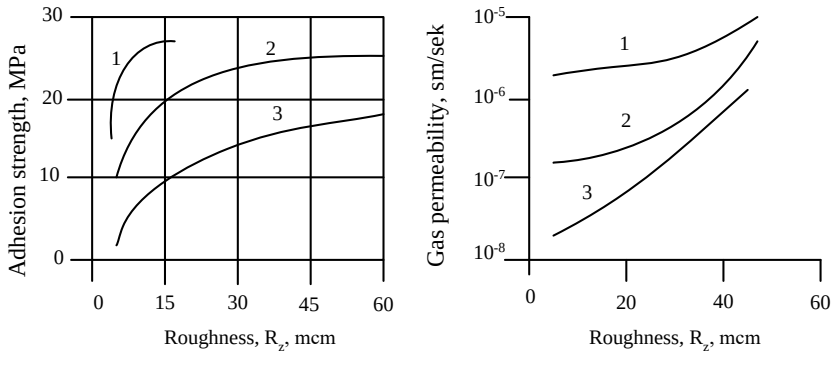

a b

Fig. 3. The effect of the base roughness on (a) the adhesion strength and (b) gas permeability of (1) FSP and (2,3) EAS at a spraying distance of (1,3) 100 mm and (2) 50 mm.

Hence, as it was before shown, for coatings produced using an EAS, a decrease in the base roughness can lead to significant reduction in their gas permeability. This should be taken into account in the development of spraying process conditions and selection of those techniques for surface pretreatment that provide a low degree of roughness, for example, blowing with quartz sand. Herein the adhesion strength decreases as well, and at low R_z in FSP coatings the adhesion strength required for the impossibility of coating detachment may not be reached, whereas in EAS the adhesion strength is high enough even in case of using a polished base surface.

Approbation of the research results

EAS was used for:

- i) renewal of worn steel cylinder parts operating under conditions of sliding friction and lubrication;
- ii) elimination of defects and protection against metal corrosion of tubes, internal and external surfaces of reservoirs and multi-aimed welded constructions as well as various decorations using spraying with aluminum, zinc and cadmium [8,9].

In addition, covering of about 50% surface of each neck is performed under conditions of strong support of the gas flow, as the crankshaft webs forms semi-closed space. The difference in the coating formation conditions causes difference in the physicomechanical characteristics of the deposited layers on different neck spots and so their different wear. The use of EAS which includes mechanical activation of coating in the course of spraying process allows one to equalize the properties of coating along its width and depth. Crankshaft necks with coatings may be repolished in the course of the next overhaul for the required size. This is not, however, reasonable as during hard and long operation the wear resistance of the coating decreases due to filling of its pores with the wear products and other impurities. It is more reasonable to remove the old coating and deposit a new one. EAS has renewed the sizes of support webs of engine camshafts. The results of the operation testing of cam- and crankshafts with using EAS process have demonstrated that the service life of these parts is 1.5-2 times longer as compared to parts renewed using FSP method.

Conclusions

1. Comparative analysis of coating properties has revealed that via using optimal spraying conditions, the porosity of EAS-derived coatings is significantly smaller than that for FSP coatings (2-4% and 9-11%, respectively), and at a coating thickness of 0.05-0.1 mm the difference reaches 2-5 orders of magnitude. The adhesion strength of EAS-coatings is 1.8-2.2 times higher.
2. When developing the EAS process for deposition of coatings, one should choose those techniques for pretreatment of the base surface which can provide reduction in the degree of its roughness (from 5 to 10 mcm) required for decreasing its gas permeability and thus porosity.
3. As a spraying gas, EAS uses the products of combustion of propane-air mixture, varying of which makes it possible to form a neutral or a reducing medium in the zone of electric wire melting, and in such a way:
   - to decrease metal oxidation and burning-out of alloying elements;
   - to increase the strength and wear resistance of coatings and so to prolong the service life of transport means parts.
4. Using the EAS technology, including mechanical activation of coating in the course of spraying, permits equalization of the properties of a coating along its thickness and width.

References

1. Highly efficient technologies in mechanical engineering: Materials of the conference (October 28-30, 1998, Kharkov). Kyiv: 1998. 126 p.

2. K.A. Yushchenko, Yu.S. Borisov, V.D. Kuznetsov, V.N. Surface engineering cake. Kiev: Naukova Dumka, 2007. 559 p.

3. Korzh V.M., Popil Yu.S. Surface engineering is a new technological direct preparation and renovation of machine parts and designs. Modern machine building. 1999. No. 1. pp. 92–94.

4. S.K. Fomichev, V.N. Lopata, M.C. Ageev, A.V. Vorona Restoration and hardening of wearing parts of armored personnel carriers by electric arc spraying. "Quality, standardization and control: Theory and practice": materials of the 15th international scientific and practical conference (September 15-18, 2015, Odessa). Kyiv: ATM of Ukraine, 2015. S. 184-188.

5. L.A. Lopata, Lopata, Medvedeva N.A., T.M. Tunic Dosledzhennya of car parts type "shaft" electric arc metallization. "Design and technology of production of agricultural machines": Collection of scientific works. Kirovograd: KNTU, 2005. No. 35. pp. 409-416.

6. Welding equipment, consumables, auxiliary equipment, raw materials for the manufacture of electrodes, gas welding equipment, equipment for special methods of welding, cutting, surfacing and spraying. - Directory. Salon "Welding". - Kyiv, 1994. 100 p.

7. List of electric welding equipment and equipment for applying coatings by gas-thermal methods. Kyiv: Institute of Electric Welding. E.O. Paton of the Academy of Sciences of the Ukrainian 1990. 68 p.

8. B. Vilage, K. Rupprecht, A. Pokhmurskaya Features of gas-thermal spraying with flux-cored wires. Automatic welding. No. 10. 2011. P. 26-30.

9. Brusilo Yu.V. S.A. Dovzhuk L.A. Lopata Influence of factors of the process of electric arc spraying on the structure formation and properties of coatings. Collection of science practices of the Kirovohrad National Technical University "Technology in the agricultural industry, galuzev machine-building, automation." 2010. Issue 23. P. 287-297.

Лопата О.В., Головащук М.В., Лопата Л.А., Солових Є.К., Катеринич С.Е. Властивості покриттів, отриманих електродуговим напиленням для реновації деталей машин і механізмів транспортних засобів

У роботі представлені результати дослідження властивостей покриттів, отриманих електродуговим (ЭДН) напиленням, і їх порівняння з властивостями покриття, отриманих газополуменевим напиленням. Пористість покриття, отриманих електродуговим напиленням, знаходилася в межах 8 10%. міцність зчеплення склала 80…100 МПа. Результати проведених досліджень показують переваги та цілеспрямованість використання електродугового напилення для відновлення та підвищення ємності деталей машин і механізмів транспортних засобів. В роботі дослідження впливу факторів процесу електродугового напилення: складу горючої суміші, дистанції напилення, дисперсності розпилення та ін. на властивості покритий. При проведенні досліджень запропоновано підвищення адгезійної стійкості, щільності покриття за рахунок керування параметрами електродугового напилення. У роботі розглянута можливість забезпечення необхідних властивостей відновлюваних поверхонь з метою підвищення ресурсу деталей машини шляхом регулювання факторами ЕДН. Зокрема, регулюючи швидкість і температуру струї транспортуючого газу і частинок можна зменшити діаметр капель, підвищити щільність і знизити окислюваність покриття. Приведені результати порівняльного аналізу властивостей покриттів, нанесених електродуговим напиленням (ЕДН) з використанням продуктів згорання пропан-повітряної суміші та газополуменевим напиленням (ГПН) з використанням газоповітряної суміші. За оптимальних умов процесу напилення пористість покриттів, отриманних електродуговим напиленням значно менша порівняно з газополуменевим напиленням: 8-10% і 20-30% відповідно. Адгезійна міцність покриттів, отриманних електродуговим напиленням підвищилася в 1,8-2,2 рази (з 30-40 МПа при газополуменевому напилені до 100 МПа при електродуговому), зносостійкість підвищилася в 2-2ю5 рази.

Ключові слова: електродугове напилення, покриття, газополуменеве напилення, пористість, адгезійна міцність, зносостійкість, зносостійкість, корозійна стійкість, товщина покриття, газопроникність

Problems of Tribology, *V. 27, No 2/104-2022, 87-93*

Problems of Tribology
Website: http://tribology.khnu.km.ua/index.php/ProbTrib
E-mail: tribosenator@gmail.com

DOI: https://doi.org/10.31891/2079-1372-2022-104-2-87-93

Kinematic analysis and synthesis of cutter movement of slotting machine

V.R. Pasika[1*], D.A. Roman[1], V.O. Kharzhevskyi[2]

[1]Lviv Polytechnic National University, Ukraine
[2]Khmelnytskyi National University, Ukraine
**E-mail: paswr@meta.ua*

Received: 20 April 2022: Revised: 25 May 2022: Accept: 10 June 2022

Abstract

The kinematic characteristics of the links and individual points of the mechanism are determined by the method of closed geometric contours and the method of designing plans. The forces of interaction between the links of the mechanism are determined by the method of kinetostatics, and the balancing moment by considering the dynamic equilibrium of the crank and the method of power balance. The drawbacks of the structural scheme of the mechanism are revealed and the ways of their elimination are offered.

The results of research are presented in the form of graphical dependences of the kinematic parameters of the cutter, reactions or hodographs of forces in kinematic pairs. The moments of resistance forces and inertia forces are determined and the dynamic and mathematical models of the movement of the mechanism are constructed. The technology of determining the power of the electric motor is shown, and its stable area of operation is approximated by a straight line.

Kinematic synthesis was performed and a modernized mechanism was obtained in which the cutter can move according to a predetermined law, in particular, without soft shocks at the boundaries of the kinematic cycle and with quasi-constant speed (error up to 5%) in the middle of the kinematic cycle.

Key words: linkage mechanisms, optimization, synthesis, kinematic analysis, law of motion, cams

Introduction

Slotting machines are used both in serial production and in repair shops to obtain grooves, flat and shaped surfaces of small height, but significant transverse dimensions, through and blind holes and cavities. The main mechanism of slotting machines is a rocker with a two-lead group attached to it, the slide of which moves in a vertical plane. The productivity of the machine is limited by the planing speed (70-80 m/min), due to the reciprocating movements of the slide with which the cutter is rigidly connected. The movement of the cutter on the working stroke is not even, which degrades the quality of the planing surface, the durability of the cutter. The presence of cutter acceleration jumps at the edges of the kinematic cycle causes soft impacts, which worsens the dynamic state of the mechanism as a whole and, as a result, further impairs the quality of the planing surface.

Literature review

Analysis of modern publications in the papers on Mechanism and Machine Science showed that the existing methods for the synthesis and analysis of mechanisms of slotting machines, both analytical and numerical, do not provide exact parameters to synthesize multi-link linkage mechanisms that could be characterized by no acceleration jumps at the boundaries of the kinematic cycle and quasi-constant velocity. cycle [1-3], including a number of modern works on this topic [8-10].

In particular, in the work [1] the methods of synthesis of linkage and cam mechanisms using unified subroutines to calculate the main kinematical parameters of linkage mechanisms are shown. It is also considered the problems of kinematic synthesis of linkage mechanisms, synthesis and analysis of cam mechanisms: a number of examples of the usage of the mathematical package Mathcad for this purpose are also provided.

Additionly, in our opinion, in the methods that are described in the existing works [1-3], there are some drawbacks that do not allow to conduct correct calculations for the entire range of initial data and according to all the neccesary requirements of the designer. For example, no analytical dependences are given for all variants of the angles of inclination of vectors of kinematic quantities and reactions in kinematic pairs.

Several calculation schemes of the structural groups are described not in the most general form. For example, for the structural group of the 2nd type, when the position of the slider will be in different quadrants, the angles of the shuttle without additional calculations can not be determined. Using modern CAD-systems, it is possible to solve numerically many problems of kinematic and dynamic analysis of technical systems, as shown in [10], but the problems of the kinematic synthesis, taking into account a number of additional criterai, require special methods, which is the subject of this publication. In this paper we will use some methods that were previously described in [4-7].

Purpose

The aim of the research is to analyze the kinematic state of the slotting machine mechanism and on its basis to suggest the ways to improve the dynamic parameters of the mechanisn and the quality of the planing surface; to synthesize such displacement of the additional slide (fixed cam profile) relative to the coupling link, where the cutter will not have soft impacts at the boundaries of the kinematic cycle and move at a constant velocity in the middle.

The kinematic analysis

The scructural scheme of the mechanism is shown in the Fig. 1 and contains: crank *OA* – 1, rocker slider – 2, coupling link (rocker) *ABC* – 3, shuttle *CD* – 4 and slider DD_1 – 5 to which the cutter is perpendicularly attached and which is affected by the planing force F_p.

The analysis is carried out on the basis of the structural qualification of mechanisms according to Assur, where structural formula for constructing the mechanism is as follows:

$$I(0-1)\rightarrow II(2-3)\rightarrow II(4-5) \tag{1}$$

Kinematic analysis is performed from the beginning of the structural formula according to the dependences obtained in [1-3]. We connect the right coordinate system *xOy* with the center of rotation of the crank. We consider the frequency of rotation of the crank and the geometric characteristics of the links as a known one.

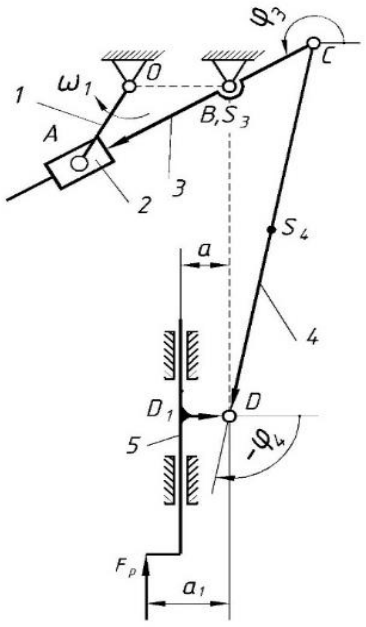

Fig.1. Structural scheme of the mechanism

Determination of the kinematic characteristics of the mechanism is carried out in groups from the beginning of the structural formula (1). Crank *OA*.

$$v_A=\omega_1 l_{OA};\ \gamma_a=\varphi_1-\pi,\ a_A=\omega_1^2 l_{OA},\ \psi_a=\varphi_1+\pi,,$$

where v_A i γ_a – modulus and angle of inclination of the velocity vector $\vec{v}_A$ to the abscissa, a_A i ψ_a – modulus and angle of inclination of the acceleration vector $\vec{a}_A$ to the abscissa.

Structural Group ABC. Calculate the kinematic characteristics of the rocker *AB*:

$$x_B = l_{OB};\ y_B = 0;\ l_{AB} = \sqrt{(x_A - x_B)^2 + (y_A - y_B)^2},\ \varphi_3 = \text{arctg}\left(\frac{y_A - y_B}{x_A - x_B}\right);$$

$$\omega_3 = v_A \sin(\gamma_A - \varphi_3)/l_{AB},\ v_{A_3A} = -v_A \cos(\gamma_A - \gamma_3);$$

$$\varepsilon_3 = \left[a_A \sin(\psi_A - \varphi_3) + 2\omega_3 v_{A_3A}\right]/l_{AB},\ a_{A_3A} = -a_A \cos(\psi_A - \varphi_3) - \omega_3^2 l_{AB}.$$

Calculate the kinematic characteristics of the kinematic pair *C*:

$$x_C = x_B + l_{BC}\cos(\varphi_3 + \pi), y_C = y_B + l_{BC}\sin(\varphi_3 + \pi);\ \ l_C = \sqrt{x_C^2 + y_C^2},\ \varphi_C = \text{arctg}(y_C / x_C);$$

$$v_C = l_{BC}|\omega_3|,\ \gamma_C = \varphi_3 + \pi + 0{,}5\pi \cdot \sin(\varphi_3),\ a_C = l_{BC}\sqrt{\omega_3^4 + \varepsilon_3^2},\ \psi_C = \varphi_3 - \text{arctg}(\varepsilon_3 / \omega_3^2).$$

Structural group CD. ξ – the angle of the guide *5* to the abscissa, $x_B = 1$ i $y_B = 0$ – sign of the point of intersection of the perpendicular dropped from the beginning of the coordinate system on the guide of the slider, $ze = \text{sign}\left\{\text{sgn}\left[y_E \cos(\xi)\right] - \text{sgn}\left[x_E \sin(\xi)\right]\right\}$,

$$\varphi_4 = \arcsin\left[e \cdot ze + a - l_C \sin(\varphi_C - \xi)\right]/l_4 + \xi,\ e = l_{OB} - a;$$

$$y_D = l_C \sin(\varphi_C) + l_4 \sin(\varphi_4) - a,\ s_D = y_{D\max} - y_D;$$

$$\omega_4 = \frac{v_C \sin(\xi - \gamma_C)}{l_4 \cos(\varphi_4 - \xi)},\ v_D = \frac{v_C \cos(\varphi_4 - \gamma_C)}{\cos(\varphi_4 - \xi)},\ a_D = \frac{a_C \cos(\psi_C - \varphi_4) - \omega_4^2 l_4}{\cos(\varphi_4 - \xi)}$$

$$\varepsilon_4 = \frac{-a_C \sin(\psi_C - \xi) + \omega_4^2 l_4 \sin(\varphi_4 - \xi)}{l_4 \cos(\varphi_4 - \xi)},\ \gamma_D = \xi + \frac{\pi\left[1 - \text{sgn}(v_D)\right]}{2},\ \ \psi_D = \xi + \frac{\pi\left[1 - \text{sgn}(a_D)\right]}{2}.$$

The analysis was performed for such parameters of the mechanism:

$$n = 120 \text{ rpm};\ \ l_1 = 0.11 \text{ m};\ \ l_{OB} = 0.05 \text{ m};\ a = 0.01 \text{ m};\ \ b = 0.02 \text{ m};\ l_{BC} = 0.11 \text{ m};\ l_4 = 0.45 \text{ m};\ \ l_5 = a;\ \ e = l_{OB} - a. \quad (2)$$

The kinematic characteristics of the cutter are shown in the Fig. 2.

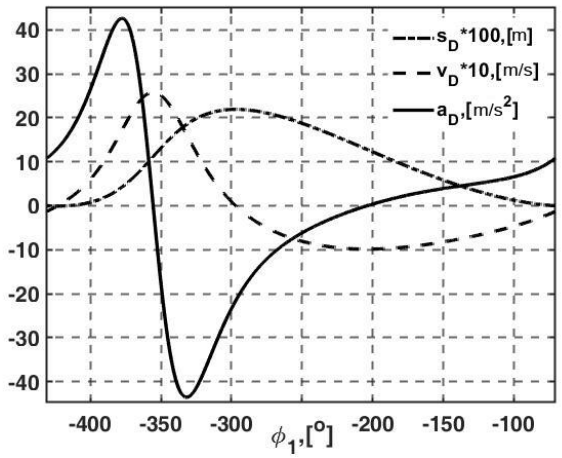

Fig. 2. Kinematic characteristics of the slider (cutter)

The results of the analysis confirm the fact that the linkage mechanisms do not provide movement of the moving link with a quasi-constant speed. The beginning and end of the planing process occurs with an acceleration jump, which causes a soft impact effect and leads to a deterioration of the dynamic state of the whole machine, its productivity and the quality of the planing surface. To avoid side effects, we need:

– to synthesize or use the known laws of periodic motion [2, 6, 7], in which there are no soft impacts, and in the middle of the kinematic cycle we have a section of quasi-constant velocity;

– to ensure the movement of the cutter according to the synthesized or selected law, replace one of the links of constant length with a link of variable length. In this case, the problem is reduced to the synthesis of such a variable length of the link at which the cutter will move according to the synthesized or selected law.

The kinematic synthesis

In the conclusions to [5] it is stated that the cutter on the working stroke has no interval of movements at a constant speed, and at the ends of the kinematic cycle acceleration is not equal to zero. Such kinematic characteristics of the cutter cannot be considered satisfactory, as soft impacts lead to a sudden action of inertia on the cutter, and variable speed degrades the quality of the planing surface. Thus, occurs the question, is it possible to modernize the mechanism to avoid such shortcomings?

It is known [1, 2] that the geometry of linkage mechanisms with one degree of freedom completely determines the qualitative kinematic characteristics of the links and it is impossible to change them. To improve the known structural scheme of the slotting machine (Fig. 3, a), it is proposed to add one more link in the kinematic chain in order to obtain a mechanism with two degrees of freedom (Fig. 3, b). The additional link of the slider *6* is connected to the shuttle 4 by a rotating kinematic pair *C* and by a translational C_3 to the slide 3. The roller *p* rotates around the axis of the pair *C* and rolls a fixed cam, which changes the length l_{BC}.

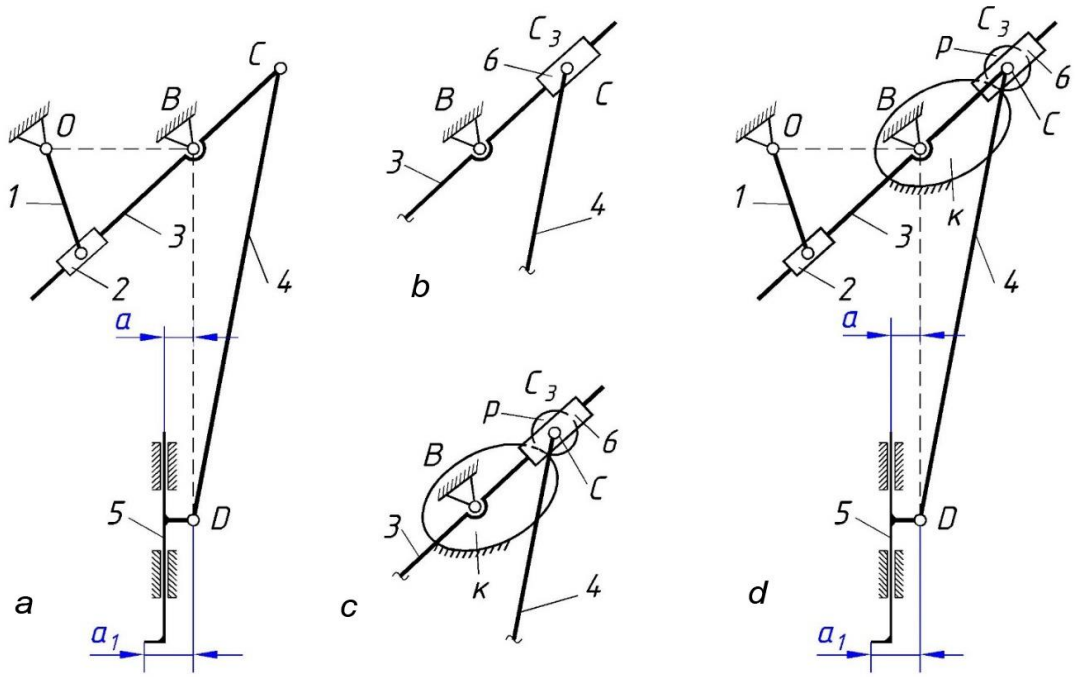

Fig. 3. The steps of modernization of the structural scheme of the mechanism of the slotting machine

With such changes, the degree of freedom of the modernized structural scheme *W=2*. Kinematic synthesis includes choosing the law of motion of the slider *6*, according to which the cutter (same as point *D*) will move according to a predetermined law.

If the crank *1* is driven by an electric motor, the additional slider can be moved in different ways. At the stage of discussions step electric motors and cam mechanisms are considered. Today, the disadvantages of step motors are that changing the position of the shaft is not a smooth line, but stepped. In addition, you need another power supply and automated control system. The use of a cam mechanism (Fig. 3, c) allows theoretically to obtain any law of periodic motion, but it is necessary to obtain a profile of a fixed cam *k*, the pressure angles of which will not exceed the allowable. Since the cam mechanism has a higher kinematic pair, this may impose additional restrictions on its use.

In our opinion, the use of the cam mechanism is simpler, cheaper and does not require special maintenance. Its use in various industries from printing engineering to internal combustion engines has proven its wide potential. The block diagram of the improved mechanism is shown in Fig. 3, d.

The essence of kinematic synthesis is to synthesize such a movement of the additional slide *6* (fixed cam profile *k*) relative to the backstage, at which the movement of the cutter 5 will occur without soft impacts at the boundaries of the kinematic cycle and at a constant speed in the middle

Theoretical grounds of kinematic synthesis

Consider links 3-5 and 6 separately (Fig. 4). Obviously, the point D and the cutter belong to the same body, and therefore the motion of the point *D* is also translational. The contour of the BC can be interpreted as a crank-shuttle mechanism (CSM) in which the length of the conditional car of the aircraft varies depending on the angle $\varphi_3' = \varphi_3 - \pi$; where φ_3 – the angle of rotation of the link *ABC* to the abscissa in the *xOy* coordinate system.

The input parameters of the synthesis, in addition to geometric dimensions, includes the law of motion s_D of the cutter (point *D*), which will achieve the objective of synthesis. The initial parameter of the synthesis is the radius vector of the fixed cam.

Denote the variable length of the conditional box $r_C \equiv l_{BC}$. Each position of point *C* must correspond to a specific given position of point *D*, and the distance between them must always be constant. This problem can be reduced to a purely mathematical one: to determine the coordinates of the point of intersection of the conditional crank of radius $r_C = \sqrt{x_C^2 + y_C^2}$ and a circle of radius l_{CD} conducted from a given point *D*:

$$\left.\begin{aligned} x_C &= r_C \cos(\varphi_3'), \\ y_C &= r_C \sin(\varphi_3'), \\ x_C^2 + (y_C - y_D)^2 &= l_{CD}^2, \end{aligned}\right\}$$

where x_C, y_C – coordinates of point *C* in the coordinate system x_1By_1.

However, we will determine in a more visual way. We show the positions of links 3 and 4 in cases where the angle μ between the links *BC* and *CD* is acute, obtuse and equal to 90° (Fig. 5). In the Fig. 5, and shows the case when the angle μ_1 is acute and straight.

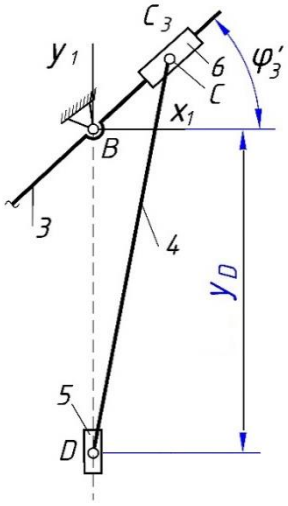

Fig. 4. Structureal scheme of the combined mechanism with variable lwngth of the conditional crank

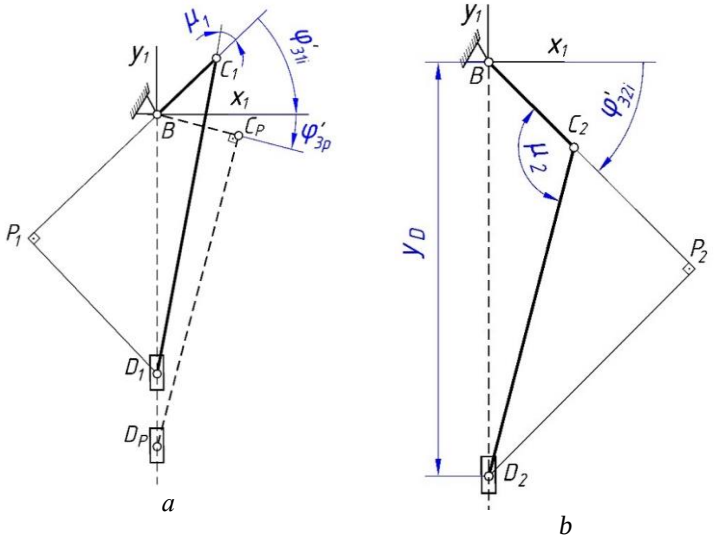

Fig. 5. For the determination of the length of the of the conditional crank *BC*

Variable radius of the conditional crank in the case of an acute angle μ_1 $r_C = C_1P_1 - BP_1$, where $C_1P_1 = \sqrt{l_4^2 - D_1P_1^2} = \sqrt{l_4^2 - \left[y_{D_1}\sin(\varphi_{31}' + \xi)\right]^2}$, $BP_1 = y_{D_1}\sin(\varphi_{31}' + \xi)$, $l_4 = l_{CD}$ – length, shuttle, $\xi = -90^\circ$ – the angle of the cutter guide to the abscissa Ox_1.

Therefore, for an acute angle, the radius is (Fig. 5, a):

$$r_C = y_{D_1}\sin(\varphi_{31}' + \xi) + \sqrt{l_4^2 - \left[y_{D_1}\sin(\varphi_{31}' + \xi)\right]^2}. \tag{3}$$

For a right angle $\mu = 90^\circ$ the radius is

$$r_C = y_{D_p}\sin\left(\varphi_{3p}' + \xi\right), \tag{4}$$

where y_{D_p} і φ_{3p}' – moving the point D and the angle of inclination *BC* in the position when $\mu = 90^\circ$.

For an obtuse angle μ_2 (Fig. 5, b) $r_C \equiv BC_2 = BP_2 - C_2P_2$, where $BP_2 = y_{D_2}\sin\left(\varphi_3' + \xi\right)$, $C_2P_2 = \sqrt{l_4^2 - \left[y_{D_2}\cos\left(\varphi_3' + \xi\right)\right]^2}$. The radius of the conditional crank for an obtuse angle:

$$r_C = y_{D_1}\sin\left(\varphi_3' + \xi\right) - \sqrt{l_4^2 - \left[y_{D_2}\cos\left(\varphi_3' + \xi\right)\right]^2}. \tag{5}$$

The obtained three dependences (3)-(5) are valid when the angle μ is obtuse, straight or acute. We apply the sign function and write the value of the variable length of the conditional crank for any angle φ_3' of the coordinate of the point *D* - y_D:

$$r_C = y_D\sin\left(\varphi_3' + \xi\right) - \operatorname{sgn}\left(\varphi_{3p}' - \varphi_3'\right)\sqrt{l_4^2 - \left[y_D\cos\left(\varphi_3' + \xi\right)\right]^2}. \tag{6}$$

Obviously, the root expression cannot be negative. But if the expression is positive, then the trajectory of point *C* has a gap of the first kind, which also does not satisfy us. Therefore, additional studies of sub-root function were performed $z = l_4^2 - \left[y_D\cos\left(\varphi_3' + \xi\right)\right]^2$ and built its graphs for three cases $z > 0$, $z < 0$ і $z = 0$ (Fig. 6). It turned out that to synthesize the radius vector $\vec{r}_C$ possible only if in a mutually perpendicular

position ($\mu=90^\circ$) of links *BC* and *CD* function *z*=0. From this condition we determine the angle of rotation of the conditional crank φ'_{3p}, for which $\mu=90^\circ$. In addition, another synthesized parameter is the length of the crank *CD*:

$$l_{4s} \equiv l_{CDs} = y_D(\varphi'_{3p})\cos\left(\varphi'_{3p}+\xi\right). \tag{7}$$

For the given geometrical characteristics, the conditional crank of *BC* and shuttle *CD* are mutually perpendicular when the angle of turn $\varphi'_3=77.79^\circ$. The length of the synthesized shuttle $l_{4s}=0,4611$ m.

With this addition, the variable length of the conditional crank (6) is equal to

$$r_C = y_D\sin\left(\varphi'_3+\xi\right)-\operatorname{sgn}\left(\varphi'_{3p}-\varphi'_3\right)\sqrt{l_{4s}^2-\left[y_D\cos\left(\varphi'_3+\xi\right)\right]^2}\quad . \tag{8}$$

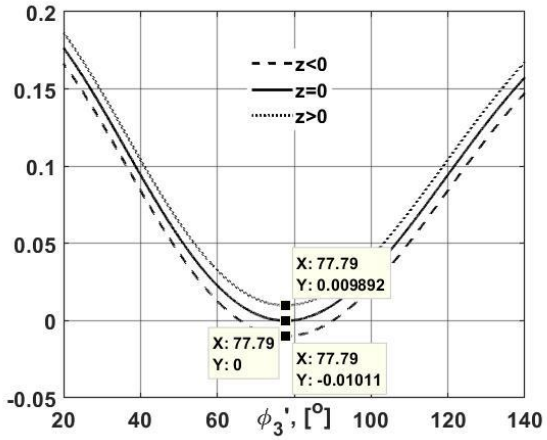

Fig. 6. To determine the synthesized length of the shuttle *CD*

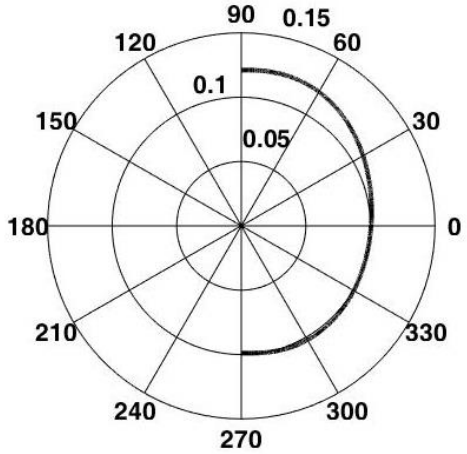

Fig. 7. The trajectory of point C of the synthesized mechanism at the stage of operation

Choice of the law of motion for the cutter

To eliminate the drawbacks of the mechanism of the slotting machine, it is necessary that the law of periodic motion (LPM) of the cutter at the edges of the stroke would not have acceleration jumps, and in the middle of the kinematic cycle there would be a constant velocity interval.

To choose a specific LPM of a cutter, we can use already known, or synthesize a new combined law. Among the known LPM [2, 6, 7] a large number of cycloid laws in which there is no acceleration at the boundaries. Among them are laws with quasi-constant velocity in the middle of the kinematic cycle.

The authors chose the law [6] that has the widest interval of quasi-constant velocity with 5% error. Invariant of moving this law:

$$a_k = (70k^3 - 245k^4 + 378k^5 - 280k^6 + 80k^7)/3, \tag{9}$$

where $k=t/T$ – dimensionless time, $0\le t\le T$ – current time, T –working period. The invariants of velocities and accelerations are calculated according to known dependencies $b_k=\frac{da_k}{dk}$, $c_k=\frac{b_k}{dk}$.

The chosen law is an algebraic law of the second type, for which the kinematic invariants are *B* = 1.46; *C* = 6.51, and the interval of quasi-constant velocity is 36.92%.

In the Fig. 7 is shown the trajectory of point *C* is built using (6) (fixed cam profile), at which the cutter on the working stroke will move according to the selected law (9). Visual analysis shows that the profile is smooth, the largest angles of pressure are observed at angles close to 30° and not exceeding about 20°. It will be possible to know more specifically after calculation of corresponding angles of pressure.

It is important to note that at half of the planing interval, the angles from $\varphi'_3=0^\circ$ to $\varphi'_3=-90^\circ$, the radius of the trajectory is close to the arc of the circle, which practically unloads the highest kinematic pair of the cam.

The kinematic characteristics of the cutter of the non-synthesized mechanism are shown in the Fig. 8, a, and the synthesized one – in the Fig. 8, b. Calculations of actual values were performed by [6]:

$$s_D = a_k[S],\ v_D = b_k\frac{[S]}{[T]},\ a_A = c_k\frac{[S]}{[T^2]},$$

where $[S]$=0.22 m – stroke of the cutter; $[T]=2\pi/|\omega_1|(\varphi_e-\varphi_s)/(\varphi_s+\varphi_e)=0{,}3251$ sec. – period of the kinematic cycle (operating time), $\varphi_e=-297.036^\circ$ i $\varphi_s=-63.964^\circ$ – the angle of rotation of the crank at the beginning and end of the stroke.

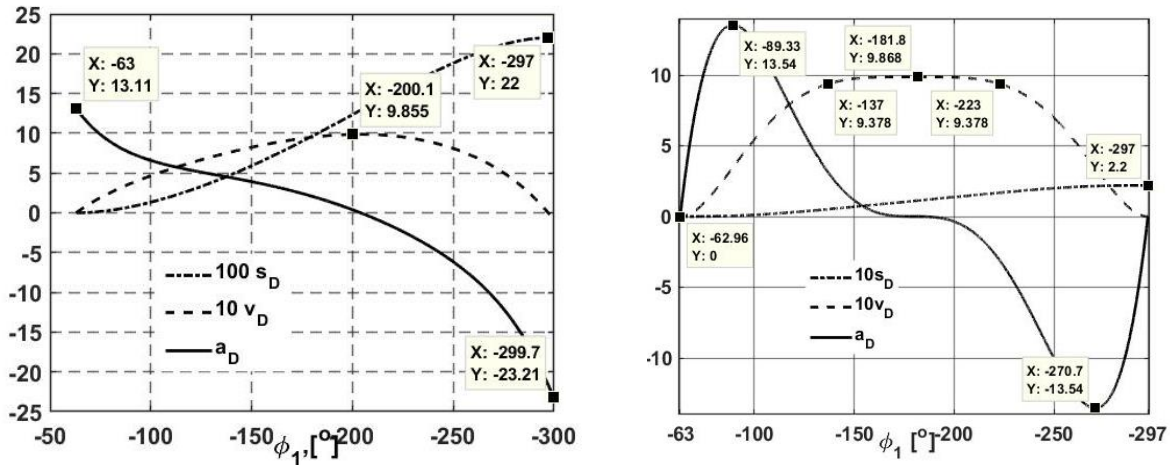

a *b*

Fig. 8. Kinematic characteristics of the cutter: a - not synthesized and b - synthesized mechanism

There are no acceleration jumps at the boundaries of the kinematic cycle, and there is a quasi-zero velocity interval in the middle. The quasi-zero velocity is almost equal to the maximum velocity of the non-synthesized mechanism. In the mechanisms of real planing machines operation does not begin at the beginning of the stroke and does not end at the finish. There is always a certain angle of rotation of the handle at the boundaries of the kinematic cycle, after which the planing process begins and ends. Therefore, the constant velocity interval of 36.92% is minimal.

Conclusions

– for the first time a six-linked linkage mechanism with variable link length was synthesized;

– changing the length of the link is proposed to provide by a fixed cam;

– the synthesized cam profile is a smooth curve and the pressure angles are clearly less than maximum that are allowed $[\gamma]\cong 40^\circ-45^\circ$ [2];

- it is received the movement of the cutter with zero accelerations at the beginning and at the end of the working stroke and with a quasi-constant speed interval of not less than 36.92% of working stroke;

– the quasi-constant velocity interval can be increased by reducing the chipping interval.

References

1.Kinytskyi Ya. T. , Kharzhevskyi V. O., Marchenko M. V. (2014) Teoriia mekhanizmiv i mashyn v systemi Mathcad: navch. posibnyk [Theory of Mechanisms and Machines in Mathcad: textbook], Khmelnytskyi, KhNU, 295 p.

2.Kinytskyi Ya. T. (2002) Teoriia mekhanizmiv i mashyn [Theory of Mechanisms and Machines], Naukova Dumka, Kyiv, 660 p.

3.Kryzhanivskyi Ye. I., Malko B. D., Senchishak V. M. (1996) Kursove proektuvannia z teorii mekhanizmiv i mashyn: navch. posibnyk [Course projecting on Theory of Mechanisms and Machines: textbook], Ivano-Frankivsk, 357 p.

4.Pasika V. R., Heletii V. M. (2019) Analitychnyi metod u doslidzhenni vazhilnykh mekhanizmiv II klasu [Analytical method in researching of linkage mechanisms of the 2nd class], Lviv-Drohobych "POSVIT", 2019. 142 p.

5.Pasika V.R., Koruniak P.S., Zokhniuk V.V., Roman D.A. (2021) Dynamichne analizuvannia mekhanizmu dovbalnoho verstatu [Dynamic analysis of slotting machine]. Herald of Lviv Agrarian University. Agroengineering researches, #25, P. 42.49.

6.Pasika V.R., Heletii V.M., Solohub B.V. (2021) Kinematychne syntezuvannia zakoniv periodychnoho rukhu [Kinematic synthesis of periodical laws of motion] : monography, Lviv, Levada, 123 p.

7.Pasika V.R. (2006) Syntez optymalnykh zakoniv periodychnoho rukhu [Synthesis of optimal laws of motion]. Scientific notes of Ukrainian Academy of printing, #9, P. 38-44.

8.Romansevych Yu. O., Rybalko V. M., Matukhno N. V. (2015) Vybir elektrodvyhuniv dlia mashyn i mekhanizmiv, yaki zabezpechuiut vyrobnychi protsesy u silskomu i lisovomu hospodarstvi [Selection of electric motors for machines and mechanisms that provide production processes in agriculture and forestry], Kyiv, 75 p.

9.Uicker J., Gordon R. Pennock, Shigley J. Theory of Machines and Mechanisms. New York, Oxford University Press, 2017, 977 p.

10. Advances in Mechanism Design II: Proceedings of the XII International Conference on the Theory of Machines and Mechanisms (ed. J. Beran, M. Bilek, P. Zabka), Springer International Publishing, 2017.

11. Kuang-Hua Chang. Motion Simulation and Mechanism Design with SOLIDWORKS Motion 2021. SDC Publications, 2021, 220 p.

Пасіка В.Р., Роман Д.А., Харжевський В.О. Кінематичний аналіз та синтез руху різця довбального верстату

Кінематичні характеристики ланок і окремих точок механізму визначені методом замкнутих геометричних контурів та методом проектування планів. Сили взаємодії між ланками механізму визначені методом кінетостатики, а зрівноважувальний момент розглядом динамічної рівноваги корби і методом балансу потужностей. Виявлено недоліки структурної схеми механізму і запропоновано способи їх усунення.

Результати досліджень подані у вигляді графічних залежностей кінематичних параметрів різця, реакцій або годографів сил у кінематичних парах. Визначені зведені до корби моменти сил опору і сил інерції та побудована динамічна і математична моделі руху механізму. Показано технологію визначення потужності електродвигуна, а його стійку ділянку роботи апроксимовано прямою лінією.

Проведено кінематичний синтез і отримано модернізований механізм у якого різець може рухатись за наперед заданим законом, зокрема, без м’яких ударів на границях кінематичного циклу і з квазісталою швидкістю (похибка до 5 %) у середині кінематичного циклу.

Ключові слова: важільні механізми, оптимізація, синтез, кінематичний аналіз, закони руху, кулачкові механізми

Problems of Tribology, V. 27, No 2/104-2022, 94-103

Problems of Tribology
Website: http://tribology.khnu.km.ua/index.php/ProbTrib
E-mail: tribosenator@gmail.com

DOI: https://doi.org/10.31891/2079-1372-2022-104-2-94-103

Using a functional approach in solving problems improve performance waterjet equipment

O. Salenko[1], M. Khorolska[1], V. Lopata [2*], A. Solovuch[3], V. Kulyzhskyi[4]

[1]*Kremenchug Mykhailo Ostrohradskyi National University, Ukraine*
[2]*E.O. Paton Electric Welding Institute of the National Academy of Sciences of Ukraine, Ukraine*
[3]*Central Ukrainian National Technical University, Ukraine*
[4]G.S. Pisarenko Institute for Problems of Strength National Academy of Sciences of Ukraine, Ukraine
**E-mail: beryuza@ukr.net*

Received: 25 April 2022: Revised: 22 May 2022: Accept: 15 June 2022

Abstract

The paper shows the influence of parameters of the calibration tube jet-abrasive devices on the quality of the process of waterjet cutting critical parts. The results of modeling the formation of two-phase flow and its movement in the calibration tube. Determined that the effects wear ductal fluid of the tube varying intensity and character. In this regard there is the need for functional-oriented approach to the choice of means to ensure the desired geometric parameters of the tube. It is concluded that the decrease in the intensity of ductal Shot material of the tube and thus maintain its geometric parameters is possible by the use of suitable protective coatings , thickness and physical and mechanical characteristics are selected on the basis of Value attributes according to the intensity and type of abrasive loading surface.

Key words: waterjet cutting, calibration tube, protective layers, functional-oriented approach.

Introduction

The appearance and widespread using in industry of new structural materials, especially composites, and new high-tech products, makes the need for new methods of treatment. One of these methods is hydroabrasive cutting. The use of hydroabrasive cutting justifies itself especially where use of traditional methods does not give a satisfactory quality. Additional costs for works or reducing of the production rate go into oblivion. An additional advantage of this method is its cleanliness and environmental friendliness. Modern systems of hydroabrasive cutting provide continuous optimization of production and quality in manufacturing. The need for high processing results requires sustainability and compactness of jet-abrasive stream.

Fig. 1. Calibration tubes, collet mixing chamber and sapphire nozzle inserts by firm SynergicInc., (Provider – ELFIHmbH, Austria)

Using of hydroabrasive processing enables significantly improve the quality of machined surface and cutting performance, which requires the development of promising new layout tools for combined treatment. Among the trends of hydroabrasive treatment the improving of the accuracy and efficiency of processing equipment is allocated. Effectiveness can be enhanced by increasing fluid pressure (600 MPa) and the number of concurrent working heads [1, 2]. However, increasing of working pressure leads to intensification of systems of wear of hydrocutting equipment, including calibration tubes (Fig. 1), which in turn reflected in the cost of processing.

Objective

Calibration tube is one of the most important elements of hydrocutting system, which affects the technological and economic characteristics of the cutting. Industrial observations suggest that most functional failures in the implementation of hydroabrasive cutting occurs due to sudden changes in geometry of jet-forming elements (nozzle and calibration tube). The tube is exposed to constant wear, resulting in internal diameter increases, which determines the wear tube. Usually firmness of tube presents 10...15 hours, and its cost arrives at 20...50 $ [2].

In this regard, an urgent task is improving the stability of calibration tube using the functional-oriented approach. To determine the peculiarities of wear of calibration tube, the impact of movement abrasive grains and species destruction are analyzed.

The research

It is known that in the motion of two-phase flow "liquid – solid particles" through the calibration tube there is chaotic action on the walls of the tube of some abrasive particles at different angles of attack and with different power of hit. Abrasive destruction of surface of the tube depends on the nature of action of the abrasive grains on its surface. Depending on the direction of action of the abrasive jet to the surface there are the following schemes of action: the destruction with a shock jet , when the angle of attack $\alpha = 90$ (Fig. 2 *a*), with sliding jet, when $\alpha = 0$ (Fig. 2 *b*), with oblique jet, when $0 < \alpha < 90$ (Fig. 2 *c*) [3, 4].

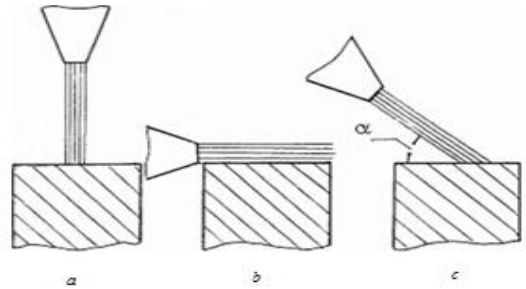

Fig. 2. Scheme of action of the abrasive jet to the surface

If on the flat surface of the material affects the flow of hard abrasive particles that fly at the speed v_u at an angle α to the surface, each share with a punch, elastically deforms the work surface and slip on it with friction. Assumed that the normal component of velocity v_0 makes only elastic deformation of the material, and tangent v_0 is partially or completely extinguished and does the work of cutting, engaging in frictional contact with the surface. With the reduced turns out that the largest processing performance theoretically should be at an angle of attack $\alpha = 45$, which is confirmed by many authors [5]. The intensity of wear in the abrasive flow is defined as the result of multiple impacts of solid particles on the surface wear at different angles of attack. Initial period of destruction of the metal is characterized by the introduction of abrasive particles in the surface layer at some depth, the second - of continuous movement of particles of the material along surface layer at some distance at which the displacement of microvolumes of the metal in layer occurs in the direction of introduction of particles and their separation from the array.

In implementing of the abrasive particle in the surface layer of metal in a free kick there is deformation near the contact zone, resulting in this layer there is a complex inhomogeneous stress-strain field with a variable limit. Stresses and strains arising from the introduction of abrasive particles in the metal depend on complex factors that characterize the parameters of the flow of particles and resistance of the metal to elastic-plastic deformations. Elastic and plastic deformations will develop in the contact zone, which will assist to metal collapse under the particle in the radial direction and subsequent tangential changes in the direction of motion of the relative particles to the surface. Depth introduction of the particle and its tangential displacement associated with the mechanical properties of the abrasive and of material of wearing surface, particles size, and deformation of the metal.

At small angles of attack due to the predominance of tangential velocity impact, the main process of destruction of the surface layer is the tangential displacement microvolumes of metal in the direction of

implementation, i.e. microcutting. At the angles of the attack close to 90º, mechanism of destruction of the surface layer of metal in a stream of abrasive particles takes a polydeformational striking character due to the predominance of the normal velocity. Destruction of structural materials under the action of abrasive particles contained in the flow of fluid is very complex and may be semifluid, brittle, polydeformational or acquires fatigue character and is complicated with phenomenon of cavitation.

Thus, the parameters of the internal profile of tube should ensure the following conditions of flow:

1) the minimum thickness of the boundary layer flow inside the tube, turbulent layer of output free jet, which reduces the thickness and the interaction of jet with the environment;

2) reducing of the possibility of separation of boundary layer of jet, helping to reduce excitation of central flow;

3) reducing of the possibility of cavitation, which provides an exception of formations of low pressures inside the tube to avoid formation of bubbles and destruction of tube.

The physical and mechanical properties of the material, which facing the particle, also have impact on the efficiency of processing. The theoretical dependence given in [5] help to assess of the impact angle of attack on the intensity of wear only qualitatively. Therefore, to analyze the phenomena that occur in calibration tube during the formation of liquid abrasive flow the software package flow vision was used. When modeling the problem of detection of conditionality of diagrams load on the cross-section of calibration tube with microhermetic parameters of jet erosion was treated, establish the role and activity of wave processes occurring in streams and exert force on the inner diameter of the calibration tube.

The core package is a unit of the numerical solution of equations of fluid motion in the orthogonal coordinate system (Navier-Stokes equation (1)) that for certain initial and boundary conditions defined by the user, provides a diagram of distribution of velocities and dynamic pressures at the point of contact with the jet or other surface:

$$\begin{cases} \dfrac{\partial v_r}{\partial t}+v_r\dfrac{\partial v_r}{\partial r}+\dfrac{v_\varphi}{r}\dfrac{\partial v_r}{\partial \varphi}+v_z\dfrac{\partial v_r}{\partial z}-\dfrac{v_\varphi{}^2}{r}= \\ =f_r-\dfrac{1}{\rho}\dfrac{\partial \rho}{\partial r}+\nu\left(\dfrac{\partial^2 v_r}{\partial r^2}+\dfrac{1}{r^2}\dfrac{\partial^2 v_r}{\partial \varphi^2}+\dfrac{\partial^2 v_r}{\partial z^2}+\dfrac{1}{r}\dfrac{\partial v_r}{\partial r}-\dfrac{2}{r^2}\dfrac{\partial v_\varphi}{\partial \varphi}-\dfrac{v_r}{r^2}\right); \\ \dfrac{\partial v_\varphi}{\partial t}+v_r\dfrac{\partial v_\varphi}{\partial r}+\dfrac{v_\varphi}{r}\dfrac{\partial v_\varphi}{\partial \varphi}+v_z\dfrac{\partial v_\varphi}{\partial z}-\dfrac{v_r v_\varphi}{r}= \\ =f_\varphi-\dfrac{1}{\rho r}\dfrac{\partial \rho}{\partial \varphi}+\nu\left(\dfrac{\partial^2 v_\varphi}{\partial r^2}+\dfrac{1}{r^2}\dfrac{\partial^2 v_\varphi}{\partial \varphi^2}+\dfrac{\partial^2 v_\varphi}{\partial z^2}+\dfrac{1}{r}\dfrac{\partial v_\varphi}{\partial r}-\dfrac{2}{r^2}\dfrac{\partial v_\varphi}{\partial \varphi}-\dfrac{v_\varphi}{r^2}\right); \\ \dfrac{\partial v_z}{\partial t}+v_z\dfrac{\partial v_\varphi}{\partial r}+\dfrac{v_\varphi}{r}\dfrac{\partial v_z}{\partial \varphi}+v_z\dfrac{\partial v_z}{\partial z}= \\ =f_z-\dfrac{1}{\rho r}\dfrac{\partial \rho}{\partial z}+\nu\left(\dfrac{\partial^2 v_z}{\partial r^2}+\dfrac{1}{r^2}\dfrac{\partial^2 v_z}{\partial \varphi^2}+\dfrac{\partial^2 v_z}{\partial z^2}+\dfrac{1}{r}\dfrac{\partial v_z}{\partial r}\right). \end{cases} \quad (1)$$

where f_r, f_φ, f_z – voltages of mass forces along the respective axes; r, φ, z; ν – kinematic viscosity; $\frac{\partial v_r}{\partial r};\frac{\partial v_r}{\partial \varphi};\frac{\partial v_r}{\partial z};\frac{\partial v_\varphi}{\partial \varphi};\frac{\partial v_\varphi}{\partial z};\frac{\partial v_z}{\partial \varphi};\frac{\partial v_z}{\partial z}$ – components of the strain rates of elementary volume of fluid (the same name derived describes the strain rate compression or stretching of line elements of the selected volume, and dissimilar – the rate of change of the angles between them); ρ – mass density of fluid; v_r, v_φ, v_z – speeds of the elementary volume of the respective coordinates.

Found stresses values of mass forces along the respective axes provided continuity $\frac{\partial(v_r r)}{\partial r}+\frac{\partial v_\varphi}{\partial \varphi}+r\frac{\partial v_z}{\partial z}=0$ determines mass force acting on the volume of liquid, which is considered:

$$F=\int_W f\rho dW\,, \quad (2)$$

where W – elementary volume.

Initial conditions are determined by geometrical profile nozzle orifice, by the pressure of liquid p_b and its properties. Boundary conditions determine the leakage of jet to the surface, which is an internal cylindrical surface of the calibration tube. Mass transfer was determined by (3) based on the Stokes equation, which determines the strength of resistance in a stream of particles:

$$F_c = \frac{18\mu\Delta w}{d^2{}_s}, \tag{3}$$

where μ – rate of fluid flow through the nozzle; d_s – diameter of tube.

Three-dimensional model of free jet was created to determine the parameters of the system and using the software package flow vision was determined the pressure and velocity in the jet. For the model studies was considered the problem of leakage of jet fluid that flows out of the hole diameter of 1 mm. In order to determine pressure and velocity of fluid in the jet the problem with free surface was created and solved.

Were given the following physical parameters:

- the initial parameters;
- basic values - temperature 273 K, pressure 101 000 Pa;
- parameters of the model - the density of liquid 1000kh/m^3;
- liquid 0 - clear water;
- adaptation of the grid up to level 2.

Boundary conditions for the elements (walls, entrance, exit) and the degree of adaptation for each of them are given. Speed jet at the inlet is 300 m/s. Initial mesh with 25652 cells where 21168 of them solidified it in the area of the exit from nozzle and at the surface of leakage is given. The general model parameters and time course of the calculation in the range from 0 to 5 • 10^{-5} are given, the calculation is standard. The calculation results derived in the form of diagrams (Fig. 3, *a, b*) fill – pressure in the range of 3,5•10^5 Pa to 7,579•10^7 Pa; rate – isolines, from 0 to 300 m/s [6].

Researches showed that most loaded from the point of view of abrasive wear are places of entrance of liquid-abrasive mixture and on an exit from a tube (Fig. 3). In these areas transversal pressure caused by wave processes maximally influences on the mobile particles of abrasive.

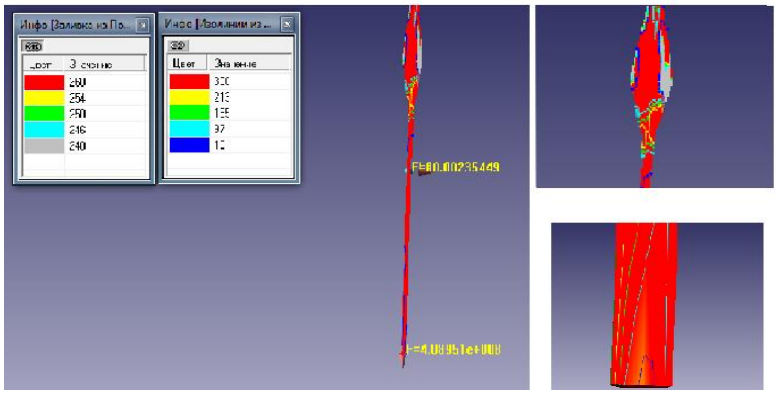

Fig. 3. The results of modeling of liquid-abrasive mixture with the walls of the calibration tube

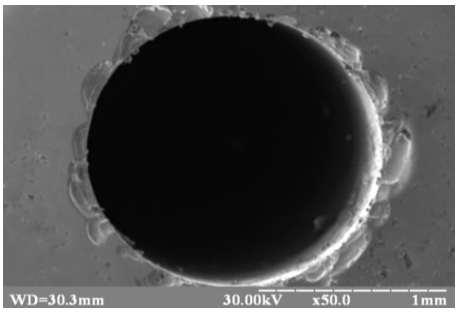

Fig. 4. The photomicrography of the worn edges of the tube

Submitted photomicrography of the edge of nozzle shows that the destruction takes place on that part of that perceived maximum hydrodynamic load (Fig. 4) caused with a back wave in time of leakage jet on an obstacle – the work surface. Thus, the picture of the damage of tube corresponds to parameters of simulated pressure diagram in the longitudinal and end sections nozzle channel. Obtained in Fig. 5 oscillogram shows a periodic increase pressure on the edge of the nozzle with amplitude from 0 Pa to 250 MPa and frequency 2 • 10-6 s, which indicates the presence of wave processes in the body of the jet.

Durability σw of materials calibration tubes with hydroabrasive wear is a complex and ambiguous function of the conditions of interaction of material with abrasive particles and the environment [3]:

$$\sigma_w = f(T; \Pi; d; K_m; K_\phi{}'; v; \alpha; \chi), \tag{4}$$

where T — duration of wear; $П$ — concentration of abrasive particles in a liquid; d — size of particles; Km — coefficient of hardness equal to the ratio of hardness of material to hardness of abrasive particles; $Kф'$ — coefficient that describes the shape of the particles; v — velocity of abrasive particles in the moment of impact with the details surface; α — angle of velocity vector of particle to wearing surface (angle of attack); χ — coefficient characterizing the decrease of mechanical properties of material resulting softening physical-chemical action environment.

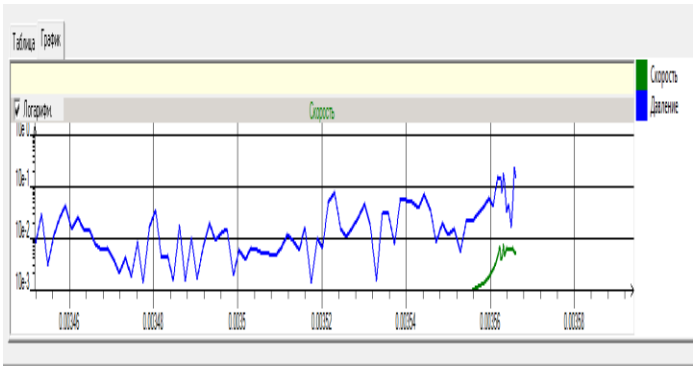

Fig. 5. Graph of velocity and pressure under leakage of jet on the walls of the calibration tube

Total volume of material seized in the interaction with the walls of hydroabrasive stream calibration tube will be:

$$w_{i\Sigma} = w_1 + w_2 = \frac{\pi\delta^2 n(3r-\delta_n)}{3} + \frac{\delta_n(6a+18b)}{15}\delta_a\,, \tag{5}$$

hole depth δ_n and its length δ_a as a function of process parameters:

$$\delta_n = \frac{mv^2{}_n}{2}\frac{R_a}{k_n z_n HB}; \qquad \delta_a = \frac{mv^2{}_a}{2}\frac{z_n}{k_a\sigma_b R_a} - \frac{k_a T^2{}_p \sigma_b R_a}{2mz_n}, \tag{6}$$

where m – mass of abrasive particles; v_n, v_a – normal and tangential component of particle impact velocity with the treated surface; R_a, HB, σ_b – parameters of roughness, hardness and strength of surface; z_n – granularity of abrasive particles; T_p – constant, taking into account the inertia of the process microcutting; k_n, k_a – constant coefficients.

Since the calibration tube takes hydrodynamic and mechanical loading from fast moving abrasive particles inserted in the flow of fluid from the nozzle cut, the reason for its withdrawal from the calibration aperture D_k growth over the limit and split of individual elements, thus changing the geometry formed by grooves cut (Fig. 6). This damage is caused with wearing phenomena. It is logical increase firmness of the calibration tubes by causing protective coatings. The use of special wear-resistant coatings can significantly improve the time of stability of materials in aggressive environments, improve the stability of the process due to less intensive changes in the dynamics of initial geometrical parameters of the channel [7]. However, currently there are no clear guidelines regarding the type of coatings that can be used in this practice and rational technologies application of such coatings on the inner surface of the channel.

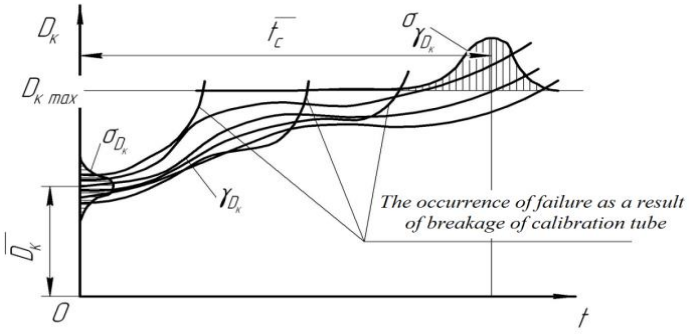

Fig. 6. The dependence of change of the calibration opening on run-in time

To address the question of whether the use of certain surface coatings on hydroabrasive resistance the samples with size 40x10x5 mm from titanium alloy VK8 were tested, which is instrumental material of elements of hydroabrasive processing, as no cover, so with a vacuum-plasma coating TiN, with the nitrided layer and the combined coverage of the nitrided layer and TiN (Fig. 7). Modes of coating are given in Table 1.

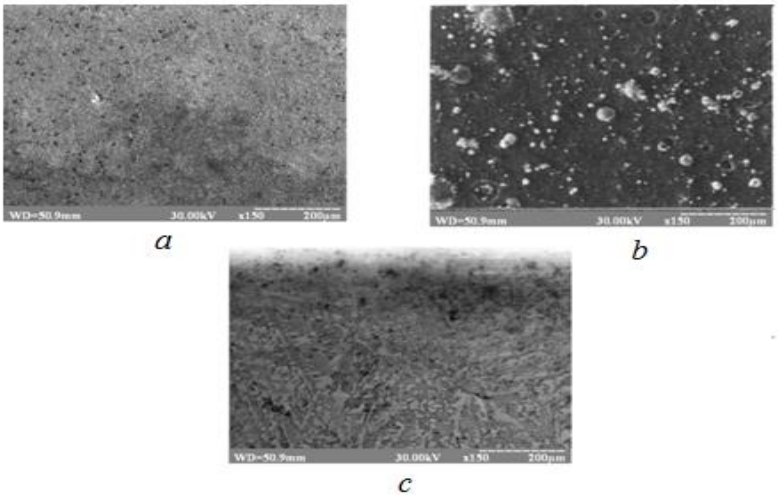

Fig. 7. Microelectronic researches of alloy VK8: *a* – without coating; *b* – with coating TiN; *c* – with the nitrided surface layer

Table 1

Modes of coating

Parameters	Vacuum-plasma spraying TiN	Ionic-plasma thermocyclic nitriding
Working pressure P	$2{,}2 \cdot 10^{-3}$ mmHg	100 Pa
Arc current Iд, A	100	10
Temperature T, ºC	520	550
Voltage U, V	500	600
Time, min	40	360

To microelectronic studies of these, coating were deposited considering functional-oriented approach to flat plates, which were established for research under certain angles to leakage jet (Fig. 8).

Functionally-oriented approach involves the production of calibration tube by special technology, which is based on strict topologically oriented implementation of the required set of algorithms of technological performance of processing in required micro and macro zones and parts of the product that meet the functional requirements of their operation in each of its zone.

Fig. 8. Installation of a test piece on desktop of hydrocutting machine LSK-5-400

For a comparative analysis all experimental studies were made at the same processing parameters, which were adopted: leakage pressure – 280 MPa, volumetric concentration of abrasive in suspension – 0,6 kg/min, processing time – 10,5 minutes. Investigation of angle of attack for wear of samples were carried out using a garnet sand from grit 30 mesh as an abrasive in suspension. The distance between the initial section of ejecting adjutage of ink-jet apparatus and the sample was 80 mm. In Fig. 9 there are comparative diagrams of coating TiN and combined coating wearing, presented as the depth of damage layer, measured relative to the plane

undamaged surface. Angle of leakage of samples is 15 ^{0} (π/12). Found that the dynamics of damage protective coatings is fundamentally different: coating TiN weared more rapidly and in 3 minutes damage reached its maximum. After that damage rate declined, and on the samples were observed area almost its complete removal. Further active destruction of substrate material began (Fig. 10). The of combined coating was more resistant to liquid cavitation abrasive wear (almost 3 times). This wear was evenly without forming complete detachment areas. In the following diagrams the dependence of the degree of damage is presented (like a deep hole that is formed on the surface (h) for a fluid time). Dependence of change of depth hole formed in function of the angle jet of leakage α is given. Impact angle of leakage boost on the speed of removal of coating was determined by measuring the penetration of the jet in the specimen at a time equal to 1 min. Measurements performed in the range of angles from 3^0 (π/60) to 30^0 (a further increase in angle leads to complete destruction of coating and base and a groove about 3-4 mm). The adequacy of the obtained models – 0,95.

According to the obtained data it is easy to conclude that most works better coverage at the tangent jet of leakage. The operation time in 1 min is not exponential, because this time is necessary to establish to ensure comparability of measurements of the dynamics of wear at the big corners of leakage (Fig. 11). The difference between the mechanisms of interaction between the abrasive particles to the surface of the tube along the canal and attempts to reach approximately the same low rate of erosion due to the development of modern functional approach discussed in the works O. Mykhaylova ([8, 9], etc.). Suggests the presence on the surface clearly deterministic function of makro zones, which require different properties and different ways of providing functions. These may be the appropriate coverage that satisfactorily be taken one or the other type of abrasive loading. However, the difficulty lies precisely in the fact that the diameter of the tube is not the same and rather small – from 4,2 mm at the inlet of the tube to 0,95–1,20 mm at its cut.

However, the use of coatings provides for a change in the design of the handset and change the material from which it is made. We suggest to use a calibration tube of fundamentally new design. Wear-resistant gauge tube to form a liquid abrasive jet cutting was made of two symmetrical parts, connected together by mechanical means, including covered clip, planted with the intention to form a longitudinal axial channel for passage of the working fluid from the abrasive surface and the longitudinal axial channel for the precedence of damage from exposure waterjet stream inflicted with durable fragmented layer, which is based on the functional-oriented approach is the adhesion of the film material, which the wear intensity for excellent action waterjet stream is the same, the length of the application layer (a fragment) is responsible length of the high intensity of the action of abrasive particles.

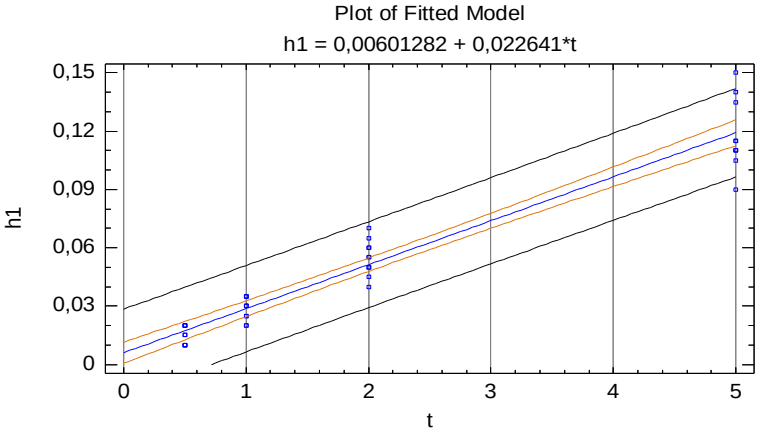

a

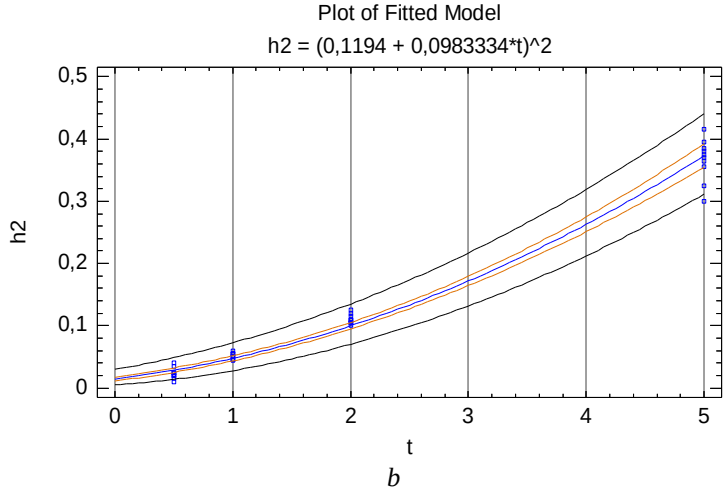

b

Fig. 9. The comparative diagrams wear of coating TiN (*a*) and combined coating nitrided + TiN (*b*)

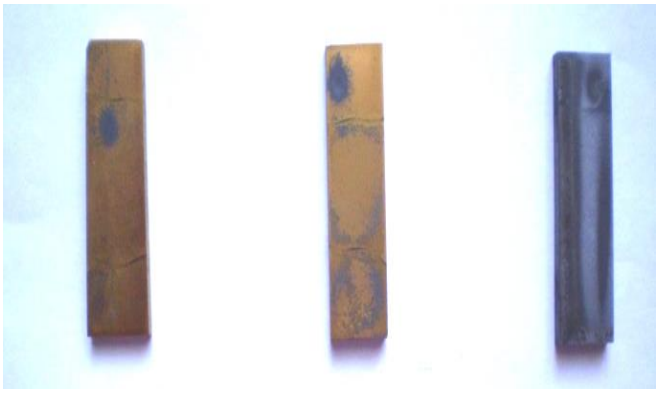

Fig. 10. Samples after testing

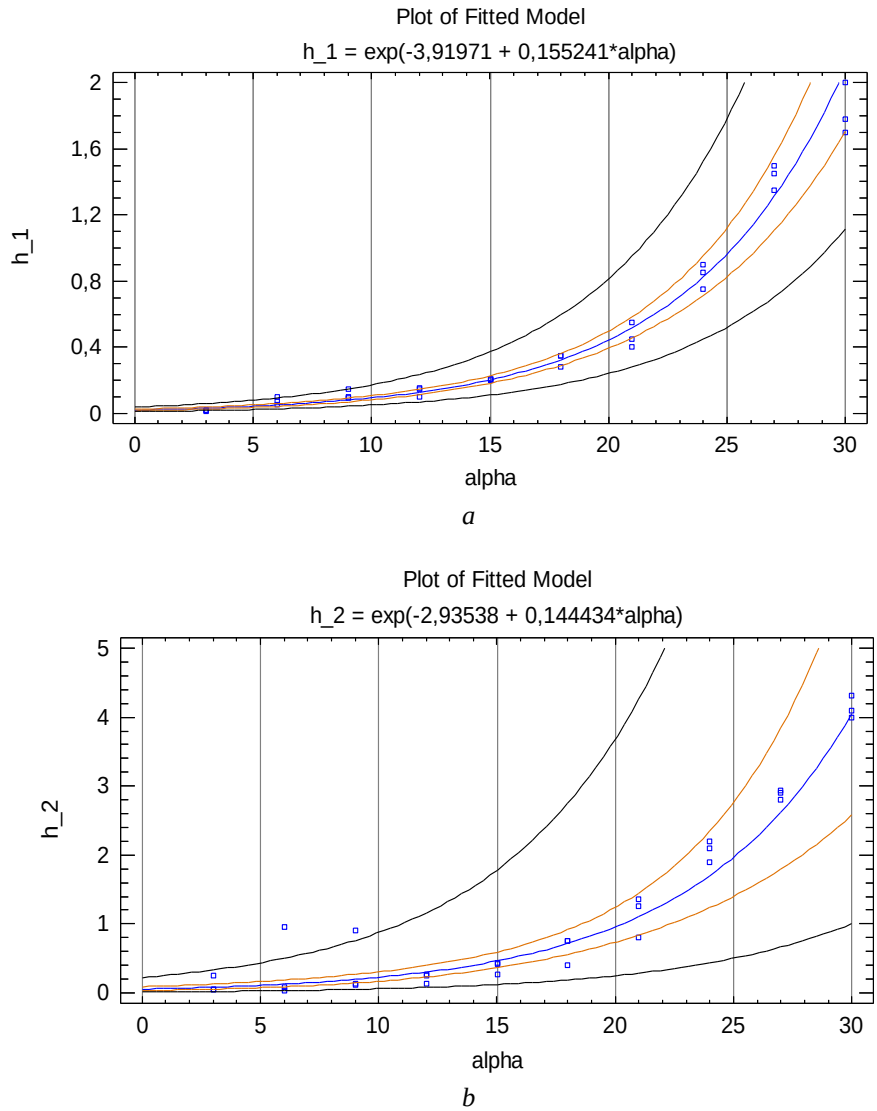

a

b

Fig. 11. Dependence of wear coating TiN (*a*) and combined coating on the corner of accumulating (*b*)

According to functional-based approach product manufacturing, it should be implemented a number of features that can be provided by individual carriers of cheaper material or work that is the least costly. Therefore, in our opinion , the use of fragmented layer is more efficient than the production of the entire tube with a wear resistant, but also more expensive in material.

To verify the presented ideas and get real wear profiles 10 gauge tubing coated with patchy layers (Fig. 12) were produced and tested after a fixed lifetime (T = 10,0 hours). Tubes material was regenerated solid alloy of VK with burning created by electrocontact TiN coating thickness of 1,5 mm (factionalism 30/50 μm) at the point where the movement of abrasive grains was ordered (in zone 1), PVD-coated in Zone 2 (where channel sees mostly rolling effect of the abrasive particles rolling and PVD- coating of nitriding (N + TiN) at the end of

the tube, where there is influence reflected from the surface treatment of the particles; nitride layer thickness – 200 μm, coating TiN – 10 μm. The results shows that the coating securely protects channel tube, embryos failed to precede the occurrence of intense destruction on the surface of the channel, while apparent space docking in different layers along the length of the channel, and the thickness of the PVD-coating of nitriding (N + TiN) 200 μm proved practically remove. However, the development of damage to the channel took place almost without disturbing the original diametric portion and quite evenly. Studies performed using laser jet set LSC-400-5. Thus, we can state that, along with other means of reducing the wear lodged in [8,9], and improve the stability of geometric parameters of channel function approach is effective and efficient.

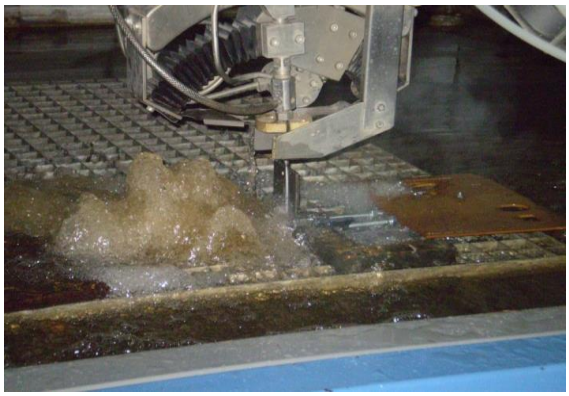

a

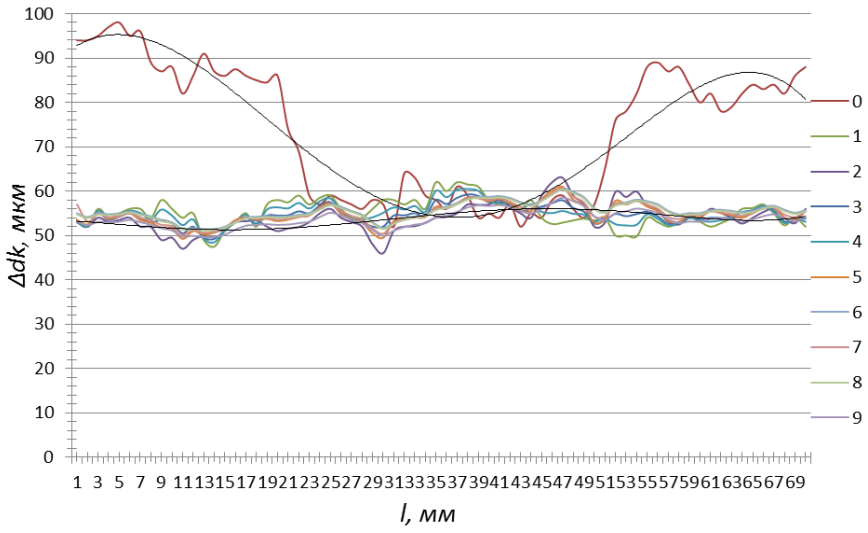

b

Fig. 12. Coated tubes (a) and wear profile of the channel after 10 hours of work (b): 0 – without layers; 1–9 – coated functional layers

At the same time, the need for further analysis of options for implementation layers, and in the future – attempts to create an inverted gauge tubes, layers that build the channel (made of a material that can then be easily removed) to the outer surface . In this case, the obvious advantage is the formation of a surface of the channel, where carbides or nitride compounds can be oriented so that the surface was formed by low hydraulic resistance. For these studies appropriate involvement of Rapid Prototyping. Further work is currently being regenerated with replacement hard metal cheaper material , such as alloyed steel. However, in our opinion, identified patterns and approaches can be used in any critical inkjet devices.

Conclusions

A model of two-phase flow of high-speed waterjet cutting stream in ductal calibration of the tube allowed to prove the existence of certain areas in which great damage processes manifested channel based on what is proposed to use a functional approach and created a new design tube which implies the existence of fragmented functional layers on the surface of the channel. Experimental tests of the proposed type gauge tubes that have proven given consideration. Of all the parameters – D_k, σ_{Dk}, γ_{Dk}, λ_{Dk} (Fig. 6), the application of functional coatings can reduce γ_{Dk}, thereby increasing the lifetime of the tube to the predicted onset of failure as $T = \frac{D_k - D_i}{\gamma_D}$

Guaranteed stability of the proposed calibration tube type stability than conventional tubes at an average of 1.5...1.8 times and averages above 17,5 hours, while the dispersion is 10–12 %. Retrieved functional dependencies wear gauge tube coated on the criteria of sustainability hydroabrasive complement general methodological information base and certainly contribute to the development of the principle of control properties of the surface layer.

References

1. Prospects of development of waterjet and water abrasive processing. Looking downstream. Amer. Mach. 2001. 145, №3, P. 80-82, 84, 86, 88, 90.

2. Salenko O.F., Fomovska O.V. (2008)"Prospects for market equipment for sheet handling", Visnyk KDPU, 2008. №6(48). P. 45-50.

3. Tsygankovskij A.B. Determining of the degree of influence of the angle of attack jet on productivity and quality of waterjet processing submerged jets, Visnyk SNU named by V. Dal. 2009. №6, P. 220-228.

4. Provolotskij A.E. Jet-abrasive treatment of details, Tehnica, Kyiv: 1989. 189 p.

5. Kleis I.R. Fundamentals of the choice of materials for operation in the gas abrasion wear. Friction and wear, 1980. №2, P. 263 - 271.

6. Dudyuk V.O. Analysis of dynamic loading of items of zone of hydrocutting using application package flow vision, Visnyk KrNU, 2010. №6(65), P. 59-62.

7. Lopata L.A. Adhesion strength and residual stress at electrocontact sintering of powder coatings, Strength of Materials, 2010. №4, P.71–76.

8. Mykhaylov A.N. Development of technologies based on the function-oriented approach. DonNTU, 2008. 450 p.

9. Sychuk V.A., Zabolotniy O.V. "New principles of designing and manufacturing nozzles for waterjet machines", Scientific Bulletin Kherson State Maritime Academy, 2012. No. 1(6), PP. 317–321.

10. Anand Umang, Katz Joseph. Prevention of nozzle wear in abrasive water suspension jets (AWSJ) using porous lubricated nozzles. The Johns Hopkins University, Department of Mecanical Engineering, Baltimore, MD 21218. Trans. ASME. J. Tribol. 2003. P. 168–180.

Саленко О. Ф., Хорольська М. С., Лопата В.Н., Соловых А.Е., Кулижський В.М. Використання функціонального підходу при вирішенні задач підвищення працездатності гідрообразивного обладнання

У роботі показаний вплив параметрів калібрувальної трубки струминно-абразивних пристроїв на якість процесу гідроабразивного різання відповідальних деталей. Приведені результати моделювання формування двофазного потоку та його руху в калібрувальній трубці. Визначено, що плинні явища зношування протокової частини трубки мають різну інтенсивність і характер. У зв'язку з цим постає необхідність застосування функціонально-орієнтованого підхіду до вибору засобів забезпечення потрібних геометричних параметрів трубки. Зроблено висновок, що зменшення інтенсивності зйому матеріалу з протокової частини трубки та, відповідно, підтримання її геометричних параметрів можливе шляхом використання відповідних захисних покрить, товщина та фізико-механічні характеристики яких обираються на основі функціонально-вартісних ознак відповідно до інтенсивності та виду абразивного навантаження поверхні.

Ключові слова: гідроабразивне різання, калібрувальна трубка, зношування, захисні шари, функціонально-орієнтований підхід

***Problems of Tribology**, V. 27, No 2/104-2022, 104-111*

Problems of Tribology
Website: http://tribology.khnu.km.ua/index.php/ProbTrib
E-mail: tribosenator@gmail.com

DOI: https://doi.org/10.31891/2079-1372-2022-104-2-104-111

Plane problem of discrete environment mechanics

O.V. Bagrii

Khmelnytskyi National University, Ukraine
E-mail: avadaro@yahoo.com

Received: 28 April 2022: Revised: 28 May 2022: Accept: 25 June 2022

Abstract

Many engineering problems related to the design of structures and machines, the mathematical description of technological processes, etc., are reduced to the need to solve a plane problem for materials with a significant effect of internal friction on their deformation. Such materials include a large class of materials in which the compressive strength is greater than tensile. These are composite materials, concretes, rocks, soils, granular, loose, highly fractured materials, as well as structurally heterogeneous materials in which rigid and strong particles are interconnected by weaker layers. The laws of deformation and destruction of such materials differ significantly from elastic ones. A feature of these laws is an increase in resistance to shear deformations and an increase in the strength of materials with an increase in the magnitude of compressive stresses. This is associated with the influence of internal Coulomb friction on the process of their deformation in the limiting and boundary stages.

The need to formulate and solve a special boundary value problem for materials with significant internal friction is because the results of solving problems using models of elasticity and plasticity differ significantly from experimental data. The difference increases when approaching the limiting state of discrete materials and depends significantly on the structure of the material and operating conditions.

The boundary value problem of the mechanics of a deformable solid is formulated as a system of equations of three types: static, geometric, and physical. For all linear and physically nonlinear problems, provided the deformations are small, the first two groups of equations remain the same. Thus, these differences can be attributed to the inconsistency of the accepted in the calculations of physical relations "stress - strain" and the real laws of deformation of these materials, which are more complex rheological objects than structurally homogeneous solids, liquids or gases.

The article uses an approach where the material is immediately considered as quasi-continuous, and the physical equations are based on the experimentally obtained relationships between the invariants of the stress and strain tensors, which consider the influence of both molecular connectivity and internal Coulomb friction.

Key words: Plane problem, internal friction, compressive stress, variable deformation modules, nonlinear physical equations

Introduction

Plane problem for materials with significant internal Coulomb friction is formulated as a boundary value problem for a flat, inhomogeneous, physically nonlinear area filled with a material, the deformations of the forms of change of which are significantly affected by the values of compressive stresses [1].

The problem is to determine the stress and strain fields when the region is perturbed by force or kinematic factors

The material in the calculation area is considered quasi-continuous. The material deformation model is a combination of a perfectly cohesive material model (Prandtl model) and an internal friction model (Coulomb model).

The physical relations of the model are written in the form of relations of mechanics of deformable solids but with variable modules of deformation, the values of which depend on the achieved level of stresses and

strains and are determined by testing macro samples of material under flat deformation.

A feature of the formulated problem is using physical equations for the active deformation process with variable deformation parameters that are different at each point of the computational area. Therefore, the problem's solution can be obtained only by specially developed iterative procedures.

The analysis of the known numerical methods allowed to choose finite elements with some limitations as the basic method for the realization of the formulated physically nonlinear problem of a flat inhomogeneous area. First, the fulfillment of the condition of invariance of stresses within one element, which is achieved by a special choice of the shape of the finite element and approximating functions. This makes it possible to assign values of variable deformation modules at a particular stage of calculation not for each point of the calculation area, but for each finite element, which allows the implementation of special iterative algorithms for solving the problem by numerous methods. The second fundamental condition is the need to consider the volume forces of gravity. Without this, the discrete material may not perceive an external load.

Therefore, it is necessary to formulate a nonlinear mathematical model of the environment using physical relations that consider the influence of internal Coulomb friction on the deformation of the environment under plane deformation conditions.

Mathematical formulation of a plane problem

To formulate the problem, we take from the array of the medium operating under conditions of plane deformation, a flat design region O of unit thickness $h=1$ (Fig. 1), which can have finite dimensions or be considered as part of an infinite plane.

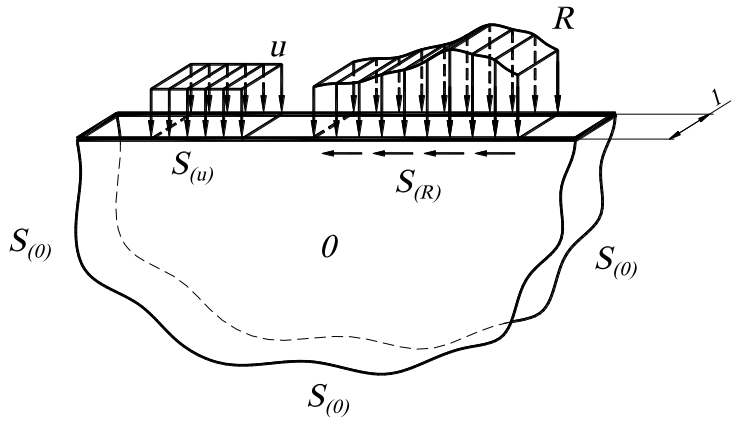

Fig.1. Calculation area of a flat problem

On some section $S_{(R)}$ of the contour, external loads (force boundary conditions) can be specified, and known displacements (kinematic boundary conditions) on the other $S_{(u)}$. On the part $S_{(0)}$, the boundaries of the displacement area may be zero.

The laws of material deformation are described by nonlinear dependencies that consider the influence of internal friction.

In this formulation, the problem is reduced to determining the fields of stresses, strains and displacements ($\sigma(x, y)$, $\varepsilon(x, y)$, $u(x, y)$) of the computational area, which correspond to the accepted model of the environment and given boundary conditions.

The problem is formulated by systems of equations:

equilibrium equations:

$$\left.\begin{aligned}\frac{\partial \sigma_x}{\partial x}+\frac{\partial \tau_{xy}}{\partial y}=V_x\\ \frac{\partial \sigma_y}{\partial y}+\frac{\partial \tau_{xy}}{\partial x}=V_y\end{aligned}\right\}; \tag{1}$$

geometric Cauchy relations:

$$\varepsilon_x=\frac{\partial u_x}{\partial x};\ \varepsilon_y=\frac{\partial u_y}{\partial y};\ \gamma_{xy}=\frac{\partial u_y}{\partial x}+\frac{\partial u_x}{\partial y};\ \gamma_{yx}=\frac{\partial u_x}{\partial y}+\frac{\partial u_y}{\partial x}; \tag{2}$$

nonlinear physical equations of discrete materials:

$$\left.\begin{aligned}
\sigma_x &= \frac{K_{3M}+2G_{3M}}{2}\varepsilon_x + \frac{K_{3M}-2G_{3M}}{2}\varepsilon_y;\\
\sigma_y &= \frac{K_{3M}-2G_{3M}}{2}\varepsilon_x + \frac{K_{3M}+2G_{3M}}{2}\varepsilon_y;\\
\tau_{xy} &= G_{3M}\gamma_{xy}\\
\tau_{xy} &= G_{3M}\gamma_{yx}
\end{aligned}\right\}. \tag{3}$$

The last relations, as noted earlier, differ from the equations of the plane problem of the theory of elasticity in that the modules K_{3M} and G_{3M} are functions of the stress-strain state and not constants of the material..

Mathematical formulation of the plane problem of the mechanics of discrete materials in a convenient for numerical implementation of the matrix form can be represented as follows.

For a flat region *O*, on the boundary of which force or kinematic boundary conditions are specified, determine the stresses $\{\sigma\}=\{\sigma\}(x,y)$, deformation $\{\varepsilon\}=\{\varepsilon\}(x,y)$ and displacement $\{u\}=\{u\}(x,y)$ corresponding to the calculation scheme and the accepted specific laws of deformation of the region's material.

The problem is reduced to solving a system of matrix equations:

$[B]^T\{\sigma\}=\{V\}$ – differential equilibrium equations (4);

$\{\varepsilon\}=[B]\{u\}$ – differential geometric equations (5);

$\{\sigma\}=[D]\{\varepsilon\}$ – physical equations for discrete material (6)

considering the experimentally obtained invariant nonlinear physical relations to determine the variable parameters G_{3M}, K_{3M}:

$$G_{3M}=\frac{n}{m+\Gamma}P,\quad K_{3M}=2G_{3M}\frac{1+\nu}{1-\nu}, \tag{7}$$

and boundary conditions:

$$\begin{aligned}
[A]^T\{\sigma\}&=\{R_S\}\ \text{– in } S_{(R)};\\
\{u\}&=\{u_S\}\ \text{– in } S_{(u)};\\
\{u\}&=\{0\}\ \text{– in } S_{(0)},
\end{aligned} \tag{8}$$

where $\{R_S\}$ – vector of known forces acting on the boundary $S_{(R)}$,

$[A]^T$ – direction cosine matrix

$$[A]^T=\begin{bmatrix} m & 0 & l\\ 0 & l & m\end{bmatrix}; \tag{9}$$

$\{u_S\}$ – known displacements at the boundary $S_{(u)}$;

$\{0\}$ – lack of movement at the boundary $S_{(0)}$.

In addition to the formulated conditions for discrete materials (primarily for bulk, granular and grainy) a fundamental restriction is introduced on the impossibility of tensile stresses. If we introduce the rule of signs, according to which the compressive stresses are considered positive, this restriction is formulated as

$$\sigma_2>0. \tag{10}$$

A feature of the formulated plane problem is that the physical equations do not include the elastic characteristics of the material G and K. Instead, functions are used with different values at each point of the computational area, which depend on the level of stress-strain state reached in it. Therefore, to solve the formulated problem, specially developed numerous iterative procedures are used.

There are many effective numerous methods that could become the basis for the development of iterative algorithms necessary to solve the problem. The most famous of them are: the finite difference method (FDM), the finite element method (FEM), the boundary element method (BEM).

The analysis of the features and capabilities of these methods made it possible to choose the implementation of the formulated physically nonlinear problem of a flat inhomogeneous region as the basic finite element method with some restrictions.

Finite element formulation of a plane problem

The idea of the method is to replace the computational area with its discrete model formed by a system of finite elements that interact with each other in nodes. At these points, the continuity conditions are always

provided. Each element is deformed according to the laws of deformation of the material of the calculation area. The distribution of stresses and strains inside the element depends on its shape and the form of the accepted approximating functions. The use of the FEM for continuum areas reduces the solution of the boundary value problem to the problem of structural mechanics, which is solved by the known method of displacements.

The convenience of using FEM for solving nonlinear problems is due to the simplicity and clarity of interpretation of all stages of the calculation, the possibility of step-by-step control of the results. However, the most important feature of the method is that for specially selected elements of the element and the approximating functions of stress and strain will not change within one element. Since the modulus of deformation of discrete materials depends on the achieved level of stress, the values of the modulus of strain at a particular stage of the calculation in this case can be assigned not for each point of the calculation area, but for each finite element. This makes it possible to implement special iterative algorithms for calculations by numerical methods.

The sequence of solving a plane problem based on the finite element method is quite fully described in the scientific and methodological literature [2, 3] and is reduced to the following operations:

1. Create a discrete model of the computational area - divide the solid domain into a grid of finite elements (see Fig. 2).

2. External loads at the boundary of the region $S_{(R)}$, and body forces lead to forces applied at the nodes $\{R\}$, and known displacements on the boundary $S_{(u)}$ lead to displacements of the nodes $\{\delta\}$. The condition of the impossibility of displacements on the boundary $S_{(0)}$ is satisfied by introducing appropriate restraints at the nodes on the boundary of the region.

3. For each finite element, a stiffness matrix $[k_e]$ is formulated that connects the vectors of nodal forces and displacements of nodes belonging to the same element.

4. Formulate a global stiffness matrix $[K]$ of the system of elements, consider the "contribution" of each finite element to the stiffness of the entire system.

5. Formulate and solve a system of canonical equations of structural mechanics, most often the displacement method, as a result, nodal displacements are found, and through them - strains and stresses in finite elements.

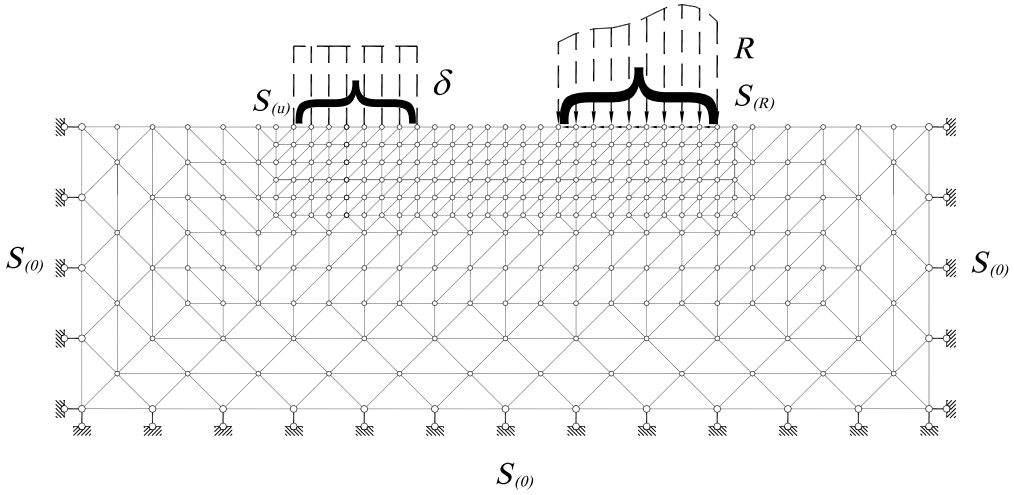

Fig. 2. Discrete model of computational area

Most of the described steps are standard for FEM. However, to implement the previously formulated physically nonlinear problem, it is necessary to consider the following features.

1. The shape of the finite element and the adopted approximating functions must ensure at each stage of calculation the invariability of the achieved values of stresses and strains within one element, which allows assigning variables of deformation modules not for each point of the region but for each finite element. This is achieved by choosing a basic finite simplex element in the form of a triangular prism of constant length $L = 1 = const$ (Fig. 3).

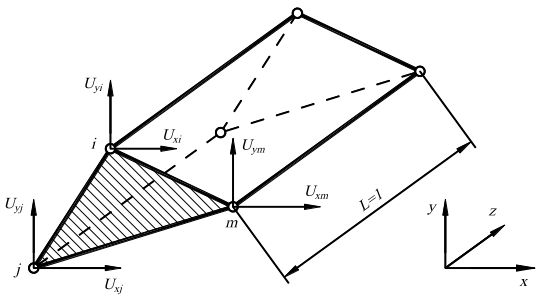

Fig. 3. Simplex element for a plane problem

An approximating function that describes the nature of changes in displacements from the coordinates of x, y points is assumed to be linear.

The displacements {u} of an arbitrary point in the middle of an element are expressed in terms of the nodal displacements {δe} of its nodes by the following relation:

$$\{u\} = \begin{Bmatrix} u_x \\ u_y \end{Bmatrix} = [N]\{\delta_e\} = \left[IN_i + IN_j + IN_m\right]\{\delta_e\}, \tag{11}$$

where I – single dimensional matrix 2×2;

N – shape function

$$N = \frac{a + bx + cy}{2A}, \tag{12}$$

where a, b, c - coefficients determined by nodal displacements;

A – element area (volume $V = A \cdot 1$).

The deformations εx, εy, γxy of the points of a finite element according to the Cauchy relations are derived derivatives of the displacements {u}. For the accepted linear approximation, the derivatives do not depend on the x, y coordinates of the points of the element. Therefore, the deformations in the middle of each element are constant. This can be easily verified by performing the following differential operations.

$$\{\varepsilon_e\} = \begin{Bmatrix} \varepsilon_x \\ \varepsilon_y \\ \gamma_{xy} \end{Bmatrix} = [B_e]\{\delta_e\} = \left[B_i, B_j, B_m\right] \begin{Bmatrix} \delta_i \\ \delta_j \\ \delta_m \end{Bmatrix}, \tag{13}$$

where B_i, B_j, B_m – submatrix of the matrix $[B_e]$ of the differential operator. For example, the submatrix $[B_i]$looks like:

$$[B_i] = \begin{bmatrix} \frac{\partial N}{\partial x} & 0 \\ 0 & \frac{\partial N}{\partial y} \\ \frac{\partial N}{\partial y} & \frac{\partial N}{\partial x} \end{bmatrix} = \frac{1}{2A} \begin{bmatrix} b_i & 0 \\ 0 & c_i \\ c_i & b_i \end{bmatrix}. \tag{14}$$

Similarly written matrices $[B_j]$, $[B_m]$.

Thus, the matrix $[B_e]$, and therefore the deformations $\{\varepsilon_e\}$ do not depend on the coordinates of the points of the element

There is an unambiguous relationship between deformations $\{\varepsilon_e\}$ and stresses $\{\sigma_e\}$:

$$\{\sigma_e\} = [D_e]_{з,м}\{\varepsilon_e\}, \tag{15}$$

where $[D_e]_{з,м}$ – matrix of deformation parameters.

Therefore, the values of the components of the stress tensor within the finite element will also be constant at each stage of the load.

Therefore, the choice of a finite simplex element in the form of a triangular prism with a linear displacement function satisfies the above requirements.

2. The second fundamental feature of the problem under consideration is the need to take into account the volume forces of gravity. Without this, the computational area of a discrete material sometimes cannot perceive an external load. As shown by O. Zenkevich [4], body forces X, Y can be reduced to nodal forces using the integral relation

$$\{R_e\} = -\int [N]^T \begin{Bmatrix} X \\ Y \end{Bmatrix} dxdy. \tag{16}$$

For the introduced shapes of the elements and the linear approximating function, after integration, we obtain that the force of gravity is equally distributed between the three nodes of the element.

The procedure for reducing the known values of the distributed load P and displacements u at the

boundary of the computational domain to nodal forces {R} and displacements {δ} does not differ from that adopted for linear problems.

3. The next stage of calculation - the formulation of the stiffness matrix of the element - under the accepted assumptions is also simplified.

In the general case, the stiffness matrix of a finite element for a plane problem is determined by the expression:

$$[k_e] = \int [B_e]^T [D_e][B_e] dxdy. \tag{17}$$

Considering the above assumptions, expression (4.22) takes the form:

$$[k_e] = [B_e]^T [D_e]_{зм} [B_e] A. \tag{18}$$

where A – the cross-sectional area of the finite element plane xy .

The components of the matrix $[B_e]$ within the finite element do not depend on the coordinates, and the matrix of deformation parameters $[D_e]_{зм}$ contains variable modules $G_{зм}$, $K_{зм}$, the values of which depend on the stresses and strains achieved in the center of gravity of the finite element.

$$[D_e]_{зм} = \frac{1}{2}\begin{bmatrix} K_{зм}+2G_{зм} & K_{зм}-2G_{зм} & 0 \\ K_{зм}-2G_{зм} & K_{зм}+2G_{зм} & 0 \\ 0 & 0 & 2G_{зм} \end{bmatrix}, \tag{19}$$

where $G_{зм} = \dfrac{n}{m+\Gamma} P, \qquad K_{зм} = 2G_{зм}\dfrac{1+\nu}{1-\nu}.$

The formation of the global stiffness matrix [*K*] of the system of elements of the discrete model of the computational area is a well-known procedure for “assembling” stiffness matrices of elements, described by O. Zenkevich [4].

After the formation of the global stiffness matrix [*K*], the continuous calculation area is considered as a normal mechanical system of deformable elements, the calculation of which is a known method of displacement of structural mechanics and is reduced to finding displacements and forces of nodes. To do this, additional restraints are set in the hinges that connect the finite elements, which make the system kinematically definable. These restraints allow many possible movements of nodes. The principle of minimizing the potential energy of the system (Lagrange principle) is used to obtain the actual displacements of the nodes [5].

The condition of the minimum of potential energy in the method of displacements is written in the form of a system of canonical equations:

$$[K]\{\delta\} = \{R\}, \tag{20}$$

where $\{R\}$ – vector of external forces applied in the nodes of the system;

$\{\delta\}$ – vector of movements of nodes.

In their physical essence, canonical equations (20) are equilibrium equations of nodes in which node displacements $\{\delta\}$ are unknown.

To obtain the solution of a specific problem, equations (20) must satisfy the boundary conditions. The form of recording these conditions depends on the structure of the basic equations and the known values of forces and displacements at the boundary of the calculation area.

If force boundary conditions in the form of known nodal forces are set at the boundary of the calculation domain, they are automatically considered by the vector $\{R\}$ of external forces (the corresponding components of the vector are equated to known forces). For nodes at the load-free boundary, the vector components $\{R\}$ are zero.

If the boundary conditions are given in the form of known node displacements at the boundary of the region, the vectors $\{\delta\}$ and $\{R\}$, as well as the stiffness matrix [*K*] are partially modified by a known procedure, for example, the procedure described in [4].

The final finite element formulation of the problem is reduced to the following operations.

Create a discrete model of the calculation area. To do this, the solid region is replaced by a grid of finite elements in the form of triangular prisms connected in nodes. The necessary matrices of connection of numbers of elements and coordinates of knots, vectors of known loadings and movements, force and kinematic boundary conditions are formed.

For each finite element, a stiffness matrix [k_e] is formed, which satisfies the conditions of equilibrium and

continuity, as well as the physical relationship between stresses and strains. These conditions are described by the following equations:

$[B]^T\{\sigma\}=\{V\}$ – equilibrium equation (4);

$\{\varepsilon\}=[B]\{u\}$ – Cauchy equation (5);

$\{\sigma\}=[D]_{з.м}\{\varepsilon\}$ – physical nonlinear equations of discrete materials (6).

Finite element stiffness matrix

$$[k_e]=[B_e]^T[D_e]_{з.м}[B_e]A. \tag{21}$$

According to the principle of "assembly" of the stiffness matrices of the elements, the global stiffness matrix [*K*] of the computational area is formed and the system of linear equations (20) of the displacement method is written.

Solving the system considering the boundary conditions, we obtain a vector of nodal displacements:

$$\{\delta\}=[K]^{-1}\{R\}, \tag{22}$$

and through it deformations are calculated $\{\varepsilon\}=[B]\{\delta\}$ and stress $\{\sigma\}=[D]_{з.м}\{\varepsilon\}$ in the middle of the element.

The described procedure can be implemented for a physically nonlinear problem only after the development of special computational iterative algorithms. Its essence is that a complex physically nonlinear problem is solved in stages. At each stage, a linear problem is solved in which the values of the deformation parameters of the element are assigned depending on the level of stresses and strains achieved in it at the previous stage.

Conclusions

In the mathematical formulation of the problem, in addition to the known equations of equilibrium and continuity of deformations, specific physical equations are used, in which instead of elastic constants variable parameters are introduced that depend on the values of stresses and strains achieved at each stage.

The described plane physically nonlinear problem of inhomogeneous region is solved by means of specially developed iterative procedures. The finite element method is chosen as the base in these procedures. The choice of finite elements in the form of triangular prisms with a linear function of the form is substantiated. The formulated finite-element matrix relations allow to obtain the solution of the problem by the numerical method using special iterative procedures.

References

1. Kovtun VV Formulation of the problem of contact interaction of structural elements with a discrete environment / VV Kovtun, OV Kolesnikova // Problems of modern engineering technology: 4th interuniversity. scientific-theoretical Conf., January 14–15, 2003: Coll. Science. work. - I., 2003. - Part II (special issue). - № 24. - P. 127–130. [in Russian].

2. Bezukhov N. I., Luzhin O. V. Using methods of the theory of elasticity and plasticity for solving engineering problems. - M. : Higher school, 1974. - 200 p. [in Russian].

3. Handbook of the theory of elasticity (for civil engineers) / [ed. P. M. Varvak, A. F. Ryabov]. - K. : Budivelnik, 1971. - 418 p. [in Russian].

4. O. C. Zienkiewicz. The Finite Element Method In Engineering Science / O. C. Zienkiewicz – McGraw-Hill; 1st Edition (January 1, 1971). – 521 p.

5. Bugrov A. K., Grebnev K. K. Numerical solution of physically nonlinear problems for soil foundations // Foundations, foundations and soil mechanics. - 1977. - No. 3. - P. 39-42. [in Russian].

Багрій О.В. Плоска задача механіки дискретного середовища

Багато інженерних задач, що пов’язані з проектуванням споруд і машин, математичним описанням технологічних процесів та ін., зводяться до необхідності розв’язання плоскої задачі для матеріалів з суттєвим впливом внутрішнього тертя на їх деформування. До таких матеріалів відносять великий клас матеріалів, у яких міцність на стиск більша ніж на розтяг. Закони деформування та руйнування таких матеріалів суттєво відрізняються від пружних. Особливістю цих законів є збільшення опору деформаціям зсуву і збільшення міцності матеріалів з ростом величини стискаючих напружень. Це асоціюється з впливом внутрішнього кулонового тертя на процес їх деформування в догранічній і граничній стадіях.

Крайова задача механіки деформівного твердого тіла формулюється як система рівнянь трьох видів: статичних, геометричних і фізичних. Оскільки для усіх лінійних та фізично нелінійних задач за умови малості деформацій перші дві групи рівнянь залишаються тими ж, відмічені розбіжності можна віднести за рахунок невідповідності прийнятих в розрахунках фізичних співвідношень „напруження – деформації” і реальних законів деформування вказаних матеріалів, які є більш складними реологічними об’єктами ніж структурно однорідні тверді тіла, рідини чи гази.

В статті використано підхід, коли матеріал одразу розглядається як квазісуцільний, а фізичні рівняння ґрунтуються на одержаних дослідним шляхом співвідношеннях між інваріантами тензорів напружень і деформацій, які враховують вплив як молекулярної зв’язності, так і внутрішнього кулонового тертя.

Ключові слова: плоска задача, внутрішнє тертя, стискуюче напруження, змінні модулі деформації, нелінійні фізичні рівняння